A Comprehensive Study on Synthesis and Bioapplication of Calcium Phosphates, Poly(glycerol sebacate) and the Biocomposite by Microwave Approaches

Chi Ching Lau

2018

A thesis submitted for the degree of Doctor of Philosophy at
University College London

Department of Chemical Engineering
University College London
Torrington Place
London
WC1E 7JE

Declaration

I, Chi Ching Lau, confirm that the work presented in this thesis is my own. Where information has been derived from other sources, I confirm that this has been indicated in the thesis.

…….....

Signature

…….....

Date

I. Acknowledgements

Firstly, I would like to express my sincere gratitude to my supervisors, Prof Junwang Tang and Prof Jonathan Knowles for their continued guidance and support to my PhD study, also for their motivation, expertise and insight throughout the entire project. Their guidance helped me all the time of research and writing this thesis.

Besides my supervisors, many people have contributed to my thesis. I'm very grateful to Dr Mustafa Bayazit, Dr Savio Moniz and Dr Philip James Thomas Reardon for their useful advices and suggestions. Also, I'm very grateful to Mark Turmaine and Dr Nicola Mordan for helping me with SEM and TEM, Dr George Georgiou and Dr Graham Palmer for helping me with DMA, DSC and contact angle measurement, and lastly Dr Mustafa Alqaysi and Nazanin Owji for helping me conduct the cell works. Without their help, much of the work presented in this thesis would not have been successful.

I would also like to thank all the members of Solar Energy & Advanced Materials research group (SEAM) at University College London for their stimulating discussions and useful feedbacks.

Finally, I would like to thank my friends and families: my parents, brothers, sister, Shok Ping, Xin Yi, Tiong Kit and my beloved boyfriend, Chee Hau, for all their encouragement and support.

II. Abstract

Microwave synthesis capable of improving reaction rate, yield and purity is highly desirable in preparing a wide range of biomaterials. Although existing conventional methods have been widely used to fabricate the biomaterial, these methods have various limitations especially time and energy consuming. In this thesis, the project aims is to fabricate two interesting biomaterials, calcium phosphates (CaP) and poly(glycerol sebacate) [PGS], with controlled properties by unique heating mechanism of microwave.

Firstly, three interesting CaP phases [i.e. hydroxyapatite (HA), β-tricalcium phosphate (β-TCP) and dicalcium phosphate anhydrate (DCPA)] with improved reaction rate and purity were first synthesised under identical microwave conditions. These CaP particles with varied morphology, specific surface area and pore size were produced after a short reaction time (5 mins) in microwave. However, the yields of these CaPs were low and the reaction time was extended to one hour. In this work, it was found that the solvent species with different solubility and microwave efficiency are crucial to control the phase and morphology of CaP. For instance, the highest solubility of calcium precursors in water produced HA particles which are the highest Ca/P ratio among these phases, and these particles grew in one-dimensional due to its slower heating rate in microwave. On the other hand, mesopores of β-TCP and DCPA particles were produced in methanol and ethanol, respectively. These particles with higher specific surface area demonstrated higher BSA loading than the nonporous HA particles. The pore size of the CaP particles also affected the release profile; larger pore size in β-TCP particles allowed faster release of BSA compared to DCPA. The phase and morphology-controlled of these CaP materials provide a platform to readily control both the drug delivery profile and loading capacity of proteins.

Secondly, pre-polymer of PGS (pre-PGS) were prepared successfully using a modified microwave approach. This approach allowed better temperature control in microwave and minimized the overheating of the monomers. In additions, water was collected to tailor the degree of esterification (DE) of the pre-PGS and this DE strongly affected the mechanical properties and degradation rate of the PGS. This method also sped up the pre-polymerisation and curing process by at least a factor of six. More interestingly, the highly branched pre-PGSs formed in microwave due to the special heating mechanism. In microwave, both primary and secondary hydroxyl groups of glycerol reacted simultaneously with sebacic acids. On the contrary, pre-polymerisation by conventional heating was mainly reacted the primary hydroxyl group. The PGS samples prepared by microwave showed a wider range (59%) of degradation rate than the conventional heating

method owing to the highly branched of polymer structure. Apart from that, a stiffer polymer obtained after 2 h of curing time as compared to the viscous polymer by conventional heating. The Young's modulus of PGS prepared after 8 h was similar with the one prepared by conventional heating after 48 h, owing to the branched structure. This microwave approach can synthesise PGS with higher degree of freedom to tune mechanical properties and degradation rate can meet demands of various applications.

Thirdly, PGS/β-TCP biocomposites were prepared by microwave method. The purpose of introducing the β-TCP particles on the polymer surface was to enhance the biocompatibility of PGS since the fast degraded sebacic acids always create cytotoxicity issue. The presence of the β-TCP particles not only increased the degree of crosslinking, but also improved the hydrophilicity which could not be achieved by single material of PGS. On the other hand, the mass loss of the biocomposites was also reduced significantly. Owing to these improved properties, the cell viability in these biocomposites also showed enhancement as compared to PGS.

Finally, the microwave synthesis of PGS was further modified without adding any solvent or catalyst. PGS was prepared successfully by single step microwave synthesis and no curing step was needed. To the best of my knowledge, this is the first study to get the biopolymer synthesised by a means of one step. It was found that a high microwave power with short reaction time is crucial for the formation of PGS. The cooling intervals minimised the monomer loss caused by the overheating issues. The prepared PGS were characterised with IR spectra, ^{1}H NMR spectra and thermal analysis, and these properties are comparable with the reported literature. The ester linkage of the PGS was confirmed by IR spectra. Surprisingly, as indicated in ^{1}H NMR spectra, both primary and secondary hydroxyl groups were activated by microwave to form linear and branched polymer, simultaneously. Both crystallisation and melting temperature were reduced with increment in reaction time, owing to limited mobility of the chains.

III. Impact Statement

Biomaterials are developed rapidly to improve human lives since soft and hard tissues in the human body are not long lasting. Generally, aging changes in tissues and some organs even lose their functions. Thus, biomaterials are crucial to help these people, especially elderly people, back to normal life.

This thesis mainly studies the preparation of calcium phosphates and poly(glycerol sebacate) using advanced microwave approaches, and also their bioapplication. Firstly, new methodology is introduced to fabricate these biomaterials. Calcium phosphate particles, poly(glycerol sebacate) and also the biocomposites of these two biomaterials, with improved properties have been successfully achieved. The prepared biomaterials could be used as drug carriers or implants. Secondly, the effects of the microwave on the material properties are also highlighted in this study and the microwave synthesis pathway method can potentially expand to synthesise other biomaterials such as polyester or hydrogel. This method could alter the material structure and properties which are very important for their application. Apart from that, the microwave chemical approach is an energy facile method and has the potential to scale-up and commercialisation. This method can save energy and time efficiently compared to conventional heating methods. These novel results have resulted in two publications and another two are still in progress.

In total, the material prepared could potentially improve human life quality and the technological outcomes related to materials in this project should benefit those scientists working in the biomaterials, nanotechnology and microwave chemistry. Finally, the fundamental understanding of the microwave chemical approach can broadly apply to other areas, e.g. chemical synthesis and manufacturing.

IV. Publications and Conferences

Publications

1. **Advanced Biocomposite of Poly(glycerol sebacate) and β-Tricalcium Phosphate Particles by Microwave Synthesis.** Chi Ching Lau, Mustafa Al Qaysi, Nazanin Owji, Mustafa Kemal Bayazit, Jijia Xie, Jonathan Campbell Knowles and Junwang Tang. *Under review.*
2. **Microwave Chemistry: Batch and Flow System.** Chi Ching Lau, Philip James Thomas Reardon, Mustafa Bayazit, and Junwang Tang. *In preparation. (Invited Review Paper)*
3. **Tailoring Degree of Esterification and Branching of Poly(glycerol sebacate) by Energy Efficient Microwave Irradiation**. Chi Ching Lau, Mustafa Kemal Bayazit, Jonathan Campbell Knowles and Junwang Tang. *Polymer Chemistry, 2017, 8, 3937-3947.*
4. **Phase-Tunable Calcium Phosphate Biomaterials Synthesis and Application in Protein Delivery.** Chi Ching Lau, Philip James Thomas Reardon, Jonathan Campbell Knowles and Junwang Tang. *ACS Biomaterials Science & Engineering, 2015, 1, 947–954.*
5. **Efficient Visible Light-Driven Water Oxidation and Proton Reduction by an Ordered Covalent Triazine-Based Framework.** Jijia Xie, Stephen A. Shevlin, Qiushi Ruan, Savio J. A. Moniz, Yangrong Liu, Xu Liu, Yaomin Li, Chi Ching Lau, Zheng Xiao Guo, and Junwang Tang. *Energy & Environmental Science, in press.*
6. **Linker-controlled Polymeric Photocatalyst for Highly Efficient Hydrogen Evolution from Water.** Yiou Wang, Mustafa Kemal Bayazit, Savio Moniz, Qiushi Ruan, Chi Ching Lau, Natalia Martsinovich and Junwang Tang. *Energy & Environmental Science, 2017, 10, 1643-1651.*
7. **Size-Controlled TiO_2 Nanoparticles on Porous Hosts for Enhanced Photocatalytic Hydrogen Production.** Chaoran Jiang, Ki Yip Lee, Christopher Parlett, Mustafa Kemal Bayazit, Chi Ching Lau, Qiushi Ruan, Savio Moniz, Adam F. Lee and Junwang Tang. *Applied Catalysis A: General. 2016, 521, 133–139.*

Conferences

1. **European Society for Biomaterials Conference** (ESB), Athens, Greece, 2017. Poster presentation.
2. Control of Poly(glycerol sebacate) properties by varying levels of crosslinking using a fast microwave approach. *Front. Bioeng. Biotechnol. Conference Abstract: 10th* ***World Biomaterials Congress****, Montreal, Canada, 2016*. Oral presentation.

V. Table of Contents

VI. List of Figures

VII. List of Tables

VIII. List of Equations

IX. Nomenclature

ATR-FTIR	Attenuated Total Reflectance Fourier Transform Infrared Spectroscopy
β-TCP	beta-tricalcium phosphate
BET	Brenauer-Emmett-Teller
BJH	Barrett-Joyner-Halenda
BSA	Bovine Serum Albumin
CaP	Calcium Phosphate
CH	Conventional Heating
DCPA	Dicalcium phosphate anhydrous or Monetite (mineral)
DMA	Dynamic mechanical analysis
DSC	Differential scanning calorimetry
EtOH	Ethanol
HA	Hydroxyapatite
IR	Infrared
JCPDS	Joint Committee on Powder Diffraction Standards
MALDI-TOF	Matrix-assisted Laser Desorption-Time of Flight
MARS	Microwave Accelerated Reaction System
MeOH	Methanol
MI	Microwave Irradiation
NMR	Nuclear Magnetic Resonance
PGS	Poly(glycerol sebacate)
Ref	Reference
SEM	Scanning Electron Microscopy
TEM	Transmission Electron Microscopy
UV-Vis	Ultraviolet-Visible Spectroscopy
XRD	X-ray Diffraction

1. Introduction

1.1 Background of Study

Turning back to history, biomaterials have evolved significantly as described previously by Hench *et al.* (Figure 1-1).[1,2] Historically, biomaterials were first reported in 1960s, aiming to replace damaged tissues like dental implants and artificial joints using bioinert materials. These materials reduce the immune response to foreign materials. Moving into the second generation of biomaterials, bioactive materials (e.g. glasses and ceramics) were introduced to elicit a controlled reaction in the physiological environment. For example, by coating hydroxyapatite on a metallic surface, a new bone grew along the coating and formed a strong interface. A convergence in resorbable and bioactive materials further upgrades the biomaterials into third generation, designed to stimulate a specific cellular response. A resorbable scaffold with seeded cells is implanted into the human body to replace damaged tissue; the scaffold resorbs and is replaced slowly by the host tissue which could provide long-lasting repair.

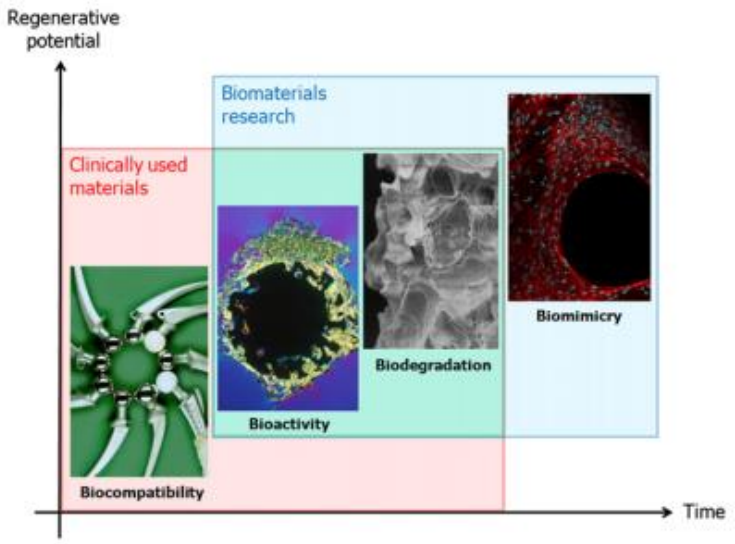

Figure 1-1 Evolution in the development of biomaterials with time.[2]

Of the various bioceramic materials, calcium phosphate (CaP) is one of the best choices for orthopaedics, dentistry and even reconstructive surgery due to its exceptional biocompatibility, biodegradability, predictability, low toxicity and

enhanced solubility compared with other materials (e.g. silica and carbon nanotubes).[3,4,5] In addition, calcium and phosphorus are two elements existing widely in the human body: bone and teeth concentrate on these elements where more than 34 wt% of calcium and 15 wt% of phosphorus are found in bone and teeth.[6] Extensive studies have been conducted to prepare these materials in different morphology, particle size and phases, depending on their applications. The solubility of CaP is relatively slow but it varies with the Ca/P ratio. β-tricalcium phosphate (β-TCP) is a bioresorbable CaP phase that is reported widely other than hydroxyapatite (HA). Its potential as a biomaterial for tissue regeneration has been highlighted by a series of *in vitro* and *in vivo* studies, and it therefore warrants further study as a bone replacement material. Along with excellent biocompatibility, β-TCP also has higher aqueous solubility and hence *in vivo* degradation when compared to HA. It could allow local delivery of therapeutic coupled with remineralisation of bone, making it an ideal candidate for both regeneration and delivery of therapeutic agents. The newest CaP may have excellent bioactive characteristics, but the phase control of CaP under mild experiments conditions is still a challenge.

Other than calcium phosphate ceramics, a variation of natural or synthetic polymers (i.e. collagen, polyester and polyurethanes) is also introduced. Poly(glycerol sebacate) [PGS], one of the interesting biodegradable polymers, is introduced by Langer's group in 2002.[7] This attractive polymer has been studied widely for various applications, such as cardiac muscles, drug carrier, cartilage and blood vessels.[8] However, the synthesis pathway of this polymer is lengthy and the relationship between the esterification degree and material properties has been less reported. Many studies have reported the application of this polymer but not its material chemistry, especially the control of these properties which is linked with a polymerisation process. Furthermore, as a synthetic material, the biocompatibility of this material is always crucial where the degraded products may cause toxicity to the system.

To understand the complexity interactions of biomaterials with the human tissues, multi-disciplines from material science, biologists, chemists, physicists, and engineering have been working together, aiming to improve human health with these biomaterials. Till now, different synthesis approaches have been applied to prepare these biomaterials, depending on the type of materials. Before proceeding to the clinical applications, the basic properties control of these materials is relatively important since the properties decide their applications. However, to control the biomaterial properties there is still a challenge. Secondly, the biomaterial synthesis using a conventional heating method always requires a long time and is energy-consuming, whilst the material society promotes green chemistry where an energy-efficient method is preferable. Lastly, scaling up the research outcome and converting into a commercial product is another challenge for the biomaterial scientist, involving cost and function effectiveness.

Considering these, the overall project goal is to utilise the unique properties of microwave heating to synthesise these two interesting biomaterials, CaP and PGS, and then a biocomposite as highly efficient and novel biomaterials for future tissue regeneration and drug delivery systems, further investigating the effect of microwave on the properties of these biomaterials. The employment of microwave heating on preparing biomaterials offers many advantages. The special rotational heating mechanism by microwave is particularly advantageous to the material preparation, especially in improving the reaction rate, crystallinity at low temperature and product selectivity. Other than that, microwave appears as a good method to control material properties, such as particle size distribution, morphology and porosity. On the other hand, the understanding and controlling of these material properties by microwave is also a missing part from literature where these are highly crucial for biomedical applications.

There are three main objectives which would enable the overall project to be successful. The first is to synthesise crystalline CaP biomaterials with controlled phases and properties by microwave. Secondly, the aim is to prepare PGS with controllable degradation rates and mechanical properties using the microwave

method. The third is to improve the biocompatibility of PGS by introducing the β-TCP particles into the PGS polymer. Ultimately, all synthesised materials were studied using a variety of functional characterisation and analytical techniques in order to offer insight into microwave-assisted material formation and factors which influence their bioapplications.

1.2 Chapter Outline

There are eight chapters in this thesis, beginning with Introduction, describing the motivation and aims and then followed by:

Chapter 2: Literature Review

In this chapter, a review of the literature summarises the current status and scientific challenges on biomaterials, especially CaP and PGS. This also includes some fundamentals on microwave irradiation which have been used in this project to prepare materials.

Chapter 3: Material Characterisation

This chapter outlines the theory of the characterisation methods, including X-ray diffraction and nitrogen sorption. For this material synthesis project, characterisation is very important to confirm the right material has been fabricated before any test.

Chapter 4: Phase Tunable Calcium Phosphates Biomaterials by Microwave Synthesis

This chapter presents the fabrication of CaP with controllable phases under identical mild microwave conditions. The protein loading and release profile is studied using these prepared CaP. Solubility, specific surface area and pore size of the prepared CaP are key factors affecting this profile.

Chapter 5: A Comprehensive Study of Poly(glycerol sebacate) Synthesis via Microwave and Conventional Heating

This chapter demonstrates the synthesis of PGS with controlled degree of polyesterification using microwave, which improves the reproducibility and provides a wider range of degradation rate that can fit into different bio-applications compared with samples synthesised by conventional approaches.

Chapter 6: Enhanced Biocompatibility of Poly(glycerol sebacate) using β-tricalcium phosphate particles via microwave synthesis

This chapter describes the preparation of β-TCP/PGS biocomposite by microwave method. Based on the cell viability results, the prepared biocomposites show excellent enhancement in the biocompatibility of PGS.

Chapter 7: Single-step Synthesis of Poly(glycerol sebacate)

This chapter presents the further improvement on preparing the PGS where a solvent and curing step are skipped during the synthesis. Under proper temperature control, the reaction rate increases, and the loss of monomers minimises, resulting into a faster and for the first time a one-step preparation of PGS.

Chapter 8: Overall Conclusion and Future Work

This chapter summarises the contribution of this thesis and proposes some future work.

2. Literature Review

Biomaterials including synthesis and application of calcium phosphates and poly(glycerol sebacate) have been reviewed firstly to understand their current progress and the limitations. Then fundamentals on microwave and its applications in materials synthesis were reviewed.

2.1 Biomaterials

2.1.1 Introduction

Biomaterials refer to any natural or synthetic materials applied to the human body and can interact with living tissues safely.[9] The creation of biomaterials is to improve the quality of life; replacing and repairing soft and hard tissue especially for the aging population. The market of biomaterials is more than $30 billion (www.marketsandmarkets.com) globally, dominated by orthopaedic applications and followed by polymer-based biomaterials. It is expected to have a huge growth potential due to the increasing number of patients suffering from diseases which need to be replaced or repaired using these biomaterials. One of the common biomaterials used clinically is orthopaedic implants and more examples are cardiac pacemaker, contact lens and artificial heart valves. An ideal biomaterial is highly dependent on three major factors: the function and biocompatibility, the health condition of patient, and the competency of a patient to adapt to it.[10]

There are four biomaterial groups: ceramics, polymer, metals and composites. Ceramics always shows good biocompatibility but are brittle, metals have high wear resistance yet low biocompatibility, polymers are flexible but reduce bioactivity during the degradation process. Due to their properties, each of these biomaterials can suit into different bioapplications and is further described in the section 2.1.2 and 2.1.2. For instance, metals are widely used for load-bearing implants such as artificial joints for hips and knees, polymers are applied for soft

tissues repairing and ceramics are employed as a restorative material in dentistry.[11]

2.1.2 Tissue Engineering

Tissue engineering aims to repair or reconstruct the damaged tissues and organs using the engineered biomaterials. As mentioned in chapter 1, biomaterials evolved and are classified into different groups depending on their properties: bioinert, bioactive and resorbable. Owing to their own speciality, the interaction between biomaterials and tissue are also varied (Table 2-1): morphological fixation, biological fixation, bioactive fixation and replacement with tissue.[12] For morphology fixation, the implant is mechanically interlocked in the body. However, it yields a non-adherent fibrous capsule surrounding the implant, resulting an isolation of the implant with the tissue. Porous materials (i.e. metal oxides, polymers and ceramics) provide biological fixation by growing the tissues into the pores on the surface of the implants. A larger surface area given by porous structure provides a firmer fixation than nonporous implants. For bioactive material, it results in a bioactive fixation by bonding the tissues with materials with the strength equal to or greater than bone. Resorbable implants are metabolically acceptable and designed to degrade gradually with time and replaced by natural host tissue. Usually these materials are polymers. For instance, polyester degrades via hydrolysis of the ester linkage.

Table 2-1 Types of bioimplants for tissue attachment.[12]

Type of Implant	Type of Attachment	Example
Nearly inert/bioinert	Mechanical interlock (morphological fixation)	Metals, Alumina, Zirconia, Polyethylene (PE)
Porous	Ingrowth of tissues into pores (biological fixation)	Hydroxyapatite (HA), HA coated porous metals
Bioactive	Interfacial bonding with tissues (bioactive fixation)	Bioactive glasses, HA, Bioactive glass-ceramics
Resorbable	Replacement with tissues	TCP, Polylactic acid (PLA)

Cells, scaffold and growth factors are three major components to repair tissues. Cells synthesise the matrices of new tissues, three-dimensional scaffolds provide a suitable environment for the cells, and the growth factors promote regeneration of new tissues during the recovery process.[13] Numerous investigations have been conducted to study these key components, including the interaction between these components with the materials, the effects of the scaffold to the tissue, the loading and delivery of growth factors to the patients, and so forth. Apart from that, structure of the scaffold, mechanical properties of the biomaterials and cell culture environment also affect the tissue recovery significantly.[13]

According to Joon *et al.* (2007), the ultimate goal of developing biomaterials is to improve human health and more specifically is to restore damaged natural living tissues and organs in the body.[9] Thus, it is essential to understand relationships between biomaterials properties and functions of these biological materials. Till now, it remains a huge challenge for all researchers working in basic science, engineering and medicine to investigate and understand the complex interactions between biomaterials and tissues in depth. It is more difficult when looking into a variety of combinations between materials and living tissues.

2.1.3 Drug Delivery

Other than tissue engineering, drug delivery systems (DDS) are also widely studied. The DDS involve drugs loading, drugs delivery in human body and total period to release the drugs. Thousands of comprehensive studies are required before applying the DDS with a specific drug in the human body. This is because an overdose could happen and may endanger the patients. Therefore, it is relatively crucial to control the drugs loading and release process.

A controlled DDS are designed to release the drugs at the specific or targeted area with minimal toxicity during the treatment process. According to Horcajada *et al.* (2010), an efficient DDS demonstrates these characteristics:[14]

i) Load or encapsulate drugs efficiently

ii) Control the drugs release process and matrix degradation without showing the 'burst effect' release
iii) Provide the flexibility to modify the surface of the carriers
iv) Able to track using the imaging techniques

The efficient DDS reduce systemic toxicity, provide excellent stability drugs toxicity and improve the impact of the drugs. For instance, Cisplatin is one of the promising anticancer agent, but it causes a lot of side effects such as renal and auditory toxicity, nausea and vomiting, therefore, targeted drugs release is preferable to minimize the side effects.[15]

Table 2-2 shows the examples of the commonly used drugs for bone regeneration, chemotherapy and anti-inflammation. Ceramics and polymers are generally used as drug carriers in the DDS owing to their superior properties, which are discussed in the following sections (2.2 and 2.3). For example, calcium phosphate ceramics is widely used to deliver growth factors for tissue recovery and release anticancer drugs for cancer treatment. In addition, degradable polymers also have the potential as drug carriers since no surgical step is needed to remove the polymer. More details on degradable polymers is presented in Chapter 2.3.1.

Drug release mechanisms involve at least one of these mechanisms: diffusion-controlled release, drug-carrier affinity or degradation of the material.[16] Diffusion-controlled release is dominated by non-degradable carriers where the engineered membrane controls the release rate by altering the solubility in the material and the diffusivity of the drug.[16] The drugs are encapsulated in the carriers and the membrane or coating allows water permeability and diffuse the drugs out the carriers.[52] Secondly, the drug release process relies on the drug-carrier affinity. This occurs when the drugs have strong and reversible chemical interaction with the carriers such as ionic bonds and hydrogen bonds between these molecules.[16]

Table 2-2 Examples of drugs used for bone tissue engineering, cancer therapy and antibiotics.

Drugs	Functions	Drug Carriers	Reference
Bone Regeneration			
Growth hormone	• Proliferation and differentiation of osteoblast • Bone remodelling • Stimulation of osteoclastic resorption activity	BCP, CaP, PACA	[17,18,19]
Bone morphogenetic proteins (BMPs)	• Proliferation and differentiation of mesenchymal stem cell and osteoprogenitor cells • Ectopic bone formation	BCP, β-TCP, PLA, collagen, gelatin, PTP	[17,20,21,22,23]
Transforming growth factor	• Angiogenic and inflammation properties • Extracellular matrix production • Recruitment, proliferation and differentiation of MSCs and osteoprogenitor cells	BCP, gelatin, HA, collagen, CPC, OPF	[17,20,22,24,25,26]
Insulin growth factor	• New bone formation and mineralization • Proliferation and migration of MSC and osteoprogenitor cells	PLGA/PEG, TCP, PLGA	[17,20, 24,27,28]
Fibroblast growth factor	• To improve angiogenesis in infracted myocardium	PLA/PGA, chitosan, ACP/PLA, gelatin	[21,22,29,30,31]
Antibiotics			
Gentamicin	• To treat serious infections caused by bacteria, such as osteomyelitis	PMMA, HA, chitosan/β-TCP, hyaluronic acid/chitosan, silica	[17,32,33,34]
Vancomycin	• To treat bacterial infections such as osteomyelitis and septic arthritis	Silica/gelatin, chitosan/alginate, HA, silica	[35,36,37,38]

Anticancer			
Cisplatin	• To inhibit growth of cancer cells • Used to treat breast, ovarian, lung and bladder cancer	HA, gelatin, PLGA/PEG, PEG/PLA	[17,39,15,40, 41]
Doxorubicin	• Anticancer drugs (e.g. leukaemia and breast cancer)	Liposomes, MOF, chitosan, PEG/PCL, CaP	[42,14,43,44,45]
Docetaxel	• To treat stomach cancer, breast cancer and prostate cancer • Inhibit cell division	PLA-PLGA, ACP, PLGA-lecithin-PEG	[46,47,48]
Anti-inflammatory			
Ibuprofen	• A non-steroidal anti-inflammatory drug • To treat inflammation caused by back pain, menstrual cramps or headache	HA, polysaccharides, silica	[49, 50,51]

BCP: biphasic calcium phosphate (mixture of β-TCP/HA); β-TCP: β-tricalcium phosphate; PACA: poly(alkylcyanoacrylate); PTP: poly(phosphazene); CPC: calcium phosphate cement; OPF: oligo(poly(ethylene glycol) fumarate); HA: hydroxyapatite; MOF: metal-organic frameworks; PMMA: poly(methyl methacrylate); PLGA: poly(lactic-co-glycolic acid); PEG: poly(ethylene glycol); PLA: poly(lactic acid); PGA: poly(glycolic acid); ACP: amorphous calcium phosphate; CaP: calcium phosphate

Thirdly, the drug release mechanism is dominated by the degradation rate, specifically for the carriers with faster degradation rate than the drugs diffusion.[16] The drug release profile can be predicted if the degradable carriers are used in the system. The degradation process of these carriers involves dissolution, hydrolytic cleavage and enzymatic degradation.[52]

Major challenges of using the biomaterials in DDS are complex preparation methods, low stability of the biomaterials, undesired degraded biomaterials, uncontrollable immune response and toxicity.[42] The efficient DDS in the human body with minimal toxicity is desired, but it is hard to control. The synthetic biomaterials can also induce the toxicity in the human body during the degradation process, and uncontrollable drugs release always causes the overdose. In short, the development in the DDS requires the convergence of knowledge in medicine, engineering, materials science, biologist, and physics to further improve the current system.

2.2 Calcium Phosphate Ceramics

Calcium phosphate (CaP) ceramic is one of the interesting biomaterials. Although there are numerous researches studying the synthesis and properties of this material, yet control of the particle size, morphology, and phase remains challenge.

2.2.1 Introduction

Ceramic materials are inorganic compounds, sharing electrons between ions or atoms by ionic or covalent bonds. The superior chemical compatibility of ceramics (i.e. alumina, zirconia and CaP) with hard tissue such as bones and teeth have resulted in a wide field of application in the medical area- as illustrated in Figure 2-1.[53] Among these ceramics, CaP have high potential in aiding bone integration and conduction process owing to their excellent biocompatibility and bioactive behaviour.[54] The first successful repair of a bone defect using CaP was

reported in 1920.[55] It is generally found that the application of CaP encompasses all the skeletal system, such as maxillofacial reconstruction and bone defect reconstructions.

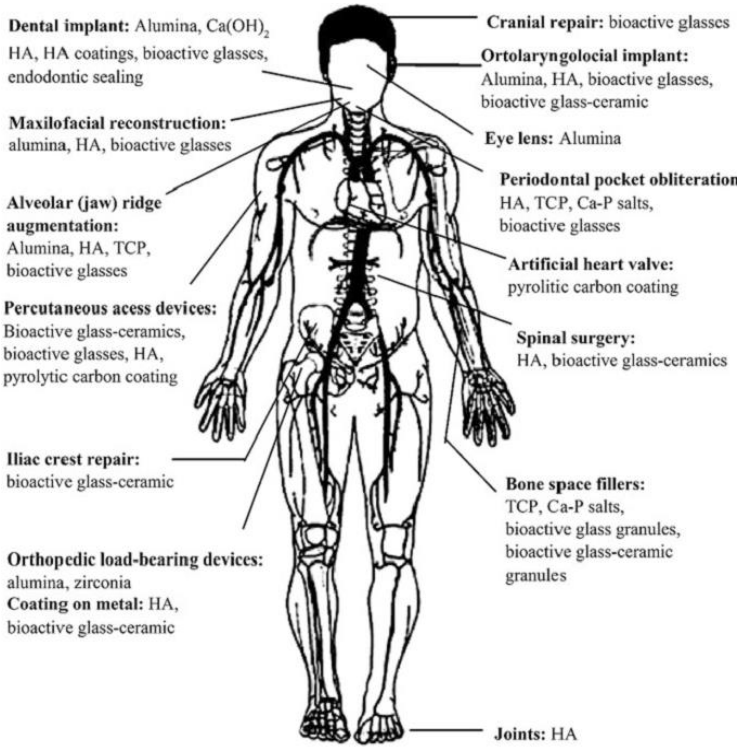

Figure 2-1 Clinical application of ceramic biomaterials in human body for repairing the damaged tissues.[53]

CaP ceramics are present abundantly in bone and teeth mineral phase and have a similarity with biological apatite's structure. CaP support osteoblast adhesion and proliferation, degrade without producing any toxic substance compared with silica, quantum dots, carbon nanotubes or magnetic particles, and their particles can permeate the cell membrane and dissolve in the cell which polymer could not achieve.[5,56] On the other hand, CaP has also been studied as drug carriers since the tuneable phase composition with different solubility of CaP phases can control the resorption rate and release rate over time and porous CaP is incorporated with hormones, vaccines, antibiotics and anticancer agents. Nonetheless, the major weakness of CaP as biomaterials is their mechanical properties, brittle with poor fatigue resistance.[56] Consequently, it is always used

as a filler and coating to support metallic implants in order to provide biological attachment.[53]

Table 2-3 Examples of registered commercial trademarks of calcium phosphates-based biomaterials.

Material	Company	Ref
Calcium deficient apatite (CDHA)	Osteogen (Impladent, NY) Calcibon (Biomet, IN,USA) Cementek (Teknimedd, France)	3,57,58
Hydroxyapatite (HA)	Osteograf (Ceramed, CO) Actifuse (ApaTech, UK) Alveograf (Cooke-Waite Laboratories, USA) ApaPore (ApaTech, UK) Bonefil (Pentax, Japan) HA BIOCER (CHEMA-ELEKTROMET, Poland)	3 ,57
β-tricalcium phosphate (β-TCP)	Vitoss (Orthovita, PA) Antartik B-TCP (MedicalBiomat, France) Biosorb (SBM S.A., France) Cerasorb (Curasan, Germany) Ceros (Thommen Medical, Switzerland) Conduit (DePuy Spine, USA)	3 ,57
Biphasic calcium phosphates (BCP)	MBCP (Biomatlante, France) Tribone (Stryker, Europe) Hydros (Biomatlante, France) Kainos (Signus, Germany)	3 ,57
BCP/collagen	Allograft (Zimmer, IN) Collagraft (Zimmer, IN, USA)	3 ,57
HA/collagen	Bioimplant (Connectbiopharm, Russia) Bonject (Koken, Japan) Collagraft (Zimmer and Collagen Corporation, USA)	57
CHA/collagen	Healos (Orquest Inc., CA)	3
BCP/fibrin	TricOS (Baxter Bioscience, France)	57

Owing to the speciality properties of CaP, they have been commercialised which is illustrated in Table 2-3. The available biomaterials are mainly osteogenic or osteoinductive or purely osteoconductive.[57] Hydroxyapatite (HA) and β-tricalcium phosphate (β-TCP) are usually applied in this area due to their high

tissue compatibility and tendency of new bone forming on these materials. Both of them promote cell proliferation and differentiation, while β-TCP biodegrades faster than HA because of its higher resorption rate.[59, 60]

2.2.2 Different phases of calcium phosphates

Calcium phosphates (CaP) consist of phosphoric or orthophosphoric acid salts which can be prepared by precipitation from Ca^{2+} and PO_4^{3-} under alkaline or acidic conditions. Generally, CaP can be distinguished by Ca/P ratio (range 0.5-2), basicity/acidity, and solubility (Table 2-4). Under different phases, CaP have their own physical properties in solubility and resorbability since most of them are sparingly soluble except in acidic conditions. The Ca/P ratio relates intimately with the acidity and solubility.[61] As the Ca/P ratio decreases, the acidity and solubility of the mixture increase. Thus, a higher Ca/P ratio of CaP is less soluble under neutral conditions and this has reduced the degradation rate. However, these two parameters drop significantly as the Ca/P ratio is close to 1.67. It is also recognized that the low Ca/P ratio (less than one) is insufficient for biological implantation usage due to their high solubility.

Monocalcium phosphate monohydrate (MCPM) or calcium dihydrogen orthophosphate monohydrate precipitates under highly acidic conditions and is used as a component in self-hardening calcium phosphate cements, mineral supplement for dry baking powders and bakery dough.[62] MCPM is the most acidic CaP phase with the highest solubility, therefore, it is not bioactive due to its acidity. At high temperature (>100 ˚C), MCPM releases water and becomes monocalcium phosphate anhydrous (MCPA) which is also non-bioactive.

Octacalcium phosphate (OCP) or tetracalcium hydrogen orthophosphate diorthophosphate pentahydrate (IUPAC name) is often found as an intermediate species during the aqueous crystallisation of thermodynamically stable phases such as calcium deficient hydroxyapatite (CDHA) which has similar crystal structure to HA. It is biocompatible, biodegradable, and osteoconductive, therefore it is medically used as a bone filler.[62]

Dicalcium phosphate dihydrate (DCPD) or brushite is easily crystallised from an aqueous solution of acidic pH (range 2-6.5) and transforms into dicalcium phosphate anhydrate (DCPA) when the temperature is above 80 ˚C.[63] It is used for CaP cements, glass production, fertilizer, toothpaste and calcium supplement in food.[62]

DCPA or monetite is a bioresorbable and biodegradable CaP.[58] It is less soluble than DCPD due to the absence of water. It can be synthesised by crystallising from the acidic aqueous solution above 100 ˚C or at room temperature in ethanol by stirring vigorously.[64] It is used in CaP cement, polishing agents, and dough conditioner in the food industry.[62]

Amorphous calcium phosphate (ACP) is an amorphous state of other CaP. It is commonly found at low temperature as an intermediate phase, precipitating first in aqueous conditions due to lower surface energy than OCP or apatites.[6263] It is used as a filling material in dentistry.

Tricalcium phosphate (TCP) is an interesting bioresorbable CaP phase, and more detailed discussion on this material is presented in section 2.2.3.

Hydroxyapatite (HA) is a relatively stable form since it is the least soluble phase of the CaP (Table 2-4). It exists in monoclinic and hexagonal crystal form, with a transition from the former to the latter above 250 ˚C. Typically it is prepared by mixing calcium and phosphate ions in an aqueous solution at pH > 9 with Ca/P ratio of 1.67 for many days and followed by calcination under high temperature (~1000 ˚C). HA does not exist as a pure form in the biological system but it has similarity to the mineral component of teeth and bone. Thus, it is widely implemented for the coating of orthopaedic and dental implants, drug delivery and in liquid chromatography of proteins.[62]

Among these CaP phases, HA and TCP have a surface that favours protein adsorption and have a high bone inductive potential.[53] HA is the most stable

phase thermodynamically at physiological conditions below pH 4, followed by β-TCP and octacalcium phosphate (OCP). Hence, the *in vivo* degradation of calcium phosphates can be predicted: MCPM> α-TCP> DCPD> DCPA> OCP> β-TCP > HA. For biphasic calcium phosphates, higher β-TCP/HA ratio creates a higher extent of dissolution.[65] By lowering the pH, brushite (DCPA) is more stable than HA.

2.2.3 β-Tricalcium phosphate

Tricalcium phosphate (TCP) exists in two polymorphs, α-TCP and β-TCP which can be distinguished by their crystal structures and solubility. Both of them are prepared by high temperature treatment (e.g. >800 ˚C for β-TCP and >1125 ˚C for α-TCP) and neither can precipitate from aqueous solutions.[58] β-TCP is less soluble in water than α-TCP at room temperature. Whitlock (β-$(CaMg)_3(PO_4)_2$) is the only biological appearance of β-TCP by substituting magnesium into β-TCP in pathological calcifications, including dental calculi, urine stones, salivary stones, and even soft tissues deposits.[62] α-TCP is a high temperature phase of β-TCP, but more reactive in aqueous systems and has a higher specific energy. It is not very popular in the biomedical field due to a quick resorption rate while it is used in cements, fertilizer, and bone grafts.[62]

Owing to its solubility, β-TCP is one of the most widely used compared to other CaP phases. HA shows quick bone adaption, however, its degradation is slow and may hinder the formation and remodelling of new bone.[53,66] By contrast, β-TCP is a more attractive biomaterial as a bone substitute due to its biocompatibility, biological safety, ease of sterilization, and long shelf life.[67] More importantly, β-TCP has proven its excellent osteogenic properties; β-TCP helps in the new bone formation without any growth factors.[68] The biocompatibility/degradation rate of β-TCP strongly depends on the porosity, crystallinity, chemical purity and surface roughness.[53]

Table 2-4 Calcium phosphates phases with listed physical properties.[57, 21]

Ca/P Molar Ratio	Phase	Chemical formula	Solubility at 25 ˚C, -log(K_s)	Solubility at 25 ˚C, g/L	pH stability range in aqueous solution at 25 ˚C
0.5	Monocalcium phosphate anhydrous (MCPA)	$Ca(H_2PO_4)_2$	1.14	~17	[c]
0.5	Monocalcium phosphate monohydrate (MCPM)	$Ca(H_2PO_4)_2 \bullet H_2O$	1.14	~18	0.0-2.0
1.0	Dicalcium phosphate (DCPA, Monetite)	$CaHPO_4$	6.90	~0.048	[c]
1.0	Dicalcium phosphate dehydrate (DCPD, Brushite)	$CaHPO_4 \bullet 2H_2O$	6.59	~0.088	2.0-6.0
1.33	Octacalcium phosphate (OCP)	$Ca_8(HPO_4)_2(PO_4)_4 \bullet 5H_2O$	96.6	~0.081	5.5-7.0
1.5	α-Tricalcium phosphate (α-TCP)	$Ca_3(PO_4)_2$	25.5	~0.0025	[a]
1.5	β- Tricalcium phosphate(β-TCP)	$Ca_3(PO_4)_2$	28.9	~0.0005	[a]
1.2-2.2	Amorphous calcium phosphate (ACP)	$Ca_xH_y(PO_4)_z \bullet nH_2O$, n=3-4.5; 15-20% H_2O	[b]	[b]	~5-12 [d]
1.5-1.67	Calcium deficient hydroxyapatite (CDHA)[e]	$Ca_{10-x}(HPO_4)_x(PO_4)_{6-x}(OH)_{2-x}$[f] (0<x<1)	~85.1	~0.0094	6.5-9.5
1.67	Hydroxyapatite (HA)	$Ca_{10}(PO_4)_6(OH)_2$	116.8	~0.0003	7-12
2.0	Tetracalcium phosphate (TTCP), mineral hilgenstockite	$Ca_4(PO_4)_2O$	38-44	~0.0007	[a]

[a] These compounds cannot be precipitated from aqueous solution.
[b] Cannot measure precisely. However, the following values were found: 25.7 ± 0.1 (pH =7.40), 29.9 ± 0.1 (pH = 6.00), 32.7 ± 0.1 (pH 5.28).
[c] Stable at temperature above 100 ˚C.
[d] Always metastable.
[e] Occasionally, CDHA is named as precipitated HA.
[f] In the case x=1 (the boundary condition with Ca/P = 1.5), the chemical formula of CDHA looks as follows: $Ca_9(HPO_4)(PO_4)_5(OH)$.

2.2.4 Synthesis of calcium phosphates using different methods

The chemical composition, morphology, size, shape, crystallinity, pores and roughness of CaP are varied with phases. These properties are critical issues in the biomedical area because they affect the resorption rate and interaction with the surrounding tissues. For instance, smaller particle size increases the surface area-to-volume ratio, allowing for a high drug payload.

In order to obtain the desired CaP phase, the molar ratio of Ca/P has to be controlled. If the molar ratio is not set to 1.67 during the preparation, extraneous phases may normally appear. For example, α-TCP or β-TCP may form at lower Ca/P value and CaO may produce at higher Ca/P value.[5] As shown in Table 2-5, a variation of synthesis approaches has been used to prepare different phases of CaP, especially those interesting phases (i.e. HA and β-TCP). Precipitation from solution and sol-gel are simple techniques to prepare materials, but both are very time consuming. Also, low temperature synthesis is not desirable since there is always the presence of a metastable phase in the final product.[5] On the other hand, hydrothermal is a better alternative to prepare materials because water can easily be removed from the products. Water can also act as a catalyst for the formation of the desired materials by tuning the temperature and pressure.[83] However, further heat treatment like high temperature calcination may be needed for these methods to improve the quality of the prepared materials, especially for their crystallinity. The calcination at high temperature is hard to produce uniform nano-sized particles and the process is always lengthy.

Time and energy saving methods are always preferable for preparing materials, therefore, high temperature calcination, mixing or milling steps are less preferable. In order to enhance the reaction kinetics and increase the ability to produce the materials, microwave coupling with hydrothermal was then used to produce CaP with improved purity and reaction rate. The fundamental of microwave will be further explained in chapter 2.4.

Table 2-5 List of methods to prepare different phases of CaP.

Parameters Control					Results	Ref
Precursors	**Ca/P ratio**	**pH**	**Process (Temperature, Time)**	**Solvent**		
Precipitation from solution						
$Ca(NO_3)_2 \cdot 4H_2O$ $(NH_4)_2HPO_4$	1.07-2.56	4.5-11	(1)P: RT, 24h (2)D: 80 ˚C, 24 h (3)C: 700-1600 ˚C, 6h, in air	SBF	• HA or mixture phase of HA/CaO/$Ca(OH)_2$/CaCO3 • 35-50 nm spherical particles • >99% purity after calcination	69
$Ca(NO_3)_2$ $(NH_4)_2HPO_4$	1.50-2.00	6.5-9	(1)P: 30-95 ˚C (2)D:100 ˚C (3)C: 1000 ˚C, 15h, air	H_2O	• Poor crystallinity of HA • Mixture phase of β-TCP/β-$Ca_2P_2O_7$, β-TCP/HA or HA/CaO depends on the initial Ca/P ratio • Specific surface area: 55-88 m^2/g • Morphology: needle-like (100 nm long) • Formation of CaP phase relies on the molar ratio of reactants but there is always a mixture of phase.	70
Mechanochemical						
Calcium pyrophosphate $CaCO_3$	1.67	NA	(1)MC :2-8 h,170 rpm (2) D: 150˚C, 24 h (3) C: 1100 ˚C, 1h	H_2O	• HA formed • Crystallinity improved by calcination • Specific surface area: 2-11 m^2/g	71
$Ca(OH)_2$ $CaHPO_4$ $CaCO_3$	NA	NA	MC: 20-80 h (45 mins milling +15 min interval per cycle)	NA	• HA or mixture of HA/$CaHPO_4$ • Nanorods and nanogranules • Hard to control the crystallinity of products where the crystallinity is not linearly related to the milling time.	72
Sol-gel						
$Ca(NO_3)_2 \cdot 4H_2O$ $(NH_4)_2HPO_4$	1.00-2.55	>9	(1)SG: 80˚C, 15 h (2)D: 37-80˚C, overnight (3) C: 300-700 ˚C	H_2O EtOH	• Mixture of HA/ammonium nitrate before calcination, • HA, calcium pyrophosphate or mixture of calcium pyrophosphate/calcium carbonate/HA after calcination • 20-40 nm long, < 40 nm wide • Formation of HA relies on the molar ratio of Ca/P	73
$Ca(NO_3)_2 \cdot 4H_2O$, $(CH_3O)_3P$	1.40-1.67	NA	(1)SG: RT, 16 h then 60 ˚C, 6 days (2)C: 600-800 ˚C, 3 h	H_2O EtOH	• HA, β-TCP or mixture HA/β-TCP • 90-150 nm particles	74

Hydrothermal						
$Ca(NO_3)_2$ $(NH_4)_2HPO_4$	1.50-1.67	10-12	(1)H: 140 ˚C, 2h (2)C: 650-1000 ˚C	H_2O	• Mixture phase of HA/β-TCP • Poor crystallinity of Ha phase after hydrothermal reaction and further heat treatment is needed. A mixture of HA/β-TCP when calcine at higher temperature (≥1100 ˚C) • Morphology: needle-like	75
Monocalcium phosphate monohydrate, $Ca(OH)_2$	0.50-1.67	2.2-5.6	(1)H: 160-200 ˚C, 4h (2)D: 40˚C	H_2O	• HA (Ca/P ratio =1.67) and DCPA (Ca/P ratio ≤ 1.5) • Morphology: whisker, platelet or needle • The formation of CaP relies on the Ca/P molar ratio and pH.	76
$CaCO_3$, DCPA	1.67	NA	(1)H: 120-180 ˚C,24 h (2)D: 80˚C	H_2O	• HA with DCPA or β-TCP as by product • Rods 2 μm x 200 nm width	77
$Ca(NO_3)_2 \cdot 4H_2O$ $(NH_4)_2HPO_4$	1.67	>10	200-400 ˚C 5 mL/min	H_2O	• CDHA (200 ˚C) or HA (300-400˚C) • 15-140 x 40-65 nm nanorods • Specific surface area: 39-100 m^2/g	78
$CaCl_2$, $K_2HPO_4 \cdot 3H_2O$,	1.67	12	(1)H: 60-150 ˚C, 12-24 h (2)D: 70˚C, 24 h	H_2O	• Using CTAB to control the morphology • HA • 15 x 75-150 nm Rod-like particles • Improved morphology and controllable size by low-temperature hydrothermal method • Poor crystallinity at low temperature (<120 ˚C) even after 20h.	79
Microwave						
$Ca(OH)_2$ H_3PO_4	1.17-1.77	NA	M:250-550 W(85-300 ˚C), 5-10 mins	H_2O	• Mixture of DCPA/$Ca(OH)_2$ or DCPA/HA • HA when >550W with Ca/P ratio of 1.67, 99.9995% purity • Needle (4-15 nm x 20-50 nm) and spherical shape (10-40 nm)	80
$Ca(NO_3)_2 \cdot 4H_2O$ H_3PO_4	1.00	NA	(1)M:60-200 ˚C, 20 mins (2) D:60 ˚C, overnight	H_2O	• Nanorods and nanoplates of DCPA • Specific surface area: 9-41 m^2/g	81
$Ca(NO_3)_2 \cdot 4H_2O$ H_3PO_4	1.4-1.67	NA	(1)M:200 ˚C, 60 mins (2) D:60 ˚C, overnight	H_2O EtOH	• Mixture of DCPA/HA • Nanowires and nanoneedle	82

SBF: synthetic body fluid; C: calcination; H: hydrothermal; MC: mechanochemical; M: microwave irradiation; P:precipitation; RT: room temperature; SG: sol-gel; D: drying; NA: not available

However, it is still a challenge to produce different phases of CaP with higher purity under mild conditions because CaP has many derivatives and the formation of the CaP phase strongly depends on the reaction conditions.

2.3 Biopolymer

Other than calcium phosphates, polymer is one the largest classes of biomaterials used in medicine for dentistry, hard and soft tissue replacement and drug carriers, owing to their physical and chemical properties, structural mobility and ease of processing shape. Natural or synthetic polymer is valuable and widely investigated, especially those degradable polymers.

2.3.1 Degradable polymer

A polymer is a large molecule which consists of many repeating units or monomers. Each polymer has its own properties in term of chemical composition, molecular weight, crystallinity, water absorption, solubility, hydrophobicity/hydrophilicity and thermal transitions. These properties can be fine-tuned by altering the type and chain length of polymer, and copolymerisation (mixing more than two polymers).[56]

Degradable polymers are widely studied because no additional steps are required to remove them from the system after accomplishing the function. However, the degradation of the polymer can be desirable or undesirable, depending on the bio-application. When using the polymer as a drug carrier, the degradable polymer is favourable since the drug is released with the degraded polymer and the process may take days or months. On the other hand, if the polymer is needed in the system for a prolonged period, the degradation in a short period is not preferable since it has to remain in the system and functions properly. The degradation rate relies on the mass loss of polymer and this is relatively important for biocompatibility issues. During the degradation process, the molecular weight of the polymer decreases and physical properties diminishes.

Polyester and polyanhydrides polymers are generally classified as degradable polymers. The degradable polyesters such as poly(glycerol sebacate), poly(ε-caprolactone), polyglycolide and polylactide are studied for soft tissues like heart, blood vessels, heart valve, nerve, bladder and gastrointestinal tract.[84] For instance, poly(ε-caprolactone) is a semicrystalline polymer with a very low transition temperature (T_g= - 60 ˚C) and low melting point (T_m= 59-64 ˚C). This polymer undergoes hydrolytic degradation due to the presence of hydrolytically labile aliphatic ester linkage. However, the degradation process is relatively slow (2-3 years) owing to its hydrophobicity.[85] On the other hand, polyanhydrides are among the reactive and unstable polymers used as biomaterials. Aliphatic polyanhydrides degrade within days, whereas aromatic polyanhydrides degrade over several years.[86] They are interesting biodegradable materials because they have two hydrolysable sites in the repeating units and the degradation rate of the polyanhydrides can be adjusted by changing the hydrophobic and hydrophilic component, where higher hydrophobic components result in slower degradation. Apart from that, polyurethanes are biostable polymers studied for long term medical implants such as cardiac pacemaker and vascular graft owing to their excellent biocompatibility and mechanical properties.[85] Interestingly, this polymer can be modified into degradable polymer by reacting them with polyester and this can improve the biocompatibility.

Degradation is a process cleaving the unstable linkage of the polymer into smaller fragments; for instance, polyester releases water when the ester linkage between acid and alcohol is cleaved. Degradable polymers can be classified into two modes which depends on the degradation medium: (i) hydrolytic in which water molecules cleave the polymer or (ii) enzymatic where enzymes breakdown the polymer. Hydrolytically degradable polymers include esters, urethanes and carbonates where these polymers have labile chemical bonds in their backbone. Enzymatic degradation occurs in the presence of various enzymes, for instance polysaccharides cleave into smaller molecules by degrading in the presence of fungi and bacteria.[87] Hydrolytic degradation of a polymer is categorised into two groups: (i) surface or heterogeneous erosion and (ii) mass or homogeneous

erosion.[53] The erosion process is mainly affected by the water absorption rate. When the water absorption rate is faster than the degradation rate, and the erosion process occurs at the whole polymer matrix. On the other hand, when the water absorption is different in polymer, the surface degrades faster than the water absorption rate into the interior polymer, the erosion occurs on the surface. Other than water absorption rate, the degradation process is also affected by a few parameters, such as structure, molar mass and its distribution, and crystallinity.[53] Crystallinity determines the space distribution of polymers chains, influencing the water absorption rate and the onset of the hydrolysis process. A good crystallinity of polymer inhibits the interaction of water into the bulk polymer, thus, decreasing the degradation rate. On the other hand, an amorphous polymer is less densely packed and is easier for degradation than crystalline regions.

In short, degradable polymeric biomaterials are preferred candidates for developing therapeutic devices such as temporary prostheses, three-dimensional porous structure as a scaffold for tissue engineering, and controlled release drug delivery carriers.[85] However, a fast degradation rate may cause the cytotoxicity issue by the acidic degraded product while low solubility may limit the applications. Therefore, a compromise between the desirable properties of the materials needs to be taken into account while considering their properties. In addition, the advances in the processing techniques to prepare these polymers and their composites are highly important for their future application, which also remains challenging.

2.3.2 Thermoplastic and thermoset elastomer

Elastomer is another interesting polymer which has the elastic deformation ability with a glass transition temperature (T_g) below room temperature: able to stretch and return to its original shape.[88] Furthermore, a biomedical elastomer must have good biocompatibility with the host tissue and its T_g needs to be lower than 37 ˚C (body temperature) in order to maintain its deformation characteristics at body temperature.[88]

Table 2-6 List of biodegradable elastomers and their applications in tissue engineering.[7,88]

Elastomers	Properties	Applications
Thermoplastic		
Polyurethanes (PU)	• Enormous diversity of chemical compositions and physical-mechanical properties • Tissue-specific biocompatibility • Tuneable biodegradability	Wound dressing and scaffolds for tissue engineering
Polyhydroxyalkanoates (PHA)	• Excellent biocompatibility • A wide range of mechanical properties and biodegradability • Expensive	Scaffolds or template for tissue engineering including bone and skin
Thermoset		
Poly(polyol sebacate) (PPS)	• Soft elasticity • Moderate biocompatibility • Tuneable degradability	Scaffold or template for soft tissues engineering, including nerve, vessel and heart muscle
Polyolefin and polydiene	• Excellent biostability • Functionality • Biocompatibility	Finger joint prostheses
Poly(glycerol sebacate) (PGS)	• Minimal inflammation compared with PLA- and PGS-based polymer • Osteoconductive material • Insoluble in water • Biocompatibility	Cartilage, cardiac muscles, nerves tympanic membranes and blood vessels

These elastomers can be classified into two categories: (i) thermoplastic elastomer, physically crosslinked, and (ii) thermoset elastomer, chemically crosslinked. The thermoplastic elastomer is remouldable. It becomes softened and more fluidic when applying heat because the curing process is reversible as no chemical bonding takes place. The thermoset polymer forms an irreversible chemical bond during the curing process. Interestingly, a crosslinked thermoset elastomer is capable of maintaining a three-dimensional geometry structure of a scaffold that could not be achieved by a thermoplastic elastomer.[88] For thermoplastic polymer, it has good processability, but its loss of mechanical strength during the degradation process is unpredictable; inversely, the

degradation rate of thermoset polymer is predictable with a linear loss of mechanical strength with time, while it has poor processability.[88] Table 2-6 shows a list of thermoplastic and thermoset elastomers with their applications. The listed elastomers, except polyolefin and polydiene, are generally biodegradable and their degradation rate can be further tuned by changing the experimental conditions.

Among these polymers, poly(glycerol sebacate) (PGS) appears as one of the interesting biopolymers since its monomers are nontoxic, and its mechanical properties and degradation rate can be easily tuned, which will be described in the following section.

2.3.3 Poly(glycerol sebacate)

Poly(glycerol sebacate) (PGS) is known as a promising polyester because of its elastomeric characteristic and excellent biocompatibility. It is designed to mimic the mechanical behaviour of a collagen in the extracellular matrix with a hydroxyl group at the backbone of PGS.[89] Additionally, PGS can be hydrophilic or hydrophobic depending on the availability of the hydroxyl group on the PGS backbone. Its degradation rate is predictable; it degrades steadily with gradual loss of mechanical strength. The mechanical properties of PGS can be modified by altering the degree of crosslink density.[89] Owing to the speciality of this polymer, a family of synthetic biodegradable polymers, composed of different polyol monomers with sebacic acid, have been developed to provide a wider range of Young's modulus (0.37 -378 MPa) that may suit into wider application.[90]

The Young's modulus of PGS is ranged from 0.02 to 1.5 MPa with 120-270 % of elongation. A comparison of physical properties between PGS and other biopolymers is given in Table 2-7. PGS is not a tough polymer when compared with other polymers, but the mechanical properties of PGS can be fine-tuned by changing the reactant molar ratio, curing temperature and time which influence

the crosslink density of PGS. For instance, an increment in glycerol molar ratio decreases the Young's modulus, owing to the excessive hydroxyl group in the polymer.[91]

Table 2-7 Comparisons of physical properties of PGS with other biopolymers. [88,92]

Polymers	Young's modulus (MPa)	Tensile strength (MPa)	Elongations (%)
Polyester urethane urea	**7-70**	**4-60**	**100-950**
Poly(caprolactone-co-lactide)	**30**	**32**	**120**
Poly(glycerol sebacate) (PGS)	**0.02-1.5**	**0.2-0.7**	**120-270**
Poly(polyol sebacate)	**0.4-380**	**0.57-17.64**	**10-200**
Poly(glycerol sebacate acrylate)	**0.05-1.4**	**0.05-0.5**	**40-190**
Poly(diol citrate)	**1.6-13.98**	**2.93-11.15**	**117-502**

PGS is reported to have a good biocompatibility *in vivo* and *in vitro*. For *in vitro* study, fibroblast cells displayed normal morphologies and showed a better growth rate than poly(lactic-co-glycolic acid) [PLGA]; PGS exhibited inflammatory in a rate similar to PLGA implants for *in vivo* test.[92] However, the crosslink density affects the degrees of cytotoxicity. Highly crosslinked PGS degrades slowly and the concentration of the potential toxic degradation products in the medium is low which can avoid any cellular death.[88] The main advantage of PGS over other elastomers is its predictable degradation rate as it degrades through surface erosion: mechanical strength and mass decrease linearly with time.[88] For instance, PGS retains its original shape after 35-day study although more than 70% of its mass degrades during *in vivo* degradation.[93] This indicates that the mechanical properties of PGS loses gradually as opposed to other polymer [i.e. poly(lactide-co-glycolide)].[92] Therefore, PGS is suitable for a wide range of biomedical applications owing to its controllable mechanical properties, such as restoration of cartilage, cardiac muscles, nerves tympanic membranes and blood vessels.[8] It has also shown promising results in creating surgical sealants by hybrid with

lactic acid and this composite improves the cell proliferation and biocompatibility.[94]

In short, the desired properties of PGS is highly dependent on its application. For instance, the degradation rate of PGS varies for different bioapplication; slower degradation may be needed for an implant (e.g. temporomandibular joint disc) because the degradation rate of the implant needs to be slower than the regeneration and restoration rate of the surrounding tissue.[95]

2.3.4 Synthesis of poly(glycerol sebacate) [PGS] via different approaches

Synthesis of PGS was pioneered by Langer's group in 2002 and it has been widely studied.[88,7] Glycerol, a tri-functional molecule, provides the hydroxyl groups to form ester linkages between glycerol and sebacic acid (Figure 2-2). PGS is generally produced by a two-step process (polymerisation and curing); (i) heating a mixture of glycerol and sebacic acid in a reaction chamber with an inert gas (nitrogen or argon) to avoid the oxidation of reactants and minimize the glycerol's evaporation, and (ii) curing in the vacuum oven. The polymerisation conditions vary from 110 to 150 ˚C and 1 to 24 h. On the other hand, the level of crosslink depends on the reaction kinetics of primary and secondary hydroxyl (-OH) groups of glycerol. Primary hydroxyl groups react faster to form the PGS primary chains at 100-150 ˚C, while the secondary hydroxyl groups crosslink the chains into a larger molecule (Figure 2-3).[88] More importantly, PGS can be processed into desired form of tissue engineering substitutes, either in a scaffold, thin film or even fibres by dissolving its pre-polymer in organic solvents (e.g. ethanol and terahydrofuran) and curing in the vacuum oven.

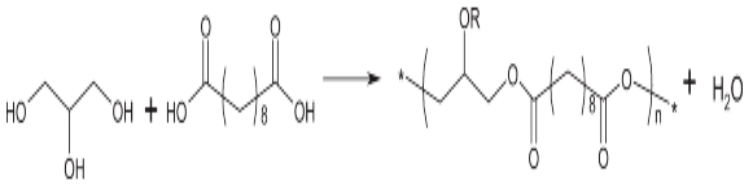

Figure 2-2 Reaction scheme for PGS where R could be the polymer chain or hydrogen.[88]

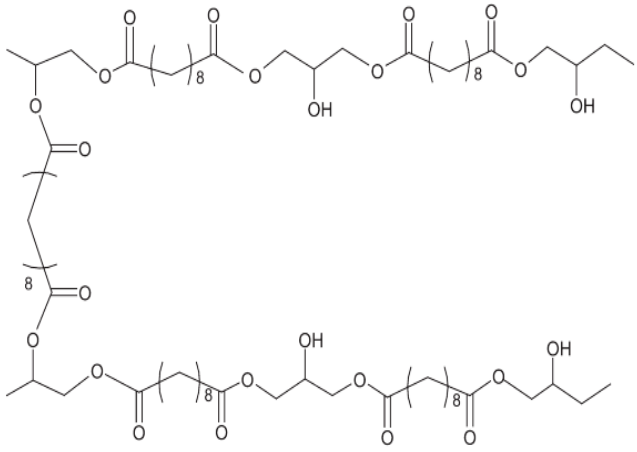

Figure 2-3 Example of crosslink scheme between two PGS polymer chains.[88]

PGS has been fabricated over a range of temperatures and durations by microwave and conventional heating methods. As illustrated in Table 2-8, the polymerisation kinetics of PGS are inconsistent. The crosslinking kinetics of PGS are strongly affected by the temperature and molar ratio of reactants. The loss of volatile glycerol depends on the flowrate of the inert gas, thus, different polymer properties are found under a 'similar' preparation method. Other than these two methods, the synthesis pathway of PGS has also been modified to prepare various structures of PGS, such as electrospinning,[96] 3D-printing[97] and salt leaching method.[98] These methods generally improve the mechanical properties and degradation rate to fit into a specific application.

Table 2-8 Comparison of the poly(glycerol sebacate) prepared by various approaches.

Experimental Conditions	Remarks/Application	Ref
Conventional heating (CH)		
P:120˚C, 24 h C:120˚C,48h	• First paper reported on this material. • No T_g detected above -80 ˚C, T_m: 5.23 ˚C and 37.62 ˚C, T_c: -52.14 ˚C and -18.50 ˚C • Young's modulus: 0.282 MPa, Tensile strength: >0.5 MPa, Elongation: ~267% • Fully absorbed within 60 days with restoration if the implantation sites (in a vivo test).	7
P:130-150˚C,8-24h C:130˚C, 24-168 h	• Degree of esterification was calculated by weight loss of water and by acid group titration. • Molecular structure was observed by NMR spectra. • Young's Modulus: 0.1-2.5 MPa, Elongation: ~25-480% • Biocompatibility was increased with the long cured periods.	99
P:120-140˚C, 24h C:120-150˚C for 6-66 h	• Young's modulus: 0.1-1.8 MPa, Tensile strength: 0.2-0.7 MPa, Elongation: ~75-500% • Physical appearance of pre-PGS and PGS was reported and it relies on the degree of esterification. • Degree of esterification was tailored. • 10-30 % mass loss after 28 days.	100
Microwave Irradiation (MI)		
Multimode MI (650W) P:3 mins MI C:150˚C, 4-24 h	• Young's modulus: 0.5 MPa, Tensile strength: 0.27 MPa, Elongation: ~180% • T_g: -35.61 ˚C, T_m: -15.82 ˚C and 61.70 ˚C • Long curing time (16 h) and high curing temperature (150 ˚C) was needed to get crosslinked PGS. • The reaction temperature was not controlled and may trigger the evaporation of monomer.	8
Multimode MI (600W) P:15-30 mins MI C:130 ˚C, 6-66 h	• Young's modulus: 0.13-1.33 MPa, Tensile strength: ~0.2 – 0.4 MPa, Elongation: ~75-230 % • Degree of esterification was tailored. • No proper temperature control during microwaving and may trigger the evaporation of monomer. • Degradation rate was not measured.	100

where P is pre-polymerisation step and C is curing step.

As introduced previously, synthesis conditions affect the properties of PGS, including its flexibility and degradation rate. Till now, the reproducibility of PGS remains challenging and this strongly affects the properties of the PGS. For instance, PGS with lower crosslinking is produced when the glycerol evaporates during the polycondensation, and this affects the biocompatibility of the PGS. This is because the dissolution of non-reacted carboxylic groups or excessive amount of carboxylic groups during the hydrolysis of ester group in PGS reduces the pH in the body medium to a level below physiological values (7.2-7.4) and unfavourable for cell viability.[101] In addition, if using the PGS with lower crosslinking as a bone implant, this rapid degradation rate is over the healing rate of bone, hence, the chemical approaches or improved synthesis approach are needed to decrease the enzymatic hydrolysis rate of the ester bond of PGS.[88] Although the degree of esterification of PGS was monitored by quantifying the glycerol loss,[100] but this is not a real time measurement and the reaction temperature in the microwave is not monitored. It can be concluded that the synthesis of the PGS needs to be further improved, especially on controlling its mechanical properties and degradation rate.

2.3.5 Poly(glycerol sebacate)-based composite

The main concerns of present biomaterials in tissue engineering are high cost, inflammation and immune responses, and difficulty in meeting mechanical requirements.[102] In order to minimise these issues, the composites are then introduced. Composites are defined as engineered materials made from two or more materials with significantly different physical or chemical properties, and remain separate and distinct at a macroscopic level within the finished structure.[57] Table 2-9 summarises the general properties of organic (i.e. polymer) and inorganic (i.e. ceramic) materials. The properties of these two materials are always in contrast with each other. For instance, inorganic material is brittle while organic material is flexible.

Table 2-9 Summary of properties from the bioorganic and inorganic materials, to be combined in various composites and hybrid materials.[57]

Inorganic	Organic
Hardness, brittleness	Elasticity, plasticity
High density	Low density
Thermal stability	Permeability
Hydrophilicity	Hydrophobicity
High refractive index	Selective complexation
Strength	Bioactivity

Fabrication of a composite is always complex and the reproducibility is also crucial. As mentioned before, the major issue of PGS is its degraded acid products which cause cytotoxicity. Therefore, inorganic particles have been added to the polymer matrix to solve this critical issue. Table 2-10 summarises some recent PGS-based composites. The incorporation of the inorganic particles improves the mechanical strength and biocompatibility. However, the presence of these particles may increase the stiffness of PGS which may not be favourable for its application.

Table 2-10 Examples of the PGS-based composites used in bio-application.

Composite	**Results/Remarks**	**Ref**
Silica-based bioactive glass	• Improved mechanical strength (Tensile strength 1-5 MPa), hydrophilicity and proliferation on osteoblast (MC3T3).	[103]
Nanosilicates	• Enhanced the mechanical stiffness without affecting the elastomeric, higher stability, enhanced cell adhesion and supported cell proliferation.	[104]
Cellulose nanocrystals	• Improved tensile strength and hydrophilicity.	[105]
Nanocarbon tube	• Increased in mechanical stiffness and enhanced the differentiation potential of human mesenchymal stem cells (hMSCs).	[106]
Bioglass particles 45wt%SiO_2,24.5 wt% CaO, 24.5 wt% Na_2O and 6 wt% P_2O_5	• Enhanced the mechanical properties, mechanical stability and improved biocompatibity.	[101]
Hydroxyapatite (HA)	• Enhanced the mechanical properties.	[107]

2.4 Microwave Synthesis of Biomaterials

After reviewing the biomaterials, fundamentals of microwave are introduced since this project focuses on preparing the biomaterials using this advanced approach. The use of microwave in chemical synthesis is still an emerging field, but it has gained more interests within these few years and could be an alternative to conventional energy sources.

2.4.1 Microwave chemistry: basic concepts

During World War II, Percy LeBaron Spencer of the Raytheon Company accidentally discovered that microwave energy could melt a candy bar when he was using the radar waves. More importantly, he also found a microwave heats food even faster than a conventional oven. This inspired him to develop the first commercial microwave oven in 1954, and it has been widely used in industrial applications since the early 1950s. Additionally, the first two papers regarding microwave-enhanced organic synthesis were published in 1986, demonstrating the benefits of using microwave energy in material synthesis.[108]

Microwave synthesis overcomes the limitation of conventional heating because microwave transfers energy directly to the reactive species by a molecular heating, instead of external heating. The advantages of microwave heating compared to conventional heating are: higher heating rates, improved yield and purity of products, and reduced by-products.[81,109,110] Many published microwave synthesis protocols were based on the multimode microwave with sealed or closed vessel processing.[110]

It is important to understand the theory of microwave before substituting any synthesis route with this method. Figure 2-4 depicts the microwave range located at the lower frequency in the electromagnetic spectrum (i.e. 300 to 300,000 megahertz (MHz) with 1 mm to 1 m of wavelengths). By supplying electromagnetic energy within this region, molecular rotation is enhanced without affecting the molecular structure.[111]

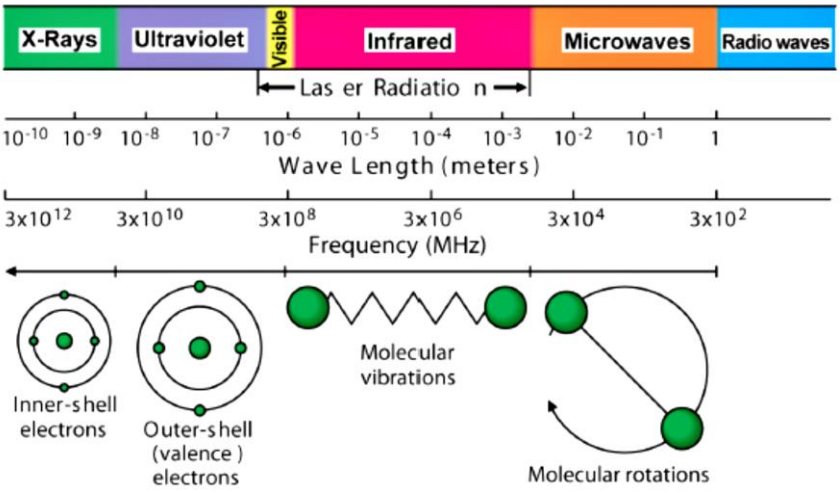

Figure 2-4 The electromagnetic spectrum.[111]

Traditionally, conventional heating provides heat externally, passing through the vessel's wall and reaching the solvent and reactants (Figure 2-5), which depends on the thermal conductivity of the various materials. Hence, it results in a variation of temperature between the wall of the vessel and the reactant-solvent, and this requires sufficient time to achieve thermal equilibrium. Conversely, microwave interacts with the molecules rapidly such that it generates heat in a short time, either dipole rotation or ionic conduction.

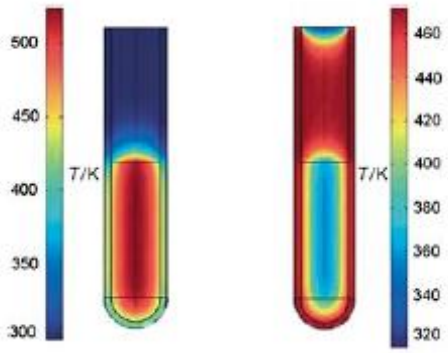

Figure 2-5 Schematic of temperature gradient in microwave (left-hand column) versus conventional heating (right-hand column).[112]

Many microwave systems use 2.45 GHz of frequency and the field oscillates 4.9 x 10^9 times per second, which is preferable for most of the dielectric heating process.[109] For dipole rotation, the polar molecules try to align themselves with

the rapidly oscillating electric field of the microwave which produces dielectric loss and molecular friction. This molecular movement creates heat as the rotating molecules hit other molecules. Ionic conduction happens when there are free ions or ionic species present in the heating substance, such as organic salts or mixtures consisting of at least one organic component (such as halide salts). The charged ions induce oscillatory movement after receiving the microwave, and this movement and interaction with the molecules generate heat. The heat is typically due to the frictional losses depending on the size, charge, and conductivity of the ions, and their interactions with the solvent.

As depicted in Figure 2-6, there are single mode and multimode microwaves. Multimode microwave is generally used in the kitchen while single mode microwave can be found in laboratories. Multimode microwave creates constructive and destructive interference patterns and results in a 'hot spot' in the cavity. The single mode system provides stronger power intensity while multimode microwave has relatively homogeneous heating due to multi-reflection.[113]

The heating efficiency of microwave may reduce with increasing microwave power as well as decreasing volume due to extra energy which could not be absorbed by the samples.[114] On the other hand, the heating efficiency is influenced by the microwave field alignment.[114] For instance, the aligned waves in single mode microwave might not be focused on the reaction vessel, therefore, a potential loss of energy occurs, while all waves can interact with the reaction vessel in a multimode microwave. Therefore, multimode microwave provides a relatively more homogeneous heating than single mode microwave. It is also reported that single mode microwave is preferable for a small-scale (< 50mL) of reaction while multimode microwave is suitable for large-scale reaction.[115]

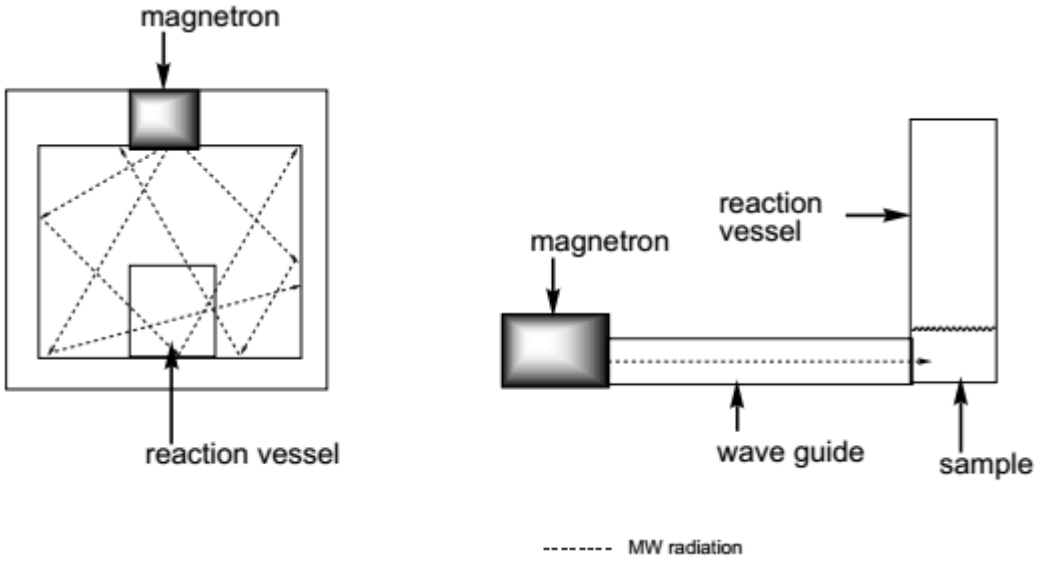

Figure 2-6 Schematic representation of a multimode (left-hand side) and single mode (right-hand side) microwave.[116]

2.4.2 Solvent role in microwave synthesis

Solvents play a vital role in the microwave synthesis method. It is crucial to select a suitable solvent for a reaction because each solvent has its own ability to couple with the microwave energy.

These three main parameters (tangent delta, dielectric constant and dielectric loss) measure the ability of a solvent to absorb microwave. The dielectric constant of a solvent is the ability to polarise the molecules in the electric field.[109] The solvent with larger dielectric constant has a greater ability to re-orientate in an applied electric field and therefore absorbs the microwave efficiently. If the applied frequency is too high, polar molecules do not have sufficient time to realign and no heat will be produced since there are no interactions. On the other hand, the ability of a substance or a solvent to convert electromagnetic energy into heat is determined by the loss tangent. The efficacy of heat production through this mechanism depends on loss tangent which varies with solvent species.[117] The loss tangent is expressed as:

$$\tan\delta = \varepsilon''/\varepsilon' \qquad \text{Equation 2-1}$$

ε'': dielectric loss factor/efficiency of energy is absorbed from the electric field and converted into heat

ε': dielectric constant (ability to polarise the molecules by the electric field)

The solvent is categorized into three groups: high, medium and low absorbing solvents, depending on the tangent loss. A high value of tan δ (> 0.5) refers to strong absorbance such as ethylene glycol and ethanol while hexane is a weak microwave absorbance (tan δ < 0.1).[118] However, polar additives (i.e. ionic liquids) are suggested to be added into a low microwave absorbing solvent to increase the absorbance level of the medium.[110] Table 2-11 summarises the loss tangent for several solvents. Several solvents may decompose to hazardous components from prolonged exposure to high temperature. Hence, the stability of a solvent at high temperature should be a concern for safety purposes.

Table 2-11 Loss tangent for different solvents, at 20 ˚C and 2.45 GHz.[109,110]

Solvent	tan δ	Solvent	tan δ
Ethylene glycol	**1.35**	**1,2-dichloroethane**	**0.127**
Ethanol	**0.941**	**Water**	**0.123**
2-propanol	**0.799**	**Chlorobenzene**	**0.101**
Formic acid	**0.722**	**Chloroform**	**0.091**
Methanol	**0.659**	**Acetonitrile**	**0.062**
Nitrobenzene	**0.589**	**Ethyl acetate**	**0.059**
1-butanol	**0.571**	**Acetone**	**0.054**
2-butanol	**0.447**	**Dichloromethane**	**0.042**
1,2-dichlorobenzene	**0.28**	**Toluene**	**0.04**
Acetic acid	**0.174**	**Hexane**	**0.02**

2.4.3 Specific microwave effects on material synthesis

There are some arguments about microwave heating giving a boost to the reaction rate of the organic chemical reaction due to purely kinetic or thermal effects.[112] It is reported that the rapid heating rates and higher bulk reaction temperature under microwave irradiation could be achieved using conventional convective heating under isothermal conditions.[119] However, it has been proven that there were

errors in these reports, especially in measuring the temperature in the microwave cavity.[119,120] Furthermore, the temperature profile in microwave (superheated) is difficult to be reproduced with conventional equipment and it limits the direct comparison under these circumstances. The temperature profiles have a dramatic effect on reaction kinetics, potentially speeding up the reaction rate.

In 2014, researchers at Florida State University published two papers on supporting the microwave-specific heating effect: Chen *et al.* reported that a 4-fold rate enhancement as compared with the convective thermal heating in homogeneous organic reaction, and Rosana *et al.* proved the observed thermal reactivity in microwave exceeded the theoretical prediction which was calculated from the temperature-based Arrhenius equation.[119,120] Based on the Arrhenius reaction rate ($k= Ae^{-Ea/RT}$), the reaction rate constant relies on two factors: (i)the frequency of collisions between molecules, and (ii) the minimum energy to overcome the activation energy barrier.[111] Without any catalyst, the activation energy is a constant for a reaction. They measured the temperature and observed the conversion of reactants to the products. By integrating these data into Arrhenius and rate equations, the expected conversion at the specific temperature was estimated. Surprisingly, conventional heating experiments matched Arrhenius predictions, but microwave method exceeded the prediction. This was because the microwave specific thermal effects perturbed thermal equilibrium between the solvent and the solute where the average kinetic molecular energy of the microwave-absorbed solute was higher.[120]

On the other hand, microwave heating eliminates the wall effects due to volumetric heating.[121] Under conventional conductive heating, the crystals nucleate on the wall of the reaction vessel and grow slowly due to randomly dispersed ions and inhomogeneity heating. Oppositely, microwave heating provides the volumetric heat internally and reduces the ‘wall effect’.

In summary, microwave heating produces heat internally and enhances the reaction rate which is favourable for material synthesis. This synthesis method

therefore potentially gives a high yield, reduces reaction time, easily controls morphology and improves crystallinity.

3. Material Characterisation

This chapter describes the general characterisation methods for the biomaterials, including calcium phosphates and poly(glycerol sebacate) and their composites. A variety of characterisation methods are employed to study the organic or inorganic materials qualitatively and quantitatively. The fundamentals of these characterisation methods are described in the following section.

3.1 Powder X-ray Diffraction (PXRD)

Powder X-ray diffraction (PXRD) is a useful characterisation method to analyse the materials. This non-destructive method is generally used to identify an unknown crystalline phase and orientation, structural properties (lattice parameters) and composition of a sample by comparing with a standard XRD diffraction pattern. An amorphous sample always shows a weak response with a broad peak over a range of degree. On the other hand, a crystalline sample has sharp peaks, but these peaks could be broadened and this depends on the particle size. For instance, larger crystal size shows a narrow peak and vice versa.

Diffraction is a phenomenon when the atoms of a crystal scatter the X-ray and cause the interference pattern of the waves owing to the unique crystal structures. The obtained diffraction data are transformed into the crystal structure by matching with the JCPDS database. The crystals diffract the incident X-ray beam and the lattice parameters of the crystals are explained by Bragg's law (Equation 3-1):

$$\boldsymbol{n\lambda = 2dsin\theta} \qquad \text{Equation 3-1}$$

Where n is an integer, λ is the wavelength of electromagnetic radiation, d is the spacing between atomic planes and θ is the angle between atomic planes and incident X-ray angles.

Other than identifying the phase of sample, PXRD is also used to estimate the crystallite size using Scherrer's equation (Equation 3-2):

$$\tau = \frac{K\lambda}{\beta cos\theta} \qquad \text{Equation 3-2}$$

Where K is the shape factor, λ is the x-ray wavelength, β is the line broadening at half maximum intensity, θ is the Bragg angle and τ is the mean size of the crystallite which is approximately grain size. Scherrer's equation is only applicable for 0.1 μm of grain size and nano-sized particles. Thus, TEM and SEM are generally used for particle size observation rather than using this equation.

3.2 Attenuated Total Reflectance-Fourier Transform Infrared (ATR-FTIR) Spectroscopy

ATR-FTIR spectroscopy is a technique to probe the vibrational modes of the chemical bonds in a material, enabling the detection of the fingerprinting for organic and inorganic compounds. More specifically, an IR active sample must have a change in dipole moment during the vibration. A dipole moment, also known as polarity of a molecule, occurs between ionic bonds or covalent bonds due to the difference in electronegativity. The dipole moment is created when a molecule shares electrons unequally. For instance, this occurs when one atom is more electronegative than another, resulting in one atom pulling more tightly on the shared pair of electrons.

In IR spectroscopy, a sample is illuminated with a polychromatic light source. Absorption occurs when the frequency of the incident light is similar to the vibrational frequency of the chemical bonds, but this light source is not energetic to excite the electrons. This vibrational energy is unique to each chemical bond in the material and depends on the chemical environment. ATR-FTIR is similar to the standard FTIR method, but it is simple and the sample can be reused. ATR-

FTIR relies on Total Internal Reflectance (TIR), instead of transmission with a diluted or thin disc sample disc. As shown in Figure 3-1, a solid or liquid sample is placed on the ATR crystal. The incident infrared light beam passes through the crystal and reflects the sample. The infrared beam undergoes 'total internal reflection', propagating along the crystal and reflecting both crystal and sample consecutively. Total internal reflection occurs if the angle of incidence is greater than a limiting angle (i.e. critical angle). On the other hand, the infrared beam that penetrates the sample is known as evanescent wave, and it does not propagate along the crystal. The beam penetration depth of the sample is approximately 0.5-2 μm.

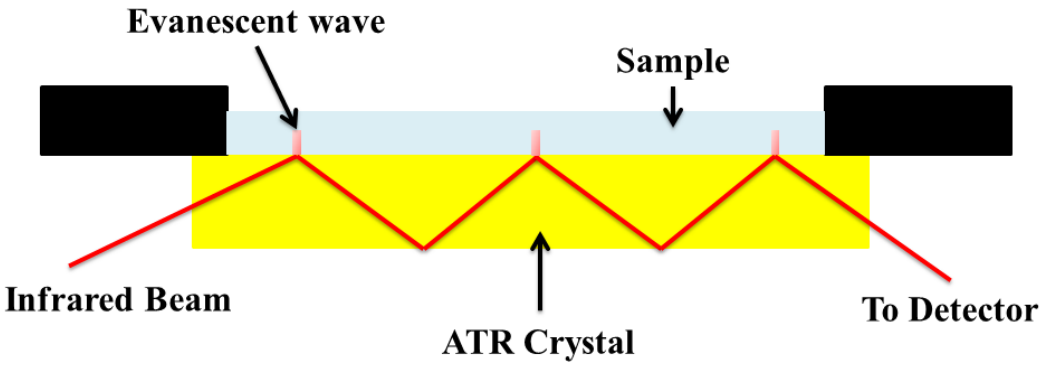

Figure 3-1 Schematic demonstration of an ATR crystal in an ATR-FTIR.

3.3 Raman Spectroscopy

Raman spectroscopy investigates the interaction between radiation and molecular vibration, identifying the chemical bonds available in the sample. In contrast to IR spectroscopy, Raman spectroscopy studies the scattering of light by vibrating the molecules, but not the absorption of light. By interacting the sample with light, it is IR active if there is a change in dipole moment and is Raman active if there is a change in polarisation.

The intensity of the scattered light relies on the amount of the polarization potential change; the polarizability measures the ability of electron cloud to deform in contrast to the atomic nuclei. When placing a molecule into an electric

field, the electrons pull towards the positive charge and the atomic nuclei move towards the negative charge. As a laser light hits an atom, it is excited after absorbing a photon and moves to a higher energy level. The scattering occurs when the atom recovers immediately from this excited state. The software in the spectroscopy compares the initial laser wavelength (λ_0) and the Raman scattered wavelength (λ), and then calculates the difference between these two wavelengths which is known as the Raman shift ($\Delta\lambda=\lambda_0-\lambda$). The vibrational bonds in the sample are identified since each molecule has its own vibrational energy level due to the unique wavelength shift of the emitted photons corresponding to the Raman shift. Thus, the Raman spectra are always plotted as a function of Raman Shift (cm^{-1}) versus the intensity.

As shown in Figure 3-2, there are elastic (Raleigh) and inelastic (Stokes and Anti-stokes) scattering. For elastic or Raleigh scattering, the energy of incident light is similar with the scattered light. When the system gains energy during this process, the scattered light loses energy and reaches a higher energy state than its beginning stage; it is known as Stokes scattering. Conversely, Anti-stoke scattering has a lower energy state than it has before.

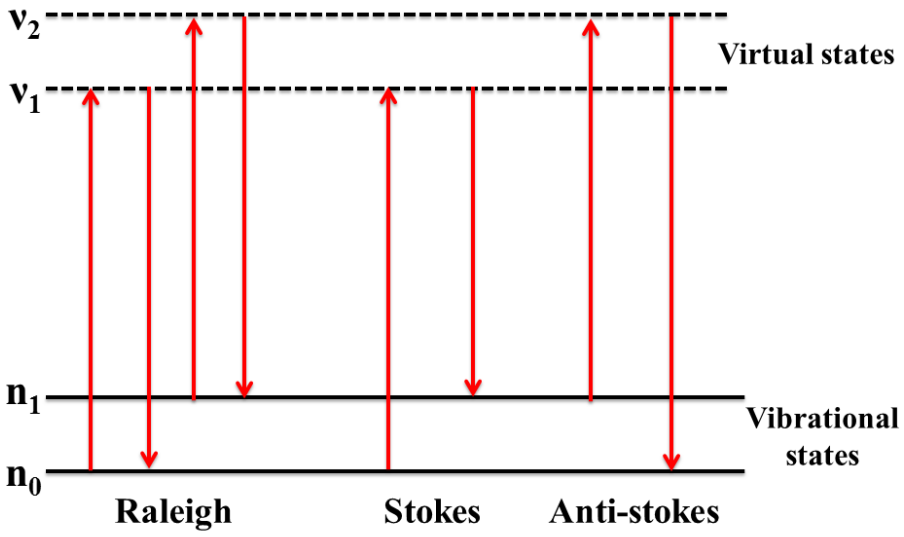

Figure 3-2 Raleigh and Stokes/Anti-stokes scattering processes in diagram.

3.4 Nitrogen Sorption

The specific surface area and porosity of materials are determined by using a nitrogen adsorption-desorption technique. The adsorption-desorption process is reversible since it is a weak Van der Waals interaction between adsorbate and solid sample.

Before running this test, the materials are degassed overnight to remove moisture and contaminants. During a typical analysis, several steps are conducted:

i) Evacuate the sample tubes,
ii) Fill the tubes with inert gas (i.e. helium) for determining the free space or dead volume at liquid nitrogen temperature (-195.5 ˚C),
iii) Remove the helium and evacuate,
iv) Adsorb the nitrogen gas on the sample until reaching the saturation pressure,
v) Desorb the nitrogen gas.

During the measurement, glass rods are placed within the sample cells to minimize the free space. The free space measurement is very critical since gas adsorbed by the sample is the difference between the doses into the sample cell and the remaining unadsorbed gas in the free space. On the other hand, liquid nitrogen is used to maintain the process at a constant low temperature because the interaction between gas molecules and the surface of the sample is stable at this temperature. This also allows the nitrogen gas to be condensed on the surface of the particles, especially for those mesopores samples.

The specific surface area is calculated by the Brunauer-Emmett-Teller (BET) equation, describing the physical adsorption of gas molecules on a solid surface. This theory applies to the multilayer adsorption by non-corrosive gas such as nitrogen. This gas does not chemically react with the material surfaces. Multi-point BET is employed at a low P/P_0 (0.025 -0.03) which covers the monolayer adsorption. The capillary condensation occurs at a higher P/P_0 (> 0.5), enabling the pore size measurement.

The BET equation (Equation 3-3) quantifies the amount of gas needed to form a monolayer on the surface of the sample:

$$\frac{1}{v_a[\left(\frac{P_0}{P}\right)-1]} = \frac{(c-1)}{v_m c}\left(\frac{P}{P_0}\right) + \frac{1}{v_m c} \qquad \text{Equation 3-3}$$

Where v_a is the volume of gas adsorbed at standard temperature and pressure (STP), P and P_o are the partial vapour pressure and saturation pressure of the physisorbed gas (generally nitrogen) at -195.5 ˚C, c is the BET constant, v_m is the quantity of adsorbed gas that form a monolayer. The relative pressure less than atmospheric pressure is achieved by creating conditions of partial vacuum. The duration needed to measure nitrogen sorption depends on its surface area; a lower surface area achieves equilibrium faster than a higher surface area.

And the BET constant is illustrated as below:

$$c = e^{\frac{(E_1 - E_L)}{RT}} \qquad \text{Equation 3-4}$$

Where E_1 is the first layer of heat adsorption and E_L is the corresponding heat adsorption for n layers >1.

Equation 3-3 is plotted as a linear line (y=Ax+I) where y is $\frac{1}{v_a[\left(\frac{P_0}{P}\right)-1]}$ and x is $\left(\frac{P}{P_0}\right)$. For a reasonable value for specific area, the R^2 value (correlation coefficient) should always be close to 1 (acceptable values are normally ≥ 0.995). Both gradient (A) and y-intercept (I) are obtained from the plot and used to calculate v_m and c:

$$v_m = \frac{1}{A+I} \qquad \text{Equation 3-5}$$

$$c = 1 + \frac{A}{I} \qquad \text{Equation 3-6}$$

The BET specific surface area is then given by:

$$S_{BET} = \alpha(\frac{v_m N_A S}{V}) \qquad \text{Equation 3-7}$$

Where α is the mass of adsorbant, N_A is Avogadro's number, s is the adsorption cross section of the powder and V is the molar volume of gas.

Other than specific surface area, pore size distribution is another important output from the nitrogen sorption analysis. Barrett-Joyner-Halenda (BJH) is a general approach used to analyse pore size distribution. The obtained adsorption-desorption profile, known as isotherm, analyses the nature of the porous material, however, this model is only applicable to mesopore (2-50 nm) and small macropore (>50 nm) size. By plotting the relationship between the amount of nitrogen adsorbed and the equilibrium pressure of nitrogen (expressed as P/P_0), a different type of isotherms is generated (Figure 3-3). Table 3-1 summarises the type of isotherms.

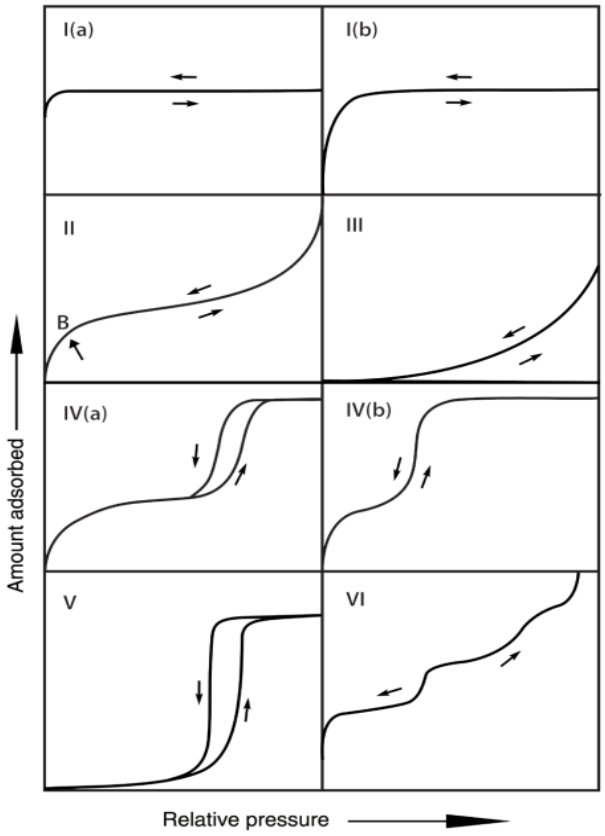

Figure 3-3 Classification of physisorption isotherms.[122]

Table 3-1 Type of isotherms correlated to their pore size. [122, 123]

Isotherm	Pore Size	Remarks
Type I	microporous (< 2nm)	• Type I(a): narrow micropores (width < ~1 nm) • Type I(b): wider micropores and narrow mesopores (< ~2.5 nm)
Type II	nonporous or macroporous	• Point B: beginning of the monolayer coverage
Type III	nonporous or microporous	• weak interaction between adsorbent and adsorbate
Type IV	Mesoporous	• capillary condensation • Type IV(a): pore size exceeds a critical pore value (i.e. wider than ~ 4 nm) • Type IV(b): conical and cylindrical mesopores with the tapered end
Type V	Porous	• weak interaction between adsorbent-adsorbate
Type VI	Nonporous	• uniform nonporous surface

Based on Figure 3-4 and Table 3-2, the hysteresis shape provides information on the pore structure. The pores in the materials are filled by nitrogen gas from the smallest to the largest pores, but are released the other way round. Four hysteresis loops, H1, H2(a), H3 and H4, are classified in the original IUPAC 1985.[123] The common feature of H3, H4 and H5 shows a steep desorption branch at a narrow range of P/Po (~0.4-0.5).

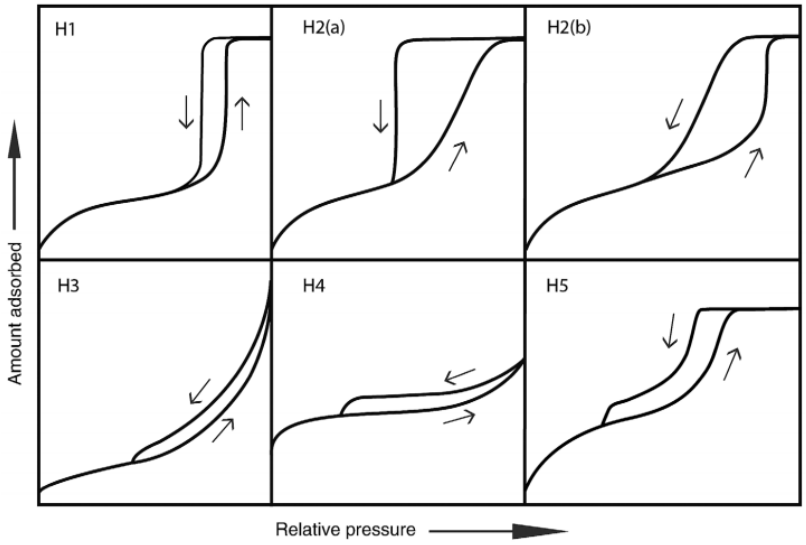

Figure 3-4 Classification of hysteresis loops. [122]

Table 3-2 Type of hysteresis loops. [122, 123]

Hysteresis	Pore structure
H1	• uniform mesopores • silica and ordered mesoporous carbon
H2	• complex pore structure • Type H2 (a): a narrow range of pore necks or by cavitation-induced evaporation, such as porous glasses and mesoporous materials • Type H2(b): wider size distribution of neck widths likes mesoporous ordered silica
H3	• non-rigid aggregates of plate-like particle or the pore network with macropores
H4	• found with aggregated crystals of zeolites
H5	• materials consisting of both open and partially blocked mesopores

3.5 Transmission and Scanning Electron Microscopy (TEM and SEM)

Transmission (TEM) and scanning electron microscopy (SEM) image the morphology of the surface and examine the particle size. In these two microscopes, electrons interact with the specimen and these electrons are scattered or transmitted. In SEM, a high energy electron beam focuses on the material surface and the emitted secondary and backscattered electrons are captured by the detector to build up the image. A layer of metal coating is needed for low conductive materials before imaging with SEM. TEM is used to observe the morphology in a higher resolution and more importantly to identify the diffraction rings from the sample. An image is formed when high energy electron beams are transmitted through the sample.

3.6 Ultraviolet-Visible (UV-VIS) Spectroscopy

UV-Vis spectroscopy is a classical and reliable technique for quantifying different analytes including transition metal ions, highly conjugated organic compounds and biological macromolecules. The presence of these compounds is detected by measuring the absorption of UV radiation of light. At a fixed path length, the concentration of these organic compounds is quantified using the Beer-Lambert law. This law (Equation 3-8) states that the absorption of a solution is directly proportional to the concentration of the absorbing species in a solution.

$$A = log_{10}(I_0/I) = \varepsilon \, x \, C \, x \, L \qquad \text{Equation 3-8}$$

Where A is the measured absorbance, I_0 is the intensity of the incident light at a given wavelength and I is the transmitted intensity, L the path length through the sample and C the concentration of the absorbing species. ε is a constant known as the molar absorptivity or extinction coefficient.

3.7 Proton Nuclear Magnetic Resonance (^{1}H NMR)

Nuclear Magnetic Resonance (NMR) spectroscopy is an important method to analyse organic compounds and it determines the molecular structure. Other than that, by integrating the peak in the H NMR spectra, the molecules with chemically equivalent proton to that peak are quantified. Deuterated solvent is used to stabilize the magnetic field strength.

NMR measures the property of the nucleus in an atom, which is known as nuclear spin, and each nucleus has different energy to bring them into beta-spin state. Based on Planck's Equation (Equation 3-9), the energy provided to a nucleus is related to the operating frequency:

$$\Delta E = h\nu \qquad \text{Equation 3-9}$$

Where h is Planck's constant (6.63×10^{-34} J·s) and ν is the NMR operating frequency.

The frequency is shown as below (Equation 3-10):

$$\nu = \frac{\gamma}{2\pi} B_0 \qquad \text{Equation 3-10}$$

γ is gyromagnetic ratio which depends on the nuclei type; B_o is the applied magnetic field strength. Based on these equations, operating frequency is proportional to the magnetic field. When increasing the NMR operating frequency, the magnetic strength is increased.

A nucleus can behave like a magnet when the number of protons or neutrons or both of an atom is odd, such as hydrogen. When placing a nucleus in a magnetic field (B), it aligns itself with the field (alfa-spin state or lower energy state). The nucleus in the lower energy state absorbs radiation energy and moves into a

higher energy state (beta-spin state). It relaxes back to alfa-spin state when the radiation energy is removed, and this relaxation process is called resonance. The amount of energy needed to create this resonance depends on the chemical environment of that specific hydrogen atom.

As illustrated in Figure 3-5, the amount of energy to move the nuclei into resonance is affected by the shielded and deshielded effect from the applied magnetic field. Larger energy is needed to move the atom into resonance and it results in a higher shift. In a deshielded environment, electrons are pulled away from the hydrogen atom. This occurs when the electronegative atom (e.g. chlorine) is near to the hydrogen atom, therefore, higher energy (E1) is needed to move into resonance (upfield). Conversely, electrons remain around the hydrogen atom in a shielded environment since these electrons are too far from the electronegative atom. These electrons cannot be pulled away from the hydrogen. Therefore, the nucleus is not altered much in this orientation and lower energy (E2) is needed to move into resonance (downfield).

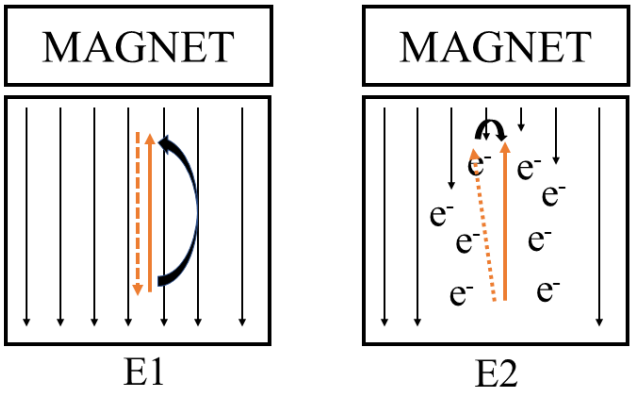

Figure 3-5 Schematic description of energy needed to bring shielded and deshielded nuclei into resonance where dotted line is α-spin state and solid line is β-spin state.

3.8 Matrix-assisted Laser Desorption Ionization Time-of-Flight (MALDI-TOF)

Matrix-assisted laser desorption ionization time of flight (MALDI-TOF) is a simple mass spectrometer, consisting of three major components, ion source,

analyser and detector. It is a soft ionization technique which does not fragment the analyte. The analyte (sample) dissolves in a matrix solution and spots on a plate. In the presence of the matrix compound, it absorbs radiation effectively before transferring the energy to the analyte molecules. The ionized analyte is observed by the detector and a plot of m/z is then generated. The matrix is always a low mass and high UV absorbance; part of the matrix heats rapidly and vaporises with the sample. One of the common matrixes that are used in this test is α-cyano-4-hydroxy-cinnamic acid (Figure 3-6).

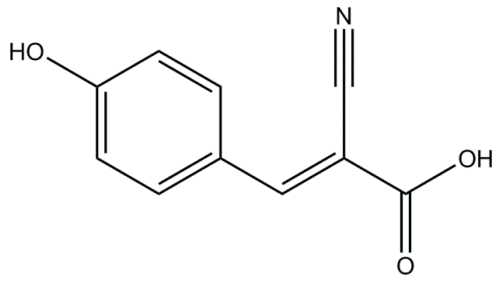

Figure 3-6 Structural formula of α-cyano-4-hydroxy-cinnamic acid.

The mass and velocity of the accelerated ions to reach the detector are crucial in this analysis. The detected separated ions are distinguished by measuring accurately the ion drift times in a high vacuum. The energy of the charged ions is shown as below Equation 3-11:

$$Energy = zeV \qquad \text{Equation 3-11}$$

Where z is the number of charges on each ion, e is the magnitude of the charge of a single electron and V is the potential difference created within this region.

These ions travel from the ion source to the detector. The kinetic energy of the ions is written as below:

$$KE = \frac{mv^2}{2} \qquad \text{Equation 3-12}$$

Where m and v are mass and velocity of the ions, respectively.

By conservation of energy, Equation 3-11 and Equation 3-12 are combined;

$$zeV = \frac{mv^2}{2} \qquad \text{Equation 3-13}$$

$$\frac{m}{z} = \frac{2eV}{v^2} \qquad \text{Equation 3-14}$$

Since the charge of electron and voltage is a constant;

$$\frac{m}{z} = \frac{k}{v^2} \qquad \text{Equation 3-15}$$

$$\boldsymbol{v = \sqrt{\frac{kz}{m}} = \frac{k}{\sqrt{m/z}}} \qquad \text{Equation 3-16}$$

Based on Equation 3-16, the velocity of the ions is inversely proportional to the square root of the m/z value. Different ions have the same kinetic energy, but with a different mass, therefore, the ions with smaller m/z value are first detected compared with heavier ions.

3.9 Differential Scanning Calorimetry (DSC)

Differential scanning calorimetry (DSC) is a type of thermal analysis, investigating the property of a sample with an elevated temperature. This is an informative method in studying the physical properties (i.e. glass transition temperature) of a compound. Specifically, calorimetry is used to determine the quantity of the heat absorbed or released by a substance. A physical or a chemical change during the measurement is known as enthalpy (ΔH) and the internal energy is measured at constant pressure.

DSC monitors heat effects on phase transitions and chemical reactions with a function of temperature. It operates at constant pressure and heat flow is

equivalent to the enthalpy change (Equation 3-17). During the measurement, the temperature of both sample and reference are increased at a pre-set rate. The difference in heat flow to the sample and a reference (i.e. inert material, such as alumina) is measured to identify the phase transitions (Equation 3-18).

$$\left(\frac{dq}{dt}\right)_p = \frac{dH}{dt} \qquad \text{Equation 3-17}$$

$$\frac{\Delta dH}{dt} = \left(\frac{dH}{dt}\right)_{sample} - \left(\frac{dH}{dt}\right)_{reference} \qquad \text{Equation 3-18}$$

Endothermic and exothermic refer to melting and crystallization processes, respectively. During the endothermic process, heat is absorbed by the sample and therefore heat flow is higher than the reference (positive value of dH/dt) and vice versa for the exothermic process. The endothermic transition upon heating changes the crystalline solid into a liquid state. The enthalpy of melting is the heat required to break down the crystalline lattice. Thus, a change in melting temperature (T_m) and enthalpy is not related to the content of amorphous material. For instance, a sharp and well-defined melting peak corresponds to a well-defined crystal structure. Furthermore, a completely crystalline sample has a sharp melting point, however, this is difficult to be achieved by polymer due to their long structure. On the other hand, during the exothermic process, heat releases from the sample and the sample crystallises upon cooling from the melt. Similar to the endothermic process, the enthalpy of crystallisation and crystallisation temperature (T_c) are measurable during the cooling process.

Other than melting and crystallisation temperature, phase transition, also known as glass transition temperature (T_g), is also another important property which can be identified by DSC. It is a reversible change from a viscous or rubbery condition to a hard and brittle condition. T_g is highly relevant to the amorphous material as it is an indicator of its stability. Additionally, the content of the amorphous material increases the T_g. Specific heat capacity is the amount of heat needed to raise the temperature of one gram of a particular material one kelvin of temperature. It is calculated when there is a T_g found in the sample and this heat

value is affected by the molecular motion; crystalline polymer with more order and a lower degree of molecular motion reduces the specific heat capacity.

In short, amorphous materials only have T_g and crystalline materials have T_m and T_c, therefore semi-crystalline materials have these three values.

4. Phase Tunable Calcium Phosphates Biomaterials by Microwave Synthesis

Although numerous papers report the synthesis of calcium phosphates (CaP), the synthesis of different phases of CaP under the same preparation conditions is extremely challenging. This chapter details the development and understanding of microwave irradiation (MI) in the fabrication of exciting CaP biomaterials, in particular β-tricalcium phosphate (β-TCP), dicalcium phosphate anhydrous (DCPA) and hydroxyapatite (HA) due to their diverse bioapplications.

4.1 Introduction

CaP biomaterials have gained increasing interest in bone regeneration and drug delivery owing to their low toxicity, excellent biocompatibility, nonimmunogenicity and osteoconductive properties.[6,54,81,124,125] Thus, they are widely used as the coatings on orthopaedic and dental implants, and also as scaffolds for bone regrowth determined by their resorbability and bioactivity.[126,127] Apart from the function as implants, CaP have been combined with protein molecules, e.g. bone morphogenetic proteins or fibronectin, to improve notably the osteogenic potential of bone substitutes and reduce the recovery period.[128] The least soluble phase HA is the most bioactive contrast to β-TCP and DCPA which are bioresorbable.[58,65] Consequently, HA is widely applied as a coating on orthopaedic and dental implants; β-TCP and DCPA, which poses a higher aqueous solubility and hence resorption rate compared with HA, can act as degradable drug carriers and scaffold materials,[81,129] with the advantage that their degradation does not create any toxic substances.[5] In addition to that, these nano-sized biomaterials are highly interesting as drug delivery agents, as their high specific surface area provides increased carrier sites.[65,130,131] Hence, the control of phase, surface structure and porosity of CaP biomaterials is crucial in improving their feasibility, especially as a drug carrier.

Calcination at high temperature can produce different phases of CaP. For instance, synthesis of β-TCP typically requires a reaction temperature above 800 ˚C to convert calcium deficient hydroxyapatite (CDHA) into β-TCP.[125] The formation of DCPA is commonly formed by heating brushite ($CaHPO_4 \bullet 2H_2O$) above 80 ˚C. Several low temperature methods have been reported for the synthesis of β-TCP and HA, but they require lengthy reaction times (e.g. more than 8 hours to crystallise β-TCP particles),[132] and control of particle size is generally poor. Hence, synthesis of different CaP phases with a high yield under mild and controllable reaction conditions remains challenging.

To solve these issues, MI heating has been proposed as an alternative method to synthesise CaP biomaterials. Compared with conventional heating, microwave generates the heat inside the solvent due to the rotation, friction and collisions of solvent molecules. Therefore, it can crystallise particles at a low temperature, with controlled morphology, short reaction times, high yields, and improved reproducibility.[81,82,133,134] This chapter investigates the employment of MI in a strong microwave absorbing solvent environment (i.e. methanol, ethanol and water) to control the phase morphology and porosity of CaP biomaterials, which is a facile route without additional steps to remove the surfactants, in an attempt to finally manipulate the protein adsorption and release properties of these CaP materials. Furthermore, underlying MI mechanisms will be discussed based on diverse material characterisations. Both protein loading and release tests will also be undertaken in an *in vitro* environment. The well-control of morphology and pore size could be a promising candidate for drug delivery with increased loading amount and controllable release profile. This work was in collaboration with Dr Philip James Thomas Reardon, where he performed the protein loading and release test. The results shown in this chapter has been published.[135]

4.2 Methodology

4.2.1 Material synthesis

All CaP biomaterials outlined in this report were synthesised using a multimode microwave-assisted hydrothermal/solvothermal method which used water or organic solvents, respectively. The solvent was heated above room temperature and the pressure was greater than atmospheric (1 atm) in a closed vessel system, but not exceeding the critical temperature and pressures for the solvents. The critical temperature and pressures for methanol, ethanol and water was 240 ^{0}C/80bar, 241 ^{0}C/63bar, and 374 ^{0}C/220 bar, respectively, while the maximum microwave temperature was 200 ^{0}C. The solution was placed into a 100 mL seal Teflon vessel and screwed with a cap (Figure 4-1) (the CEM company). The solution was then irradiated with microwave to produce high temperature and pressure condition, and followed by a cooling down process. The cooling time was ca. 30 minutes.

Figure 4-1 Microwave-assisted reaction systems (MARS) and its vessels.

Synthesis of different phases of CaP by changing the experimental conditions

Preparation of CaP biomaterials was completed in a two-step process. For β-TCP preparation, 0.79 g of $Ca(C_2H_3O_2)_2•H_2O$ (Sigma Aldrich) and 0.33 g of H_3PO_4 (Acros Organics) were dissolved in 20 mL of methanol, respectively at room temperature. Next, H_3PO_4 solution was added drop-wise into the other precursor solution. The mixture (Figure 4-2) was then transferred into a sealed PTFE

container (Figure 4-1) before putting into a microwave (MARS model, CEM company). The whole hydrothermal/solvothermal reaction was pre-set at 25 minutes of ramping time and 5 minutes of holding time at 200 ^{0}C. The output power of microwave was adjusted automatically for maintaining at the pre-set temperature. The product was then cooled to room temperature. The suspended product was then centrifuged, in order to separate the solid phase product from its solvent, and washed several times with deionized water before being dried overnight in the oven (Advantage Lab oven 50-L) at 70 ºC. The whole procedures were repeated by replacing methanol with ethanol and water for preparation of DCPA and HA, respectively. For optimizing the experimental conditions to prepare these phases, the reaction time was extended to 60 minutes in microwave without changing other parameters.

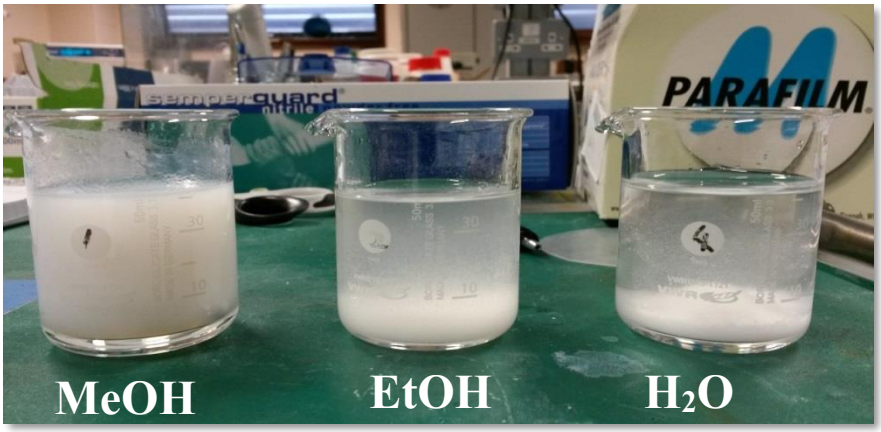

Figure 4-2 Mixture of calcium and phosphate precursors in methanol, ethanol and water before reacting in microwave.

Other than that, the calcium precursor was then replaced with calcium nitrate tetrahydrate (Sigma Aldrich) without changing other parameters to understand the role of calcium precursor in the formation of phases of CaP. The whole procedures were repeated as mentioned above.

4.2.2 Characterisation

Powder X-ray Diffraction

Different phases of calcium phosphate were confirmed using PXRD owing to the unique crystal structure of these phases. The phase identification by PXRD was

carried out using a Bruker D4 Advance Powder X-ray Diffractometer with a CuK_α (λ = 0.154060 nm) radiation source for all the prepared calcium phosphates. Diffraction patterns were collected from 10 º to 80 º with a step size of 0.02 º and 10 seconds of step time. These patterns were compared with the standard spectra from the JCPDS database.

Raman Spectroscopy

Raman spectra data of the samples were acquired using a Renishaw Raman Microscope with helium-neon laser at a wavelength of 514.5 nm and 20 scan numbers.

Nitrogen Sorption

The specific surface area of samples was measured using a Micromeritics TriStar gas adsorption analyser and the Nitrogen (N_2) adsorption/desorption isotherms at 77 K after degassing the samples at 130 ˚C overnight. The degassing process aims to remove adsorbed contaminants from the surface and pores of a sample.

Transmission/Scanning Electron Microscopy

The morphologies of samples were observed using a JEOL 1010 Transmission Electron Microscope (TEM) which was operated at 80kV. For sample preparation, the synthesised calcium phosphates were highly dispersed in an ethanol solution by sonication and then dropped onto a carbon mesh TEM grid (Agar Scientific) with a micropipette.

A JEOL JSM-7401F high resolution Field Emission Scanning Electron Microscope (SEM) operating at 3-5kV was used to observe the size and shape of calcium phosphates. Owing to low conductivity of calcium phosphates, samples were coated with Au to reduce discharge.

4.2.3 Protein/BSA loading and release

The protein loading and release test were conducted with Dr Philip James Thomas Reardon, who previously worked in the same research group. Bovine serum albumin (BSA) was used to study *in vitro* protein loading and releasing profile. The loading and release experiments were conducted as previously reported.[81] Briefly: 0.25 g of sample was added to 50 ml of BSA solution (1mg/mL) and then stirred for 24 hours without any heating. The loaded sample was centrifuged without washing since this eliminates some loosely bonded

proteins. The BSA loading amount was calculated based on the depletion of BSA in the solution measured by Ultraviolet-vis (UV-Vis) spectra. 0.25 g of loaded sample was then incubated in 10 mL of phosphate buffer solution at room temperature. 2 mL aliquots of solution were removed and then replaced with a fresh buffer solution at pre-set time intervals. The BSA concentration at different time points was measured by UV-vis spectrometer (Shimadzu UV-2550 UV-vis spectrophotometer) at 277-280 nm. Baseline with a water or phosphate buffer was performed before each measurement. A calibration plot (0.1-1 mg/mL) using known BSA concentrations was undertaken to calculate the concentrations of the loading and release samples. Then the amount of protein in the solution was calculated by measuring the concentration in the solution; a higher released amount of BSA in the solution indicated a larger absorption value.

4.3 Results and Discussion

Microwave-assisted hydrothermal/solvothermal technology with different parameters, such as the type of solvent, microwave radiation time, reaction temperature and vapour pressure of the solvent have been investigated in this study. By varying these parameters, the changes in the calcium phosphates phases, morphologies and porosities were observed. The products were then tested for the protein loading capacity and release profile.

4.3.1 Study of different experimental parameters on formation of calcium phosphates (CaP)

As mentioned in chapter 2, properties of CaP vary with their phases and each phase can suit into different applications. After 5 mins of holding time in microwave, three important CaP phases, including β-TCP, DCPA and HA, were synthesised in methanol, ethanol and water respectively when fixing other experimental parameters, e.g. calcium acetate monohydrate and phosphoric acid precursors, Ca/P ratio of the reactants, reaction temperature and time.

As depicted in Figure 4-3, all XRD patterns are matched with JCPDS database; β-TCP (JCPDS #09-0169), DCPA (JCPDS #9-80) and HA (JCPDS #09-0432). The synthesised calcium phosphate particles appear to have a preferred growth orientation depending on the solvent species, resulting in a variation in morphology as observed by TEM (Figure 4-4). DCPA particles are elliptical (50-110 nm x 40-90 nm), HA materials are plate-like in shape (1-5 µm x 0.4-1.2 µm), while β-TCP are needle-shaped nanoparticles (20-80 nm x 10-20 nm). However, short reaction times resulted in low yields, for example, less than 10 % β-TCP are produced after 5 minutes in microwave. Therefore, the experimental conditions were then further optimized by extending the reaction time, which will be further explained in the following section. When using calcium nitrate tetrahydrate as a calcium precursor, DCPA is obtained in methanol instead of β-TCP while DCPA and HA are produced in ethanol and water, respectively (confirmed by XRD pattern in Figure 4-5). Therefore, calcium acetate monohydrate is found to be a suitable precursor to synthesise different phases of CaP by only changing the solvents while no adjustment in pH and Ca/P reactant ratio is needed.

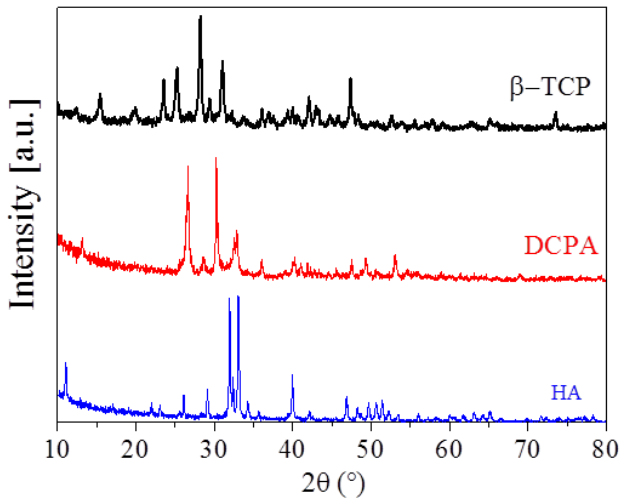

Figure 4-3XRD patterns of calcium phosphates (β-TCP in methanol, DCPA in ethanol and HA in water) prepared at 200 ^{0}C after 5 minutes of microwave heating.

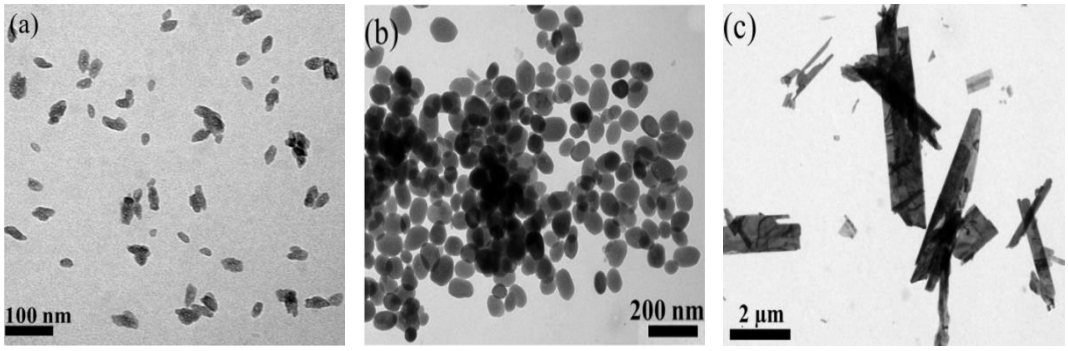

Figure 4-4 TEM images of (a) needle-like β-TCP prepared in methanol, (b) elliptical DCPA in ethanol and (c) plate-like HA particles in water. synthesised after 5 minutes of microwave holding time at 200 ^{0}C.

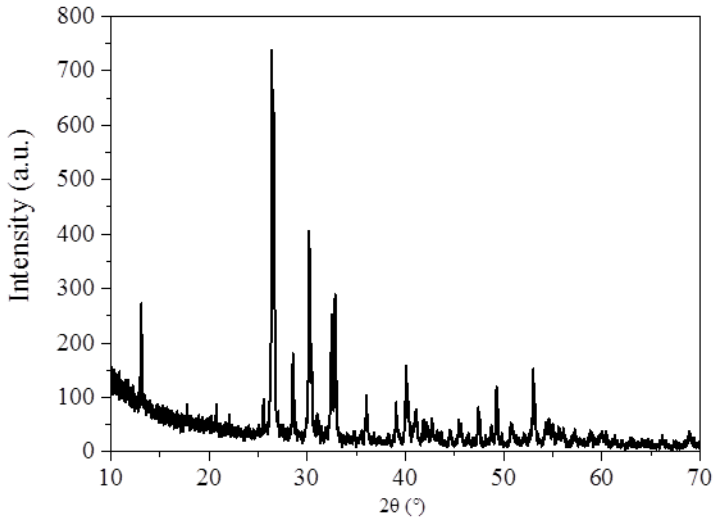

Figure 4-5 XRD pattern of DCPA (JCPDS 70-1425) that produced after one hour in methanol at 200˚C using microwave method (calcium nitrate tetrahydrate as calcium precursor).

4.3.2 Optimization of microwave conditions for higher yields

For solving the low yield issue, the reaction time was further extended to one hour. At this stage, no change in CaP phase is found, as verified through XRD (Figure 4-6), but with higher yields of these CaP products (see Table 4-1).

Table 4-1 samples synthesised at 200 ˚C and one hour holding time in microwave.

Type of solvent	Phase	Yield (%)	BET Specific Surface Area (m^2/g)
Methanol	β-TCP	80.72	31.7 ± 2.3
Ethanol	DCPA	85.11	72.2 ± 5.6
Water	HA	91.99	13.6 ± 2.5

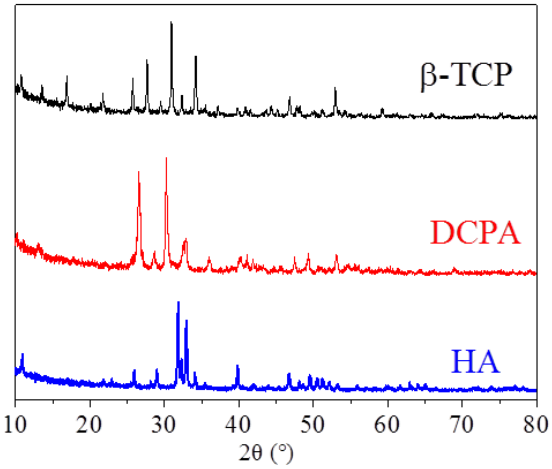

Figure 4-6 X-ray diffraction pattern (XRD) of samples prepared using the microwave method at 200 ˚C and one hour reaction time. CaP phases are readily controlled by solvents used, e.g. methanol (β-TCP), ethanol (DCPA) and water (HA).

The Raman spectra of β-TCP, DCPA and HA samples prepared with one hour microwave reaction time are similar to the literature (Figure 4-7).[136,137,138,139] All visible peaks are attributed to the P-O stretching and bending modes of the vibration. For example ν_1 is the symmetric P-O stretching mode (ca. 900-990 cm^{-1}), ν_2 is the doubly degenerated O-P-O bending mode (ca. 370-500 cm^{-1}), ν_3 is asymmetric P-O stretching mode (ca. 1000-1100 cm^{-1}) and ν_4 is the triply degenerated O-P-O bending mode (ca. 550-650 cm^{-1}).[5] Raman peaks at 291, 404, 470, 548, 611, 631, 948, 967 and 1005 cm^{-1} are corresponded to those found in β-TCP, while Raman peaks at 392, 419, 562, 576, 591, 901, 987 and 1097 cm^{-1} are the characteristic peaks of DCPA. HA sample only has four main Raman peaks, which are found at 430, 592, 962 and 1046 cm^{-1}.

When the reaction time is further increased to two hours, the yield of the calcium phosphate nanoparticles is similar to that achieved after one hour reaction time. This indicates that the temperature of 200 ˚C is high enough to provide sufficient energy to drive the reaction and it can be concluded that the optimum synthesis conditions are a temperature of 200 ˚C with one hour of residence time in the microwave, resulting in a high yield and controlled phases of CaP, (e.g. 80.72 % for β-TCP. 85.11 % for DCPA and 91.99 % for HA).

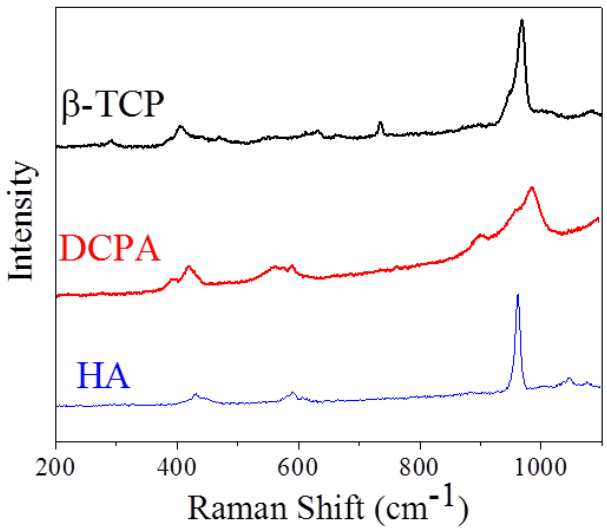

Figure 4-7 Raman spectra of β-TCP, DCPA and HA samples synthesized at 200^{0}C and 1 hour reaction time via microwave method.

The mesoporosity of β-TCP, DCPA and HA particles prepared at 200 ˚C with one hour holding time was further analysed by nitrogen adsorption/desorption analysis. DCPA shows a Type IV isotherm with a H1 hysteresis loop, indicative of a mesoporous material with a relatively narrow distribution of pore diameters as shown by the sharp peak in the range of 4-12 nm in the BJH plot (Figure 4-8). β-TCP nanoparticles also exhibit a similar Type IV isotherm with a H1 hysteresis loop while a larger pore size of 10-40 nm. Only HA particles obtained in this study show a Type II isotherm with zero pore volume, indicating that they are nonporous. In term of specific surface area, DCPA particles have the largest specific surface area (72.2 ± 5.6m^2/g), followed by β-TCP (31.7 ± 2.3 m^2/g) and then HA particles (13.6 ± 2.5m^2/g) (see Table 4-1), consistent with their pore volume.

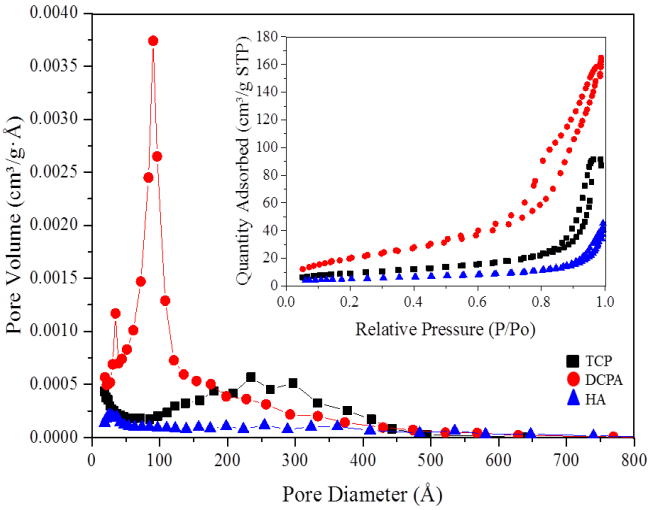

Figure 4-8 Pore size distribution and N_2 adsorption-desorption equilibrium isotherm of β-TCP, DCPA and HA particles prepared at 200 ^{0}C and one hour residence time in microwave.

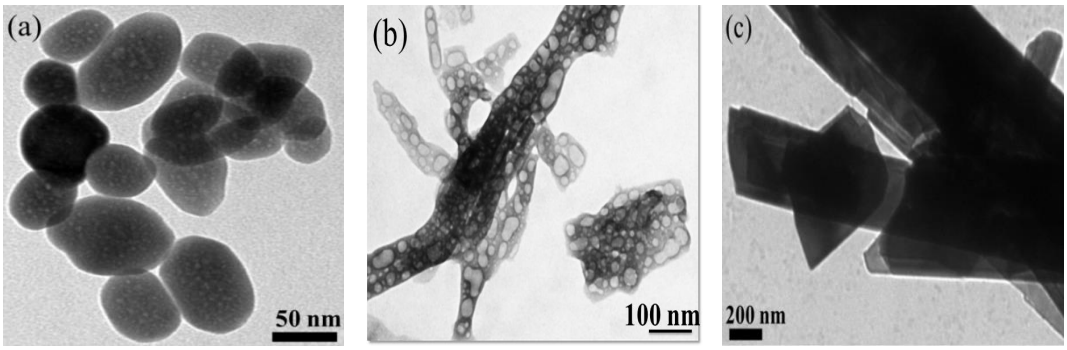

Figure 4-9 TEM images for (a) β-TCP nanoparticles, (b) DCPA and (c) HA particles produced using microwave method at 200 ^{0}C for one hour.

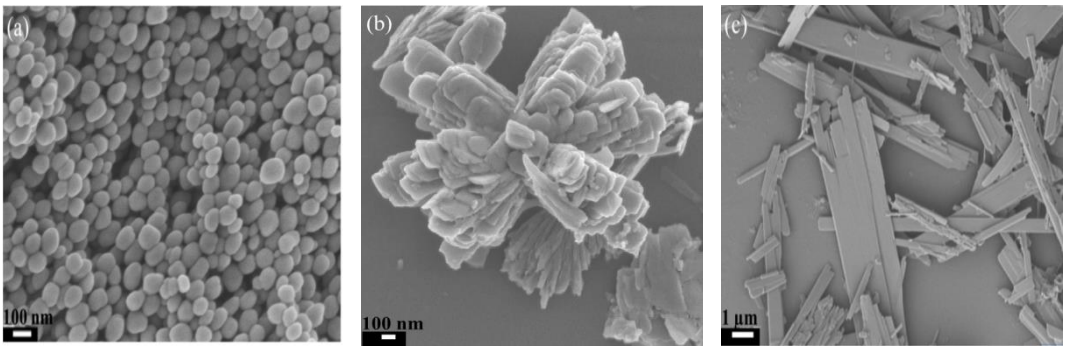

Figure 4-10 SEM images of (a) β-TCP in methanol, (b) DCPA in ethanol and (c) HA in water synthesised at 200 ℃ and one hour reaction time.

Interestingly, a longer reaction time not only increases the yield of the samples, but also changes the shape of particles (Figure 4-9 and Figure 4-10). After one hour, β-TCP nanoparticles grow from needle-shaped to elliptical with dimensions 50-120 nm x 40-80 nm (Figure 4-9). DCPA particles transform from elliptical into larger flat plate-like particles with dimensions of 140-950 nm x 100-240 nm. The shape of HA particles does not change but they increase in dimensions to 2-10 μm x 0.4-2 μm. Both β-TCP and DCPA can be seen full of pores. However, these CaP particles are not very stable under the high electron beam and their pore size also changes when the imaging time is too long and therefore the pore size of DCPA looks larger than that of β-TCP in TEM images.

The morphology of CaP produced is strongly influenced by the type of reaction solvent. Solute-solvent interaction can change the crystal growth kinetics and surface energy, thus enhancing or inhibiting growth at certain crystal faces.[140,141] Reardon *et al.* reported that the morphology evolution of CaP materials relied on the concentration of the residue precursors in the solution after the formation of nuclei; a higher precursor concentration favours one-dimensional growth and a lower precursor concentration allows three-dimensional growth of nanocrystals.[82] A measure of the efficiency of a solvent to convert the absorbed microwave energy to thermal energy is known as the dissipation factor tan δ, as listed in Table 4-2; higher tan δ values indicate greater heat dissipation to the solvent molecules, allowing a more rapid achievement of the desired temperature.[142] Therefore, a faster heating and higher vapour pressure produce an environment in which nucleation is faster, herein the order is methanol > ethanol > water. Larger amounts of nuclei decrease the precursor ions' concentration or the chemical potential in alcoholic solvents, thus favouring three-dimensional growth of crystals and leading to small needle-shaped β-TCP and elliptical DCPA particles in methanol and ethanol, respectively. Inversely, a high precursor ions' concentration in water results in a preference for one-dimensional growth. Furthermore, reaction time also affects the size and morphology of the crystals; larger crystals are obtained with longer reaction times. As the reaction time extends, the needle-shaped β-TCP particles transform into regular elliptical

shapes in methanol while DCPA particles agglomerate into larger plate shapes in ethanol. HA particles retain their morphology but increase in size. On the other hand, the specific surface area of CaP increases with the longer chain length of solvent but reduces with the presence of H_2O. This phenomenon is in agreement with a previous study, proposing that the alcohols may create pores or defects on the surface of CaP.[143] Specifically, alcohols act as surfactants due to their amphiphilic nature. Alcohols interact strongly with the phosphate group via hydrogen bonding and also interact between hydrophobic parts of alcohols with the solute molecules.[143]

Table 4-2 Microwave assumption factors tan δ, pK_a of phosphoric acids in solvents and polarity data for methanol, ethanol and water.[142,144,145]

Solvents	pK_a	Polarity index	tan δ ($x10^{-4}$)
Methanol	5.15	5.1	6400
Ethanol	6.15	5.2	2500
Water	2.11	9.0	1570

4.3.3 Mechanism on CaP formation

Chemical reactions in MI synthesis highly depend on the nature of the reaction solvent. The chemical reactions occurring in microwave are acid-base reactions, referring to acidic phosphoric acid with basic calcium acetate. The produced β-TCP is the neutral phase, whilst DCPA and HA are slightly acidic and basic, respectively.[146] No reaction occurs in both alcohol solvents (methanol and ethanol) before MI due to the low solubility of calcium precursors in alcohols, while brushite (matched with JCPDS #09-0077) directly form after mixing both precursors in water (Figure 4-11).

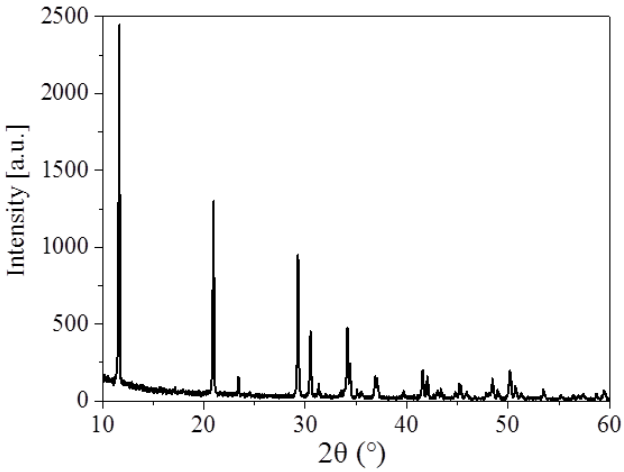

Figure 4-11 XRD pattern of brushite ($CaHPO_4 \bullet H_2O$) (JCPDS 09-0077) produced after mixing both the precursors in water at room temperature.

Reactions in methanol (Equation 4-1 and Equation 4-2), ethanol (Equation 4-4) and water (Equation 4-5 and Equation 4-6), with overall reactions (Equation 4-3, Equation 4-4 and Equation 4-7) are described as below:

$$Ca(CH_3COO)_2 + H_3PO_4 \rightarrow ACP + CH_3COOH \quad \text{Equation 4-1}$$

$$ACP \rightarrow Ca_3(PO_4)_2 \quad \text{Equation 4-2}$$

$$3Ca(CH_3COO)_2 + 2H_3PO_4 \rightarrow Ca_3(PO_4)_2 + 6\,CH_3COOH \quad \text{Equation 4-3}$$

$$Ca(CH_3COO)_2 + H_3PO_4 \rightarrow CaHPO_4 + 2\,CH_3COOH \quad \text{Equation 4-4}$$

$$Ca(CH_3COO)_2 + 2\,H_2O + H_3PO_4 \rightarrow CaHPO_4 \bullet 2\,H_2O + 2\,CH_3COOH \quad \text{Equation 4-5}$$

$$CaHPO_4 \bullet 2\,H_2O \rightarrow Ca_{10}(PO_4)_6(OH)_2 \quad \text{Equation 4-6}$$

$$10Ca(CH_3COO)_2 + 2H_2O + 6H_3PO_4 \rightarrow Ca_{10}(PO_4)_6(OH)_2 + 20CH_3COOH \quad \text{Equation 4-7}$$

The overall reaction process is described below. β-TCP and HA follow a two-step reaction sequence. Bow *et al.* reported that amorphous CaP (ACP) was initially obtained through mixing these two precursors at room temperature using methanol as a solvent.[132] After undergoing microwave dielectric heating, the ACP transforms into a crystalline calcium phosphate (β-TCP) in methanol with acetic acid as the by-product (Equation 4-3). For DCPA, no initial phase is formed when mixing the two precursors at room temperature as calcium acetate is totally insoluble in ethanol at room temperature as observed experimentally. However, after microwave assisted heating, slow dissolution and calcium ion release allow

the formation of DCPA (Equation 4-4). In water, brushite immediately precipitates after addition of the phosphoric acid into the calcium precursor solution and acts as the precursor to HA (Equation 4-5). Indeed, water is always needed in the chemical transformation of brushite, therefore, it is hydraulic compared to other phases.[146]

The solubility of precursors in different solvents plays a critical role in controlling the phase of CaP. The nucleation rate of CaP is determined by the concentration of calcium and phosphate ions in solution.[146] This concentration is dependent on the solubility of precursors (calcium acetate monohydrate and phosphoric acid) in the different reaction solvents. The calcium and phosphate ions, from calcium acetate monohydrate and phosphoric acid, interact chemically and precipitate as the end product or form the intermediates for additional CaP phases. For instance, brushite which precipitates before microwave heating acts as an intermediate precursor for HA in water. Water is a highly polar solvent, therefore, the degree of dissociation of both precursors is relatively higher. Calcium acetate monohydrate dissolves in water, but only partially dissolves in alcohols at room temperature.[147] Consequently, the higher solubility of precursors in water leads to the insoluble HA phase produced in water. Furthermore, the pK_a value of phosphoric acid in water (pKa=2.11) indicates a higher dissociation of phosphoric acid than the phosphoric acid in alcohol (pKa = 5.15-6.15) (Table 4-2), which shifts the reaction from left to right (Equation 4-8) and more HPO_4^{2-} ions favour brushite and then HA formation in water.[148]

$$\boldsymbol{H_3PO_4 \rightleftharpoons H_2PO_4^- \rightleftharpoons HPO_4^{2-} \rightleftharpoons PO_4^{3-}} \qquad \text{Equation 4-8}$$

In addition, the Ca/P ratio of these phases and the solubility of precursors are intimately related. Indeed, the use of alcohols tends to reduce the Ca/P ratio of the final calcium phosphate phase.[149] HA, with the highest Ca/P ratio, can be prepared in water because the degree of dissociation of both precursors in water are relatively higher than both in alcohols, and OH^- ions present in water. Calcium acetate monohydrate is slightly soluble in methanol and almost insoluble

in ethanol, hence, the Ca^{2+} ion concentration in ethanol at room temperature would be lower than in methanol. Amorphous calcium phosphate, with a Ca/P molar ratio of 1.2-2.2, was observed when mixing the two precursors in methanol after a few hours at room temperature.[63,132] Therefore, β-TCP preferably was formed in methanol due to slightly higher concentration of calcium ions than that in ethanol in which DCPA with a low Ca/P ratio of 1.00 was produced.

Microwave in a closed vessel system produces a high vapour pressure that can also facilitate CaP nucleation and growth. For example, methanol is a highly volatile organic solvent. Hence, it produces the highest vapour pressure, 400-550 psi, followed by ethanol with approximately 300-400 psi and water at 110-200 psi which was measured by a pressure probe located in the cavity of the microwave reaction system used in this study (Figure 4-12). However, the vapour pressure of the solvents does not play a decisive role in the final product phase formed, but contributes in combination with solubility of precursors in solvents to accelerate the reaction rate, as β-TCP, DCPA and HA were reported to be synthesised at room temperature in similar solvents but with a much long reaction time.[64,132,150] For instance, synthesis of both β-TCP and DCPA requires only five minutes microwave irradiation, instead of approximately eight and three hours, respectively observed at room temperature.[64,132] Therefore, rapid synthesis and phase selectivity of these biomaterials is the product of both a highly pressurized system and rapid heating associated with our microwave assisted synthesis.

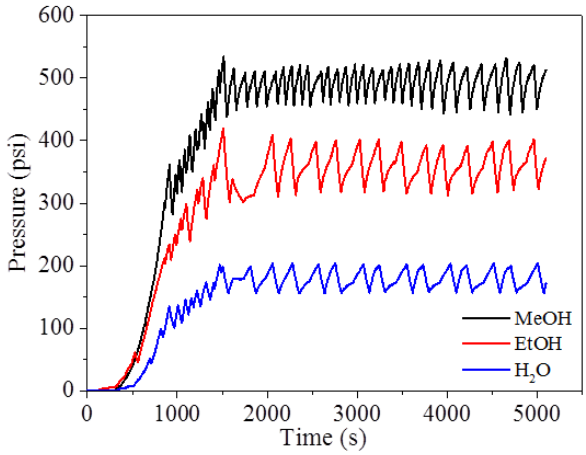

Figure 4-12 Pressure profile for all solvents (i.e. methanol, ethanol and water) irradiated in microwave at 200 ^{0}C with 60 minutes of holding time.

4.3.4 Temperature influence on crystallisation of β-TCP

Additional experiments were conducted for studying the minimum reaction temperature to produce high temperature phase, β-TCP. As illustrated in Figure 4-13, temperature is crucial to obtain the highly crystalline phase of β-TCP at a fixed reaction period (one hour). A decrement in temperature could not provide sufficient energy to complete a reaction in a short reaction time. Thus, β-TCP could not be produced in one hour when the reaction temperature was reduced to 70 ˚C in microwave. On the other hand, when increasing the reaction temperature to 90 ˚C and 130 ˚C, β-TCP was obtained after one hour and the yield increased with the reaction temperature. The yield is 63% and 74% for β-TCP prepared at 90 ˚C and 130 ˚C, respectively. Apparently, the microwave temperature is highly important to produce the crystalline high temperature β-TCP phase.

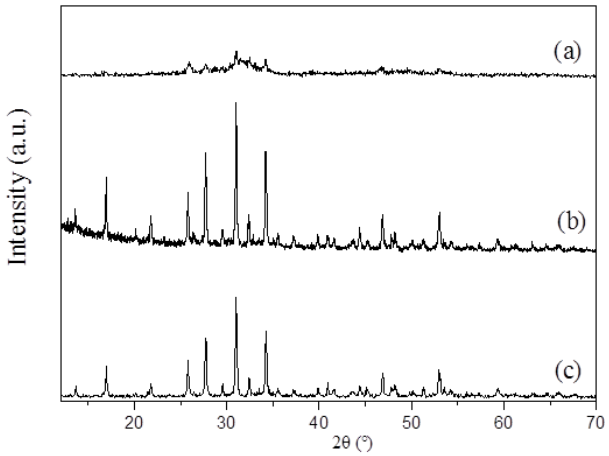

Figure 4-13 XRD patterns of samples produced after one hour in methanol at (a) 70 ˚C, (b) 90 ˚C and (c) 130 ˚C using microwave heating method.

4.3.5 Protein loading and release

After investigating the effects of experimental conditions on CaP formation, these CaP prepared at optimized experimental conditions (one hour) were then studied for the protein loading efficiency using bovine serum albumin (BSA) as a protein model. BSA loading was carried out for 24 hours to ascertain the drug delivery performance of the CaP biomaterials. It is well known that the specific surface area and pore size of CaP materials should influence the protein adsorption capacity. As mentioned in Section 4.3.2, DCPA particles have the largest specific

surface area (72.2m^2/g), followed by β-TCP (31.7 m^2/g) and then HA particles (13.6 m^2/g), consistent with their pore volume. Table 4-3 summarises the specific surface area of the prepared CaP materials with their BSA loading (%). The micron plate-shaped HA particles prepared in water as a solvent show a 15 wt% BSA loading due to its comparatively small surface area of 13.6 m^2/g. A threefold increase in loading efficiency (i.e. 50 wt%) for DCPA particles compared to HA particles is found, which correlates with the 380 % increase in surface area and higher meso-porosity observed. β-TCP particles represent a 41 wt% loading of BSA, 18 wt% less than DCPA although its surface area is 2 times smaller than DCPA.

Table 4-3 Specific surface area (m^2/g) of the prepared CaP in different solvents and their BSA loading (%).

Phase	BET Specific Surface Area (m^2/g)	BSA Loading (wt.%)
β-TCP	31.7 ± 2.3	41
DCPA	72.2 ± 5.6	50
HA	13.6 ± 2.5	15

The adsorption of BSA molecules onto the CaP particle surface is mainly driven by the electrostatic interaction between the BSA molecule and the CaP particles. The highly ionic CaP surface exerts great electrostatic forces to interact with the functional groups in BSA molecules. [130,151,152] Specifically, this interaction occurs between Ca^{2+} in the CaP and COO^- in BSA molecules. A higher surface area increases the overall charge per unit weight (more Ca^{2+} ions on the surfaces) which results in a higher degree of electrostatic interaction between CaP and BSA.[130] Therefore, the smallest surface area HA with fewest Ca^{2+} adsorption sites on the surface adsorbs the least amount of BSA molecules. Zhu *et al.* reported that greater amounts of protein adsorbed onto porous surfaces, concluding that the higher specific surface area produced more binding sites,[128] and is in agreement with our results- higher specific surface area of DCPA adsorbs the highest amount of BSA. It is also reported that the pore size also affects the BSA adsorption capacity; large mesopores allow more large biomolecules such as BSA (ellipsoid with dimensions 14 nm x 3.8 nm x 3.8 nm) to be adsorbed.[153,154,155] The

β-TCP material has less than half the surface area of the DCPA sample, but demonstrates ca. 82% of the BSA loading amount achieved by DCPA. This strongly indicates that the mesoporous structure of β-TCP (15-40 nm) can host more BSA molecules in comparison to the smaller pores (4-12 nm) in DCPA. Conversely, HA has the smallest surface area and a nonporous structure, resulting in the smallest loading amount of BSA. This characteristic suggests that drug loading may be controlled by not only surface area but also pore size.

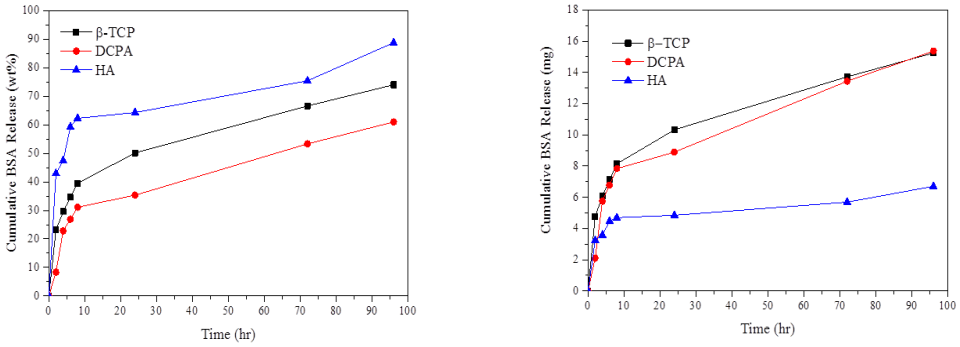

(a) **(b)**

Figure 4-14 Protein release profile for: (a) Cumulative BSA release rate (wt%) using different CaP (β-TCP, DCPA and HA) based on loading efficiency. (b) Cumulative amount of BSA release (mg) from β-TCP, DCPA and HA surfaces over 96 hours. The release profile of BSA was conducted in the phosphate buffered solution (pH 7.4, 37 ˚C) for 96 hours. All the CaP samples were synthesised at 200 ^{0}C, with one hour of microwave heating.

The other important aspect of a drug delivery medium is its release profile. The BSA-loaded CaP samples were incubated *in vitro* to examine this property. All materials exhibit a two-stage release profile (Figure 4-14 (a) and (b)) consisting of an initial fast release stage (0-10 h), followed by a slow linear release stage (10-96 h). Based on Figure 4-14(a), the BSA released (wt%) over the whole delivery period is the largest for HA, in comparison, DCPA exhibits the smallest release (wt%), regardless of loading amount. It is found that 62 wt% of BSA (4.7 mg) is released from HA, 40 wt% (8.2 mg) from β-TCP and only 31 wt% (7.8 mg) of BSA from DCPA particles after the first 10 hours (Figure 4-14(b)). According to Figure 4-14 (a) and (b), the BSA released (in wt % and mg) on three samples at the second stage is much slower compared with the first stage. It is estimated 100% of the protein would be released after 7 and 9 days from the β-

TCP and DCPA particles respectively, in contrast to just 6 days for HA due to its lower adsorption capacity. During the second release phase (10-96 h), DCPA shows the largest release amount of BSA (15.4 mg), compared to 15.2 mg for β-TCP and only 6.7 mg for HA. The total amount of BSA released from DCPA is expected to surpass β-TCP after 96 hours.

The two-stage release mechanism for all CaP phases is determined by the physical states of the adsorbed molecules and dissolution rate of CaP material.[130,128,156] The fast initial release is attributed to loosely bonded BSA molecules (physical adsorbed molecules) present on the outer adsorption layers where the electrostatic forces are weak and dominated by the surface area. The increase in the thickness of BSA layers on the CaP surfaces results in the molecules not being tightly bound. The second release stage is dominated by the dissolution rate of CaP; higher solubility of CaP has a higher dissolution rate, enabling a larger amount of the BSA to be released (Figure 4-14 (b)).[130] Thus, the protein release amount is directly linked to CaP solubility: DCPA > β-TCP > HA. However, another important factor influencing the protein release rate is the pore size in which the BSA molecules are captured. Gao *et al.* reported that the drug molecules easily leaked out or were released from the larger pore surfaces.[155] Therefore, the larger pores of β-TCP can also explain the higher release rate of BSA compared to DCPA over the same release period. Therefore, it can be concluded that the release profile is affected by a trifecta of surface area, CaP dissolution rate and pore size.

4.4 Conclusion

In this chapter, three major CaP phases (β-TCP, DCPA and HA) have been successfully synthesised under mild microwave conditions. There were four significant results in this work, including (i) formation of the CaP phases, (ii) morphology of the produced CaP particles, (iii) factors affecting the protein loading and (iv) release profile. Firstly, the produced CaP phases was closely

related to the solubility of the precursors in the solvent, regardless of Ca/P precursor ratio and reaction temperature. Calcium acetate monohydrate produced different phases of CaP by only changing the solvent species, while the microwave conditions remained unchanged. The selective interaction between microwave and solvent molecules manipulated the phases of CaP. Secondly, the morphology of the produced CaP particles was also controlled. The morphology was strongly linked to the solvent species, specifically the concentration of the residue precursors in the solution after the nuclei formation. A faster heating rate by microwave in methanol favoured three-dimensional growth and a slow heating rate in water resulted in one-dimensional crystal. Thirdly, the BSA loading was strongly related to their specific surface area and pore size. Increasing the specific surface area provided more binding sites. DCPA particles represented the highest loading amount of BSA (50 wt%) in the study due to the largest surface area. In addition, mesopores were formed in β-TCP and DCPA during preparation in alcohol solvents (methanol and ethanol) and resulted in higher BSA loading. The larger pore size of β-TCP exhibited a 'cage effect' by increasing the adsorption of BSA macromolecules. Fourthly, the release of BSA from different CaP biomaterials was a two-stage profile. This release profile was controlled by surface area, dissolution rate of CaP and pore size. A higher dissolution rate of CaP facilitated a larger BSA release amount. Importantly, the larger pores in the β-TCP material also influenced the release rate of BSA compared to DCPA (smaller pore size) over the same release period.

In short, the phase and morphology-controlled CaP materials by the microwave approach provide better control of drug delivery and loading owing to improved materials properties.

5. A Comprehensive Study of Poly(glycerol sebacate) Synthesis via Microwave and Conventional Heating

Following on the successful MI synthesis of different phases of CaP with a demonstration of controllable protein loading and release profiles in chapter 4, this chapter represents a comprehensive study of an interesting biopolymer, poly(glycerol sebacate) [PGS]. A highly branched pre-polymer of PGS (pre-PGS) has been prepared, leading to a wider range of degradation rate which is crucial for diverse bio-applications.

5.1 Introduction

PGS has been studied intensively after the first reported by Langer's group in 2002 due to its unique properties.[7] The specialities of PGS are its rapid degradation rate, relatively compatible with the healing rate of tissues (*i.e.* 6-12 weeks), modulated degradation rate favours for drug carrier, and tailored mechanical properties as a nerve guide material.[157–159] More importantly, both reactants of PGS are endogenous monomers that can be naturally found in human metabolites.[90,160] Because of its non-toxic monomers, PGS has proved less inflammatory than poly(lactide-co-glycolide), a currently widely utilized biomaterial.[159] Other than its tailored mechanical properties, the cytotoxicity of PGS can be further reduced by adding filler into the system or by controlling the crosslink density. For example, the percentage of dead cells decreased significantly as the crosslink level of PGS increased (*e.g.* by adding Bioglass);[101,161] a highly toughened or crosslinked PGS showed excellent cytocompatibility compared to a soft PGS.[162] The rapid degradation of soft PGS could induce an acidic and cellular toxicity environment. Therefore, controllable degradation of highly crosslinked PGS maintains a low concentration of potentially toxic degraded sebacic acid in the medium,[157,162,163] which is highly preferable but very challenging.

Apart from that, the preparation of PGS is very time and energy consuming under conventional heating (CH), which normally requires pre-polymerisation under inert gas condition to prevent oxidation of reactant for 24 h, and curing under vacuum condition for 48 h.[7] Over the past 10 years, MI has shown a great potential to replace CH.[87] It offers a homogeneous and fast heating due to volumetric and selective interaction between microwave and polar molecules, leading to increased reaction rates and high reproducibility.[81,82,165] A few reports discussing the effect of microwave irradiation on the pre-polymerization of PGS have been published,[8,166] in which a household multimode microwave oven was used. However, an ineffective control of the temperature rise and reaction rate could both trigger the evaporation of the monomer (e.g. glycerol due to a low boiling point of 290 ˚C) and change the stoichiometric ratio of the reactants that potentially altered the physical and chemical properties of the resulting PGS.[167] In addition, this multimode domestic MI provides much weaker energy density than single mode MI,[168] which can influence the degree of crosslinking of a polymer that is very important to biocompatibility of the polymer.

In order to solve these limitations, this chapter studies the PGS synthesis using both single mode and multimode MI approaches. A finely-tuned polyesterification of sebacic acid and glycerol to prepare PGS by single mode and multimode MI was carried out. The degree of esterification (DE) was thoroughly investigated in order to control the mechanical properties and degradation rate of PGS. For comparison, PGS synthesis was also conducted using CH. The mechanism underlying PGS formation by MI was also discussed. All interesting results led to a high quality publication.[169]

5.2 Methodology

5.2.1 Synthesis of Poly(glycerol sebacate)

Generally, there are two microwave systems (MARS and Discover SP, CEM company) used in the project. Specifically, MARS is a multimode microwave and

Discover SP is a single mode microwave. Both systems control the reaction temperature, where a fiber optic sensor is plugged into the reaction vessel in MARS system and an infrared temperature sensor detects the reaction temperature change during the material synthesis in Discover SP system. MARS is usually applied for large scale reaction and Discover SP is more suitable for small scale production. In this chapter, the two microwave systems were employed and further compared with conventional heating methods. PGS is hygroscopic, therefore, they are stored in air-tight, sealed containers after synthesis.

Microwave synthesis at constant temperature without solvent in batch and closed system

Initially, the synthesis of pre-polymer of PGS (pre-PGS) was conducted in a closed vessel system. Equimolar of glycerol (99%, Sigma Aldrich) and sebacic acid (> 99% Sigma Aldrich) were weighed and added into a reaction vessel (MARS, CEM company). The reaction was pre-set at 25 minutes of ramping time with a variation of holding time (10-60 mins). The microwave power was adjusted automatically to control the reaction temperature at 120 ˚C. After the cooling process, the mixture in the vessel was collected and further characterised.

Microwave synthesis at constant power without solvent in open system

After that, the synthesis of pre-PGS was modified in an open vessel system and N_2 gas was purged during the reaction. Similar to the previous step, equimolar of glycerol (99%, Sigma Aldrich) and sebacic acid (> 99% Sigma Aldrich) were weighed and put into a round bottom flask connected to a Drechsel bottle. The reaction temperature was controlled by alternating the microwave power. The applied microwave time was 3- 6 minutes and the resultant polymer was characterised. The resultant polymer was then cured in a vacuum oven for 24 h.

Microwave synthesis at constant power with solvent in single mode and multimode microwave

The procedures (Figure 5-1) were further modified by adding toluene into the previous system. Equimolar of glycerol (99%, Sigma Aldrich) and sebacic acid (> 99% Sigma Aldrich) were measured and pre-mixed in a round bottom flask before adding dry toluene (30 mL) into the mixture. Concentrated H_2SO_4 (3 μL)

was then added into the mixture. The reactor was connected to a Drechsel bottle for water collection. This mixture was then ramped under nitrogen gas with Dynamic mode (150 W) in CEM Discover SP system (single mode) for 3 minutes (one cycle) with a temperature limit of 130 ˚C. It was then cooled to room temperature. The cycle was repeated to obtain 12 and 27 minutes samples. The abovementioned experimental procedures were repeated using MARS system (multimode microwave) under similar microwave conditions (150W, 3 mins/cycle). The cycle was repeated 7 times to get a total 21 minute reaction time. Condensed water was collected for calculating the degree of esterification. The pre-PGSs were purified by removing the unreacted glycerol and then were dried using the diaphragm pump. Then, the pre-PGSS were left in the fumehood overnight at room temperature. The dried pre-PGSs were then cured in the vacuum oven at 120 ˚C for 2-48 h. PGSs were then cooled to room temperature under vacuum condition.

Figure 5-1 Experimental set-up of microwave-assisted synthesis of pre-PGS in single mode Discover SP system.

Conventional heating to prepare poly(glycerol sebacate)

For the control experiments, the pre-polymerisation step was carried out by conventional heating methods. Equimolar of glycerol and sebacic acid with toluene as solvent were heated in an oil bath at 120 ˚C. The same reactor was connected with a Dean-Stark for water collection. The curing procedure remained unchanged.

5.2.2 Characterisations

Fourier Transform Infrared Spectroscopy

The chemical bonds were confirmed using Perkin-Elmer 1605 FT-IR spectrometer in attenuated total reflection (ATR) mode with the frequency range 400-4000 cm^{-1} at 4 cm^{-1} resolution. Polymer samples including pre-polymer and crosslinked PGS were placed on the ATR crystal, and then compressed using a flat axial screw. Spectra collected were then compared with literature to distinguish the characteristic bonds of the samples.

Scanning Electron Microscopy

For observing the morphology of crosslinked PGS, the samples were fractured into small pieces and coated with Au. The SEM images were taken using JEOL JSM-7410F field emission-scanning electron microscopy operating at 2-3 kV.

Tensile Tests

Tensile strength tests were carried out on the crosslinked PGS samples by cutting into rectangular strips (4-5 mm x 15 mm x 1-2 mm of thickness) by Perkin-Elmer Dynamic Mechanical Analyser (DMA 7e, Perkin-Elmer Instruments, USA) at room temperature. All the measured dimensions of the samples were counted during the test. The initial load was set at 1 mN and increased to 6000 mN with a rate of 200mN min^{-1}. Six or more repeats were carried out for each sample and the final results were the average of these measurements. The Young's Modulus of each specimen was calculated from the gradient of stress-strain curve using the Pyris^{TM} software.

Matrix-Assisted Laser Desorption/Ionization-Time of Flight Mass Spectrometry (MALDI-TOF)

Mass spectrometric studies were used to identify the molecular weight of the oligomers and data were acquired in UCL Chemistry Mass Spectrometry Facility MALDI. It was operated in positive Reflectron mode using the mass range of m/z 500 to 5000 with 100 shots/spectrum. Pre-PGS samples were dissolved in THF to prepare a concentration of 9-10 mg mL^{-1}. Samples were then prepared by 1:1 dilution with matrix (α-cyano-4-hydroxy-cinnamic acid) in water-acetonitrile (2:8, v/v), 0.5 % formic acid. 3 μL of the resulting sample was spotted onto the MALDI target plate and allowed to dry. Samples were analysed using a Waters

MALDI micro MX (Waters, UK) with a nitrogen laser in reflection mode using delayed extraction (500 nsec) and an accelerating voltage of 120V, pulse 2500, and detector 2000. The simulated isotopic peak patterns were constructed using online software MoIE- Molecular Mass Calculator v2.02 (http://mods.rna.albany.edu/masspec/MoIE).

NMR spectroscopy

NMR spectra were recorded using a Bruker Avance III 600 MHz NMR spectrometer equipped with a 5 mm cryoprobe (^{1}H 600.13 MHz). NMR spectra of the pre-polymers (pre-PGS) were obtained in acetone-d6. All chemical shifts (δ) were given in ppm, where the residual C_3H_6O peak was used as an internal reference for ^{1}H NMR (δ_H = 2.09 ppm). The pre-PGS samples were pre-treated by washing with ethyl acetate to remove the unreacted sebacic acid. The filtrate was then dried under vacuum before the NMR analysis. The resulting data were processed and analysed using ACD/NMR Processor software.

5.2.3 Degradation study

For each sample, five or more polymer specimens were cut into dimensions of 5x5 mm^2 before storing in the standard phosphate buffer saline (PBS, 1X) at 37 ˚C for 28 days. The initial weight of the PGS samples was recorded before putting into the PBS solution. At a pre-set time (after 7, 14, 21, 28 days), these degraded specimens were dried in a drying oven at 60 ˚C for 12 h and the residue mass of the specimens was recorded.

5.3 Results and Discussion

5.3.1 Preliminary study on microwave synthesis of poly(glycerol sebacate) [pre-PGS]

Temperature monitoring and accurate control are important to avoid fast evaporation of volatile glycerol in PGS synthesis. In this study, the temperature was monitored and well controlled throughout the experiments. The experiments were firstly conducted in a closed vessel system without any solvent. After a pre-

set reaction time in a microwave, the resultant products was in wax form, which was consistent with the previous study.[38] As shown in Figure 5-2, the prepared pre-PGS shows a significant peak at 1688 cm^{-1}, corresponding to the unreacted C=O bond of the carboxylic bond, and a shoulder peak at 1730 cm^{-1} is the characteristic bond of the ester linkage. A broad peak at 3300-3500 cm^{-1} is associated with the unreacted OH bond from the glycerol, and the bonds at 2848 and 2915 cm^{-1} are attributed to C-H stretching of polymer backbone.[8,166] It can be concluded that the conversion of glycerol and sebacic acid into ester is low, proven by weak peak of ester linkage.

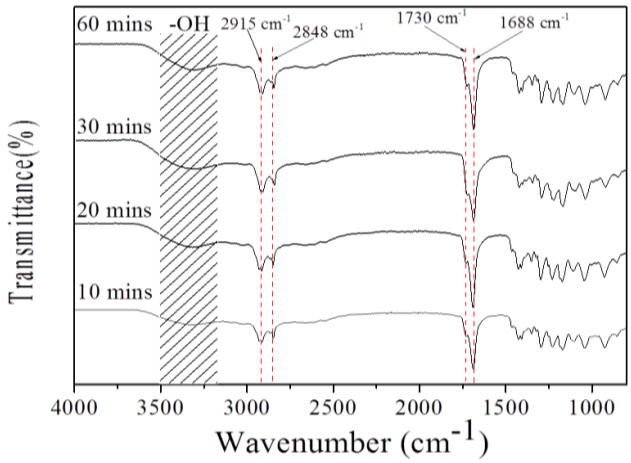

Figure 5-2 ATR-IR spectra of the prepared pre-PGS after 10-60 mins of holding time in a closed vessel system.

To increase the reaction rate in the microwave irradiation, an open system was then proposed to prepare pre-PGS. This allows the removal of the side product, water, by flowing N_2 continuously into the system, which was collected in the Drechsel bottle to judge the degree of esterification (DE). As presented in Figure 5-3, after 3 or 6 minute microwave reaction, a characteristic ester linkage at 1730 cm^{-1} is shown, and the C=O bond of the sebacic acid is still intense in both samples. The esterification process was preceded in the vacuum oven after the curing process, which is proven by a more intense ester peak in the IR spectra. The conversion of sebacic acid and glycerol into ester remains low in this open system and it is relatively hard to control the degree of esterification of pre-polymer without any indicator. In addition, the microwave power is capped

because higher microwave power may cause overheating if there is not any solvent used in the system. This pre-polymerisation highly relies on the microwave power applied to the system, thus, a better MI system has to be used which will be discussed in next section.

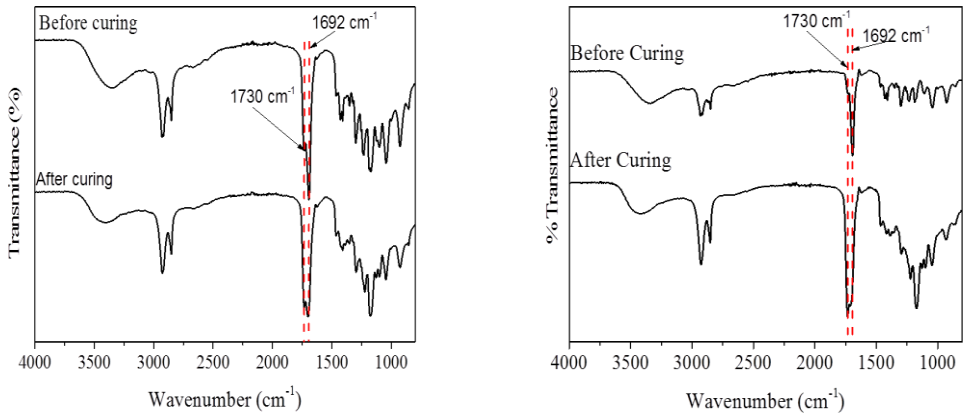

Figure 5-3 ATR-IR spectra of pre-PGS after 3 mins (left) and 6 mins (right) in MI and followed by 24 h of curing.

5.3.2 Synthesis of poly(glycerol sebacate) pre-polymer [pre-PGS] using single mode and multimode microwave irradiation (MI)

To improve the previous MI system, a solvent (i.e. toluene with lower boiling point 110˚C) was induced to protect the evaporation of glycerol (boiling point at 290 ˚C) and further set the maximum reaction temperature of 130 ˚C. All these have maintained a constant reactants ratio in the medium throughout the MI reaction with a well-controlled reaction temperature in an open system.

Although pre-PGSs have been prepared by multimode domestic microwave,[8,166] single mode pre-PGSs synthesis was not reported. Based on the obtained results, single mode MI has been found to be more energy efficient than multimode MI to synthesise viscous pre-PGS with a similar degree of esterification. For instance, 12 mins of microwave treatment is needed to synthesise the pre-PGS with ca. 70% DE by single mode MI, which was not achieved until 21 mins irradiation using multimode while the pre-PGSs prepared by both methods show a similar

characteristic ester linkage (C=O bond) at 1734 cm^{-1} and 1730 cm^{-1}, respectively (see Figure 5-4). The faster reaction time by single mode MI is attributed to the higher intensity provide by single mode microwave than that by multimode MI.[116,168]

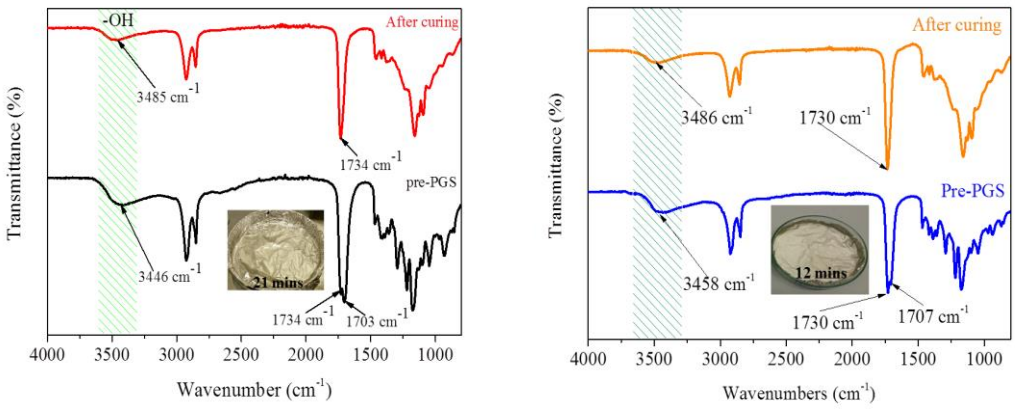

(a) **(b)**

Figure 5-4 ATR-IR spectra of pre-PGS (DE~ 70%) and cured PGS prepared by (a) 21 minutes in multimode and (b) 12 minutes in single mode microwave and followed by 8 h curing.

Other than the reaction time, the mechanical properties of the crosslinked PGSs, obtained by 8 h curing of pre-PGSs synthesized by both microwave methods, were also studied (see Figure 5-5). Based on Figure 5-5 (a), Young's modulus of the PGSs synthesized by single mode MI is 2.60 ± 0.34 MPa and the PGSs synthesized by multimode MI is 3.31 ± 0.30 MPa. The elongation at break for PGSs is 27.73 ± 1.87 % and 17.00 ± 7.77%, for single mode and multimode MI, respectively (Figure 5-5(b)). The ultimate tensile strength of the PGSs by single mode MI is also similar (approximately 0.46 ± 0.06 MPa for single mode MI and 0.41 ± 0.15 MPa for multimode MI-Figure 5-6). Independent sample t-tests were performed to compare the mechanical properties of the PGS prepared by both microwave methods. There was not a significant (NS) difference in the mechanical properties (i.e. Young modulus, elongation at break and ultimate tensile strength) of the PGS samples prepared by single mode and multimode microwave ($p > 0.05$).

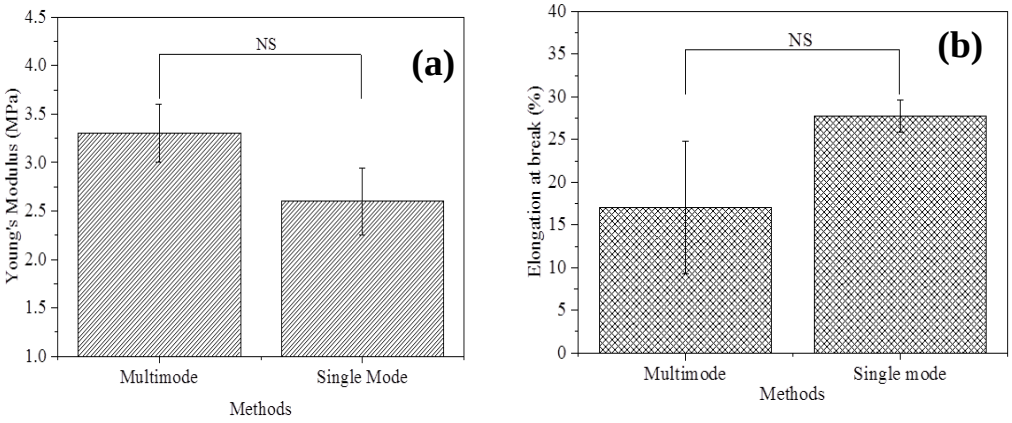

Figure 5-5 (a) Young's modulus and (b) elongation at break of PGSs prepared by 12 min single mode MI and 21 min multimode MI, followed by 8 h curing. The difference in the Young's modulus for the samples prepared by single mode (mean=2.60, SD=1.24) and multimode (mean=3.31, SD=0.67) was not significant (t(16)=-1.20, p=0.248). The difference in the elongation at break for the samples prepared by single mode (mean= 27.73, SD=6.74) and multimode (mean=17.00, SD=17.38) was not significant (t(16)=1.95, p= 0.069). NS: not significant.

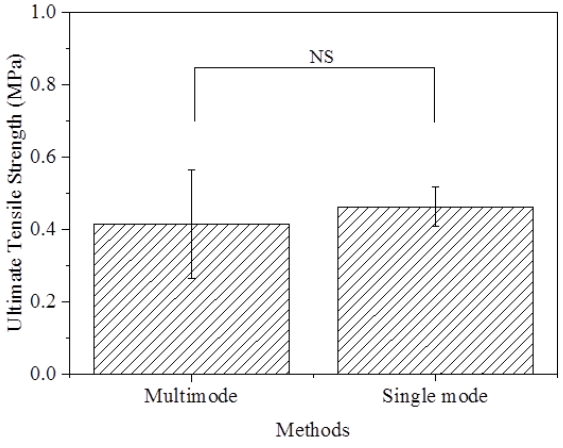

Figure 5-6 Ultimate Tensile Strength (MPa) of PGSs prepared by 21 minutes in multimode and 12 minutes in single mode microwave and followed by 8 h curing. The difference in the Ultimate Tensile Strength for the samples prepared by single mode (mean=0.46, SD=0.20) and multimode (mean=0.41, SD=0.34) was not significant (t(16)=0.381, p= 0.708). NS: not significant.

This summarises that the PGS synthesised by single mode MI can achieve similar Young's modulus compared with those samples prepared by multimode MI, but with a shorter reaction time. Owing to faster reaction rate and higher energy efficiency, the experimental conditions were then optimised using single mode MI and further comparisons with CH are discussed in the next section.

5.3.3 Preparation of poly(glycerol sebacate) pre-polymer [pre-PGS] using single mode MI and CH

Similar to the previous step, a two-step preparation procedure was applied to synthesise all PGSs, which were pre-polymerisation under MI or CH conditions and the curing in the vacuum oven. In a typical procedure, a mixture of sebacic acid and glycerol in dry toluene was heated to reflux temperature to prepare pre-PGSs in an open system and the condensed water was collected as a measure of degree of esterification (DE) - as illustrated in Figure 5-7.[89] In this mixture, glycerol interacts much more strongly with microwave than others. This is because the loss tangent of glycerol (tan σ = 0.651) is higher than toluene (tan σ = 0.040) due to multi-hydroxide groups attached, and the long chain of polar molecules (i.e. sebacic acid) always has a weaker interaction than a short chain with microwave.[109,170] The pre-PGSs were then purified by only removing unreacted glycerol which is soluble in toluene and further characterised.

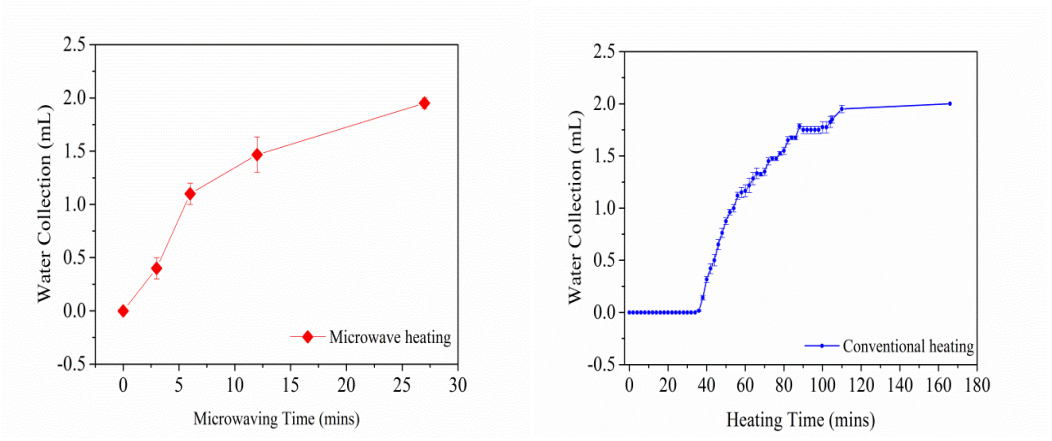

Figure 5-7 Water collection profile of polymerisation process by single mode microwave irradiation (MI) and conventional heating (CH) method.

DE can be used as a measure of the degree of polymerization and more importantly for predicting the unreacted alcohol groups after the pre-polymerisation process. In this study, the DE is calculated using the Equation 5-1 stated as below:

$$DE(\%) = \frac{Amount\ of\ water\ collected\ (mL)}{Theoretical\ amount\ of\ water\ formed\ (mL)}\ x100\% \qquad \text{Equation 5-1}$$

The percentage of DE was calculated based on two mole of water produced in order to fully react the sebacic acid. The results of DE are shown in Table 5-1. It was also observed that pre-PGSs prepared by MI method with 18.18 % DE and 66.82% DE were in wax and viscous liquid form, respectively, comparable with the previous reports. [38] On the other hand, the DE increases with a longer reaction time in both heating methods, however, this increment is dramatic by MI. In other word, a minimum six-fold increase in reaction rate can be obtained by MI compared to by CH (ca. at similar DE 70%).

Table 5-1 Water collected and degree of esterification (DE) by MI and CH methods.

Methods	Heating Time (mins)	Volume of Water (mL)	DE (%)
MI	3	0.40	18.18
	12	1.47	66.82
	27	1.95	88.64
CH	50	0.90	40.91
	77	1.50	68.18
	166	2.00	90.91

According to the water collection profile (see Figure 5-7***)***, MI almost starts the esterification process when MI is turned on. However, it takes more than 30 minutes to collect water droplets by CH. MI (dielectric heating) speeds up the reaction rate significantly by aligning the polar species (e.g. glycerol molecules) with the rapidly changing electrical field of the microwave as such the reactants could be activated selectively. More importantly, MI provides the heat internally

and tends to eliminate the 'thermal wall effect'.[121,171] The condensed water molecules produced are also evaporated fast in the microwave due to large dielectric loss of water molecules, which further shifts the reaction towards polymer formation.[172–174]

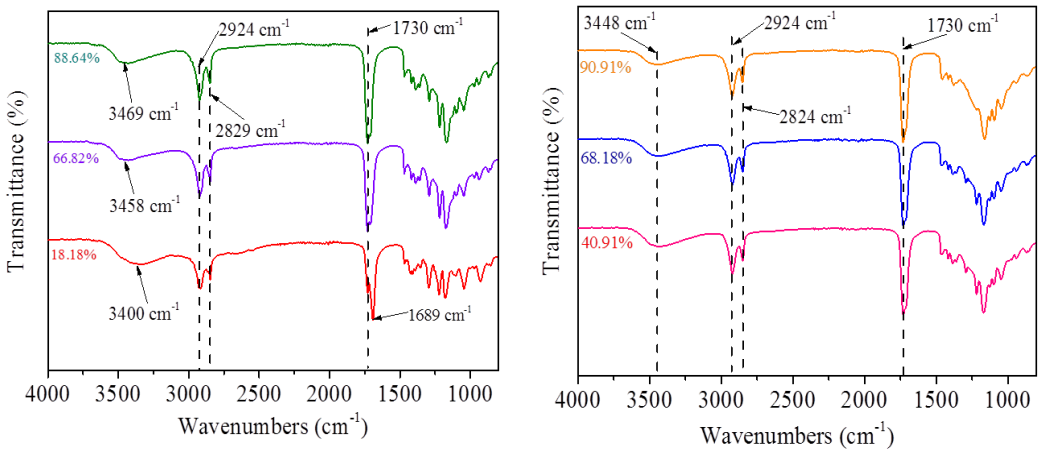

(a) **(b)**

Figure 5-8 ATR-FTIR spectra of pre-PGS prepared at different DE by (a) MI and (b) CH methods. These pre-polymers show strong signal of ester bond (C=O) at 1730 cm^{-1} and hydroxyl bond (—OH) around 3400-3469 cm^{-1} when using MI method. Similarly, the pre-polymer prepared via CH also showed C=O signal at 1730 cm^{-1} and —OH signal at 3448 cm^{-1}.

ATR-FTIR was used to confirm the formation of ester functional groups (Figure 5-8). A sharp peak is found at 1730 cm^{-1} which corresponds to the carbonyl (C=O) stretching mode of the ester linkage, and the bands appearing at 2924, 2829 and 2824 cm^{-1} are attributed to C—H stretching of the polymer backbone.[8,166] The relative intensity of the characteristic ester carbonyl increases as reaction time increases, suggesting a high degree of polymerisation.[17] The peak at 1689 cm^{-1} refers to the carbonyl stretching of the remaining free sebacic acid after pre-polymer formation. The pre-PGSs prepared by CH and MI show a broad peak around 3448 cm^{-1} and 3400-3469 cm^{-1}, respectively, attributed to hydroxyl (alcohol group) stretching of pre-polymer. As the MI time increases, the alcohol group of the pre-PGS prepared by MI shifts to higher wavenumber. The precursor glycerol contains two alcohol groups. One is the primary and the other

is the secondary alcohol group, which have a mixed peak around 3290 cm^{-1} (Figure 5-9). The primary alcohol group has higher frequency compared to secondary alcohol.[175] The observed continuous shift may indicate the pre-PGS prepared by MI contains more primary than secondary alcohol groups, which is interesting since the secondary alcohol group is esterified slowly and responsible for crosslink.[99] In other words, the MI approach uses more secondary alcohol group than the CH approach.

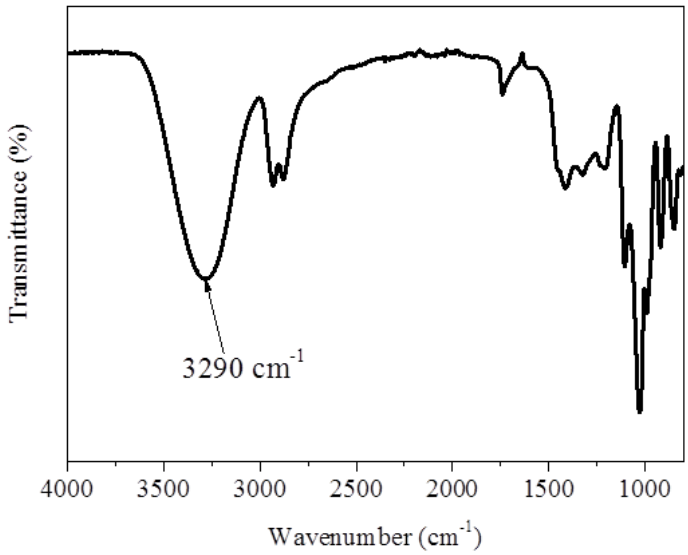

Figure 5-9 ATR-IR spectra of glycerol before polymerisation process.

Based on the obtained IR spectra, the highly branched pre-PGS structure by MI approach is proposed as depicted in Figure 5-10**.** MI interacts strongly with glycerol as mentioned above, leading to the activation of both alcohol groups in glycerol which react more efficiently with sebacic acid compared to that happening in CH approach. In order to justify this hypothesis, the obtained pre-polymers were further characterized by MALDI-TOF and ^{1}H NMR. ^{1}H NMR spectra of the obtained pre-PGSs, synthesised using both heating methods, were recorded using acetone-d6 (δ2.09 ppm) as the deuterated solvent. As shown in **Scheme 1,** 5 different sets of protons (H_{a-e}**)** can be assigned to the repeating units of pre-PGS.[176]

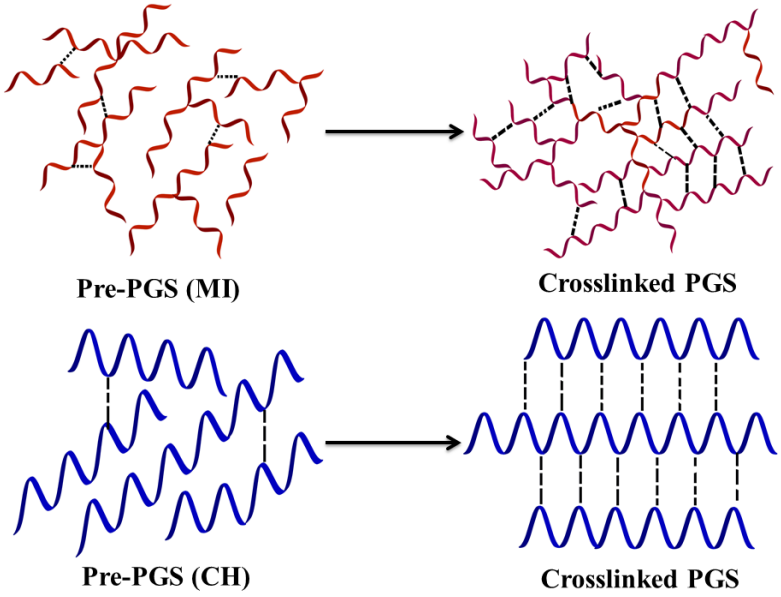

Figure 5-10 Proposed scheme for the possible structure of pre-PGS that prepolymerised via MI and CH methods, and crosslinked PGS after the curing process. The dotted line in the figure indicates the cross-linking.

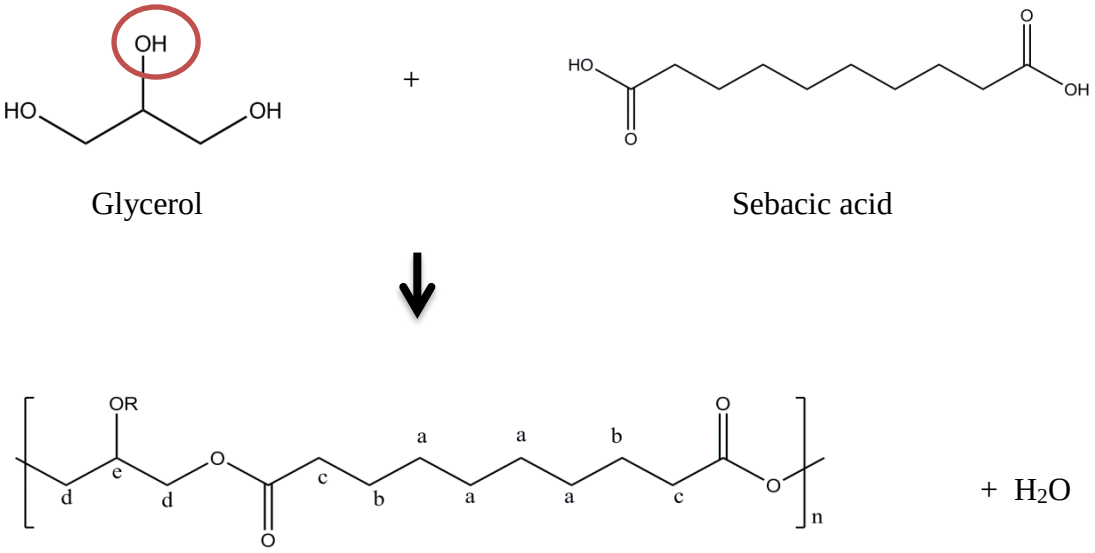

Scheme 1. Polycondensation of PGS using equimolar glycerol and sebacic acid where R can refer to hydrogen or a branched chain. The red circled region refers to the secondary alcohol group of glycerol.

^{1}H NMR spectra of the pre-PGSs, prepared by MI (18.18-66.82 % DE) and CH (40.91-68.18 % DE), display the chemical shifts at δ1.32 ppm (H_a), δ1.59 ppm (H_b), δ2.32 ppm (H_c), which are attributed to –CO-CH_2-CH_2-CH_2- group in the pre-polymer from the precursor sebacic chain (Figure 5-11**)**.[177,178] The additional peaks at δ 3.50-5.50 ppm identified in the spectrum are ascribed to the H_d and H_e in PGS molecular chain from glycerol.[179]

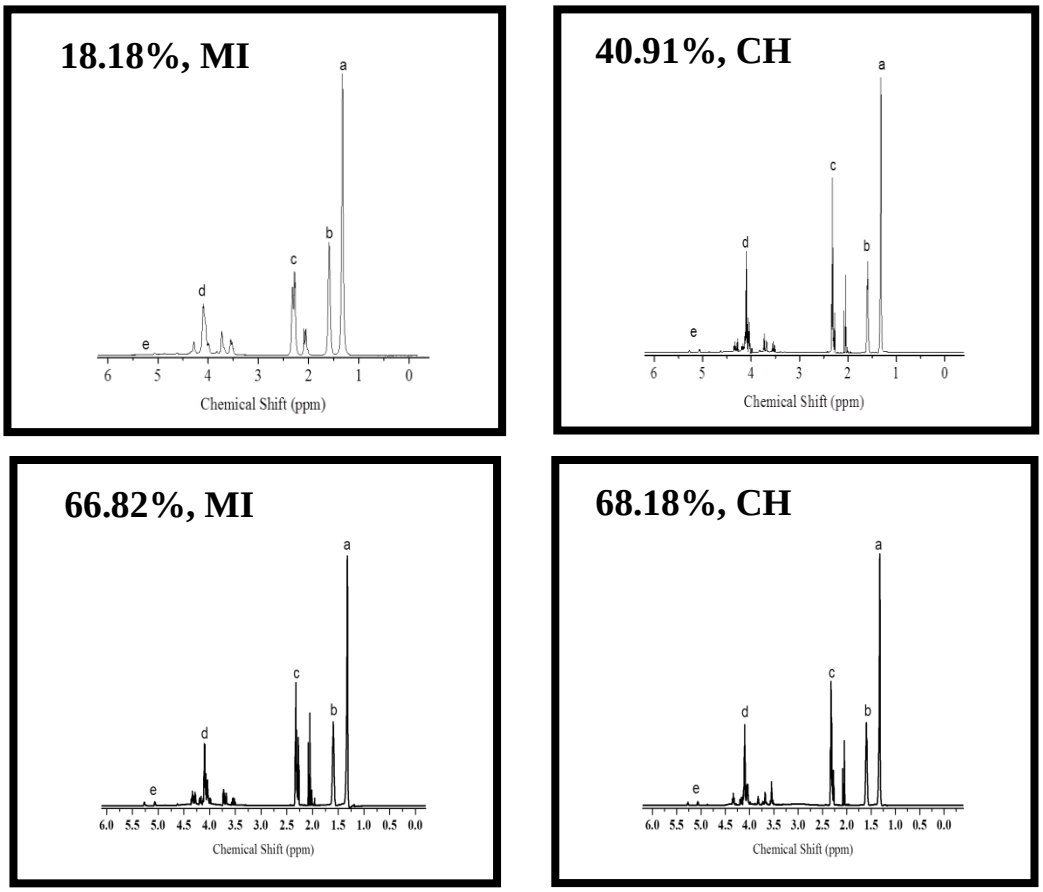

Figure 5-11 ^{1}H NMR spectra, in acetone-d6, of the pre-polymer with 18.18-66.82% of DE (MI) and 40.91-68.18% of DE (CH). The sebacic chain peak in the pre-PGS is illustrated at δ1.32 ppm (H_a), δ1.59 ppm (H_b), δ2.32 ppm (H_c) while H_d and H_e attributed to the glycerol chain in the pre-polymer. The ^{1}H NMR spectra demonstrate the typical molecular structure of pre-PGS where the additional peak at 2.09 ppm is from solvent acetone-d6 peak.

Further study was carried out to understand MI induced branching by observing the ^{1}H NMR between δ 4.9 and δ 5.3 ppm which corresponded to H_e and more specifically referred to 1,2,3-triacylglyceride (δ 5.27 ppm)- as illustrated in

Figure 5-12.[99] Relative signal intensity ratios can be used to understand the change in the amount present of secondary alcohol groups of glycerol. The relative signal intensity ratio of H_b or H_c to H_a is a constant (ca. 0.5). This is because these protons are not involved in the esterification process. Interestingly, the relative ratio of H_e/H_a corresponding to 1,2,3-triacylglyceride (δ 5.27 ppm) are 0.012 and 0.010 for MI (18.18% DE) and CH (40.91% DE), respectively. The higher the relative H_e/H_a ratio at δ 5.27 ppm, the higher the esterification of secondary alcohol groups of glycerol. When reaching ca. 70% DE, this relative ratio of H_e/H_a is 15% higher under MI (0.0132) than that under CH condition (0.0115). This indicates a higher branched pre-polymer achieved by MI method.

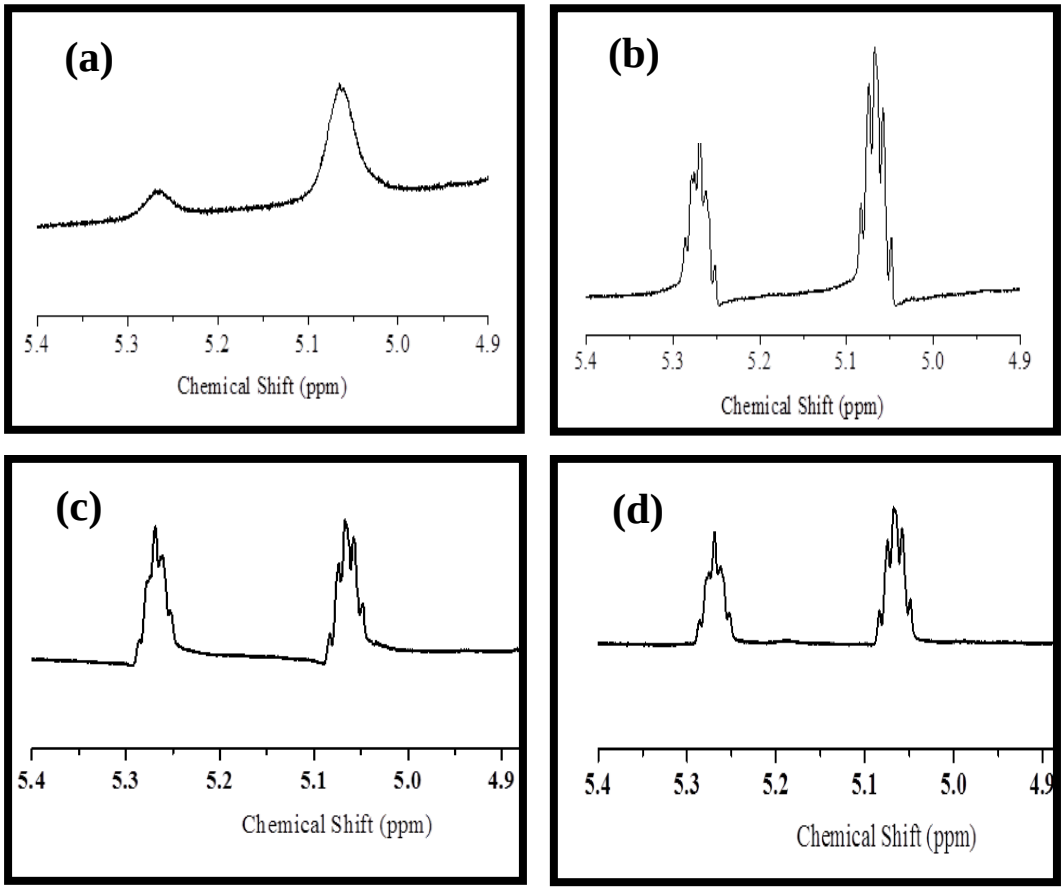

Figure 5-12 The last two figures are illustrated the region at δ 4.90-5.40 ppm for the pre-PGS with (a)18.18%-MI (b)40.91%-CH (c)66.82 %-MI and (d) 68.18%-CH. These two peaks assign to H_e which corresponded to 1,2-diacylglyceride (δ 5.07 ppm) and 1,2,3-triacylglyceride (δ 5.27 ppm).

More importantly, a significant broad signal is observed at δ 2.65-3.30 ppm in the ^{1}H NMR spectrum of the pre-PGS (68.18% DE) prepared using CH method (Figure 5-13). This signal is assigned to the secondary hydroxyl groups of glycerol (H_e in **Scheme 1**), in agreement with the previous reports.[180] In contrast, no such signal is observed in the ^{1}H NMR spectrum of the pre-PGS (66.82% DE) prepared using MI (Figure 5-13). The presence of excessive secondary alcohol groups in the pre-PGS prepared by CH suggests that the CH method produces linear polymer chains, whereas MI facilitates branching by selectively activating all alcohol groups as indicated in Figure 5-10**,** which is crucial to control the property of the final polymer.

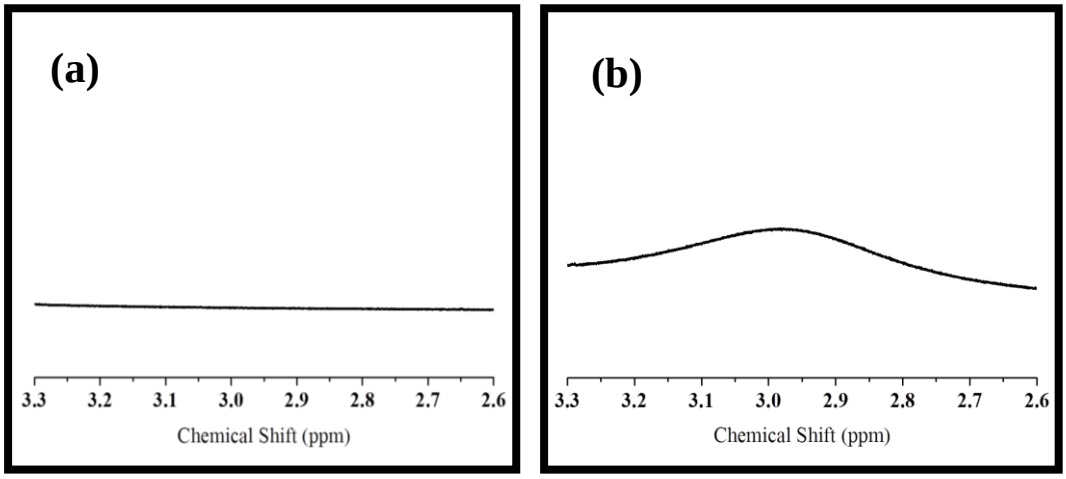

Figure 5-13 These two figures refer to the region of δ 2.65-3.30 ppm for (a) 66.82 % and (b) 68.18% of pre-PGS that were synthesized by MI and CH, respectively. The significant peak in (b) suggests the excess of secondary hydroxyl group (H_e) of glycerol existing in the pre-polymer prepared by CH method.

Other than ^{1}H NMR spectra, the MALDI-TOF mass spectra, recorded from 500 to 5000 *m/z*, of the pre-PGSs synthesized by both methods were also used to verify the formation of oligomeric structures (Figure 5-14 and Figure 5-15). The profile of experimental spectra of the samples prepared by either MI or CH is consistent with the theoretical spectra (Figure 5-14 and Figure 5-15), suggesting the validity of the modelling. However, the pre-PGS prepared by MI (DE=18.18%) shows monoisotopic mass at *ca.* 2360 *m/z* (Figure 5-14), appearing

to be shifted by 4 *m/z* when compared with the theoretical monoisotopic mass at 2364 *m/z* ($[C_{117}H_{200}O_{46}Na]^+$) that was calculated using a likely linear PGS with 9 repeating units. The shift (4 *m/z*) is thought to be most likely due to the esterification reaction of secondary alcohol groups of glycerol to produce branched PGS, which is in agreement with the NMR spectra. However, the pre-PGSs prepared by CH (DE=68.18%, Figure 5-15**)** shows monoisotopic mass at *ca.* 1405 *m/z* ($[C_{68}H_{118}O_{28}Na]^+$, consisting of a linear PGS with 6 glycerol and 5 sebacic acid units) which is very close to the theoretical monoisotopic mass at *ca.* 1406 *m/z* ($[C_{68}H_{118}O_{28}Na]^+$) (Figure 5-15-both theoretical and experimental monoisotopic patterns). This different monoisotopic mass also suggests that MI produces a different pre-polymer structure than CH.

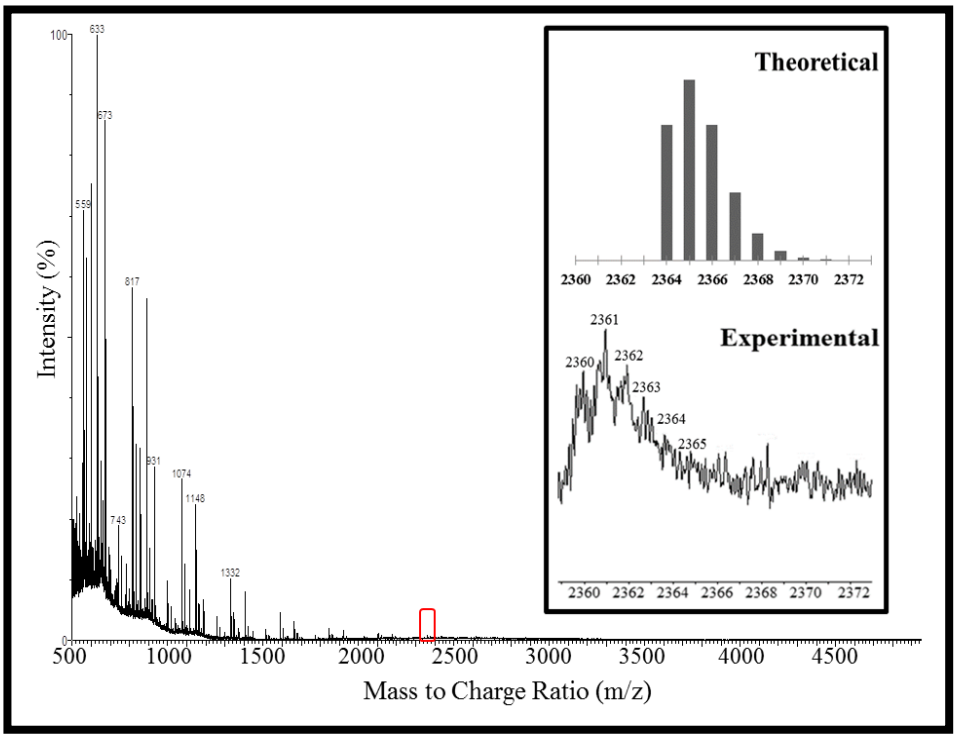

Figure 5-14 MALDI-TOF spectra of pre-PGS (18.18% DE-MI) show the maximum detected oligomer mass at 2360 m/z. This spectra is slightly left shifted when compared to the theoretical MALDI spectra, GSGSGSGSGSGSGSGSGS $[C_{117}H_{200}O_{46}Na]^+$.

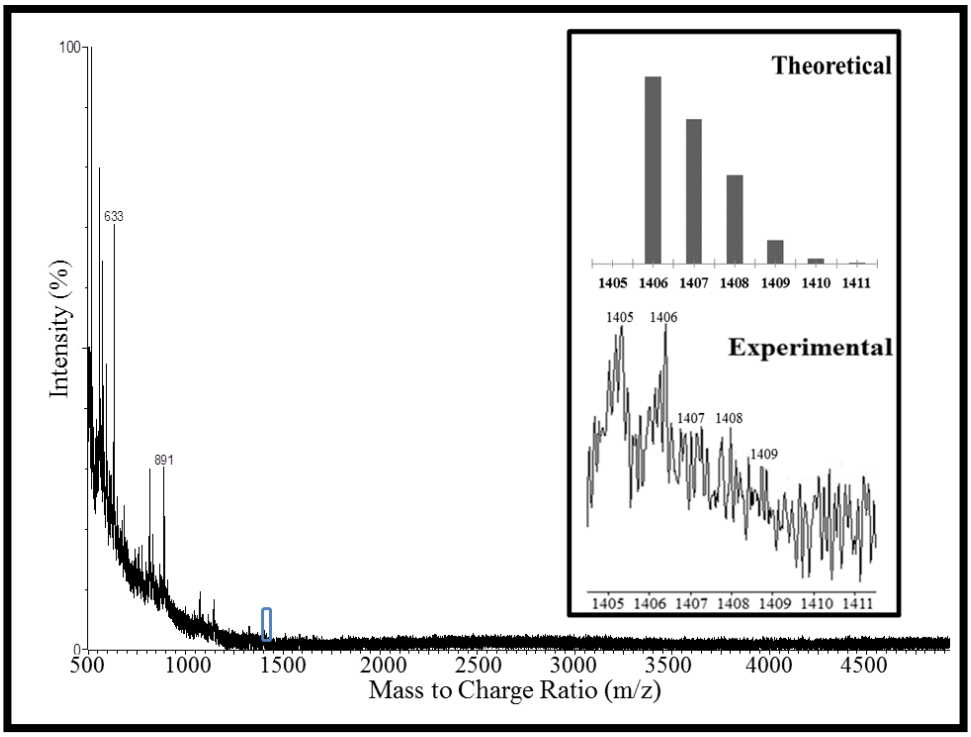

Figure 5-15 MALDI-TOF spectra of pre-PGS (68.18% DE-CH) depict the maximum oligomers mass at 1405 m/z which is well-fitted with the theoretical spectra created by the software, i.e. GSGSGSGSGSG, $[C_{68}H_{118}O_{28}Na]^+$.

Previous studies reported that a range of possible oligomers could only be produced from the reactants glycerol and sebacic acid when tuning their ratio.[181] Surprisingly, different PGS structures (*e.g.* branched/heavily crosslinked or linear) can be obtained by only changing the heating method while maintaining a constant stoichiometric ratio of glycerol to sebacic acid (1:1) here. Overall results obtained from NMR and MALDI-TOF spectra suggest that the microwave promotes the formation of branching oligomers in pre-PGS (detailed structure is represented in Figure 5-10). Naturally, the primary alcohol group is likely to react with the carboxylic acid group to generate polymer linear chains, while the secondary alcohol group facilitates the branching. Microwave can produce a polymer with higher molecular weight,[182] thus, it very likely activates both secondary and primary alcohol groups simultaneously due to their similar polarity which couples well with MI. Therefore, at low DE, MI prefers branching in different directions while CH is likely to form a shorter chain prior to the curing process.

5.3.4 Morphology of crosslinked PGS samples

After curing the pre-PGS in the vacuum oven, a significant reduction in the intensity of the hydroxyl band was observed, as seen in Figure 5-16. In order to investigate the effect of the heating method on the surface morphology, SEM images of both appearance and cross section of the samples were obtained (Figure 5-17***)***. For the internal structure analysis, the specimens were fractured in the liquid nitrogen instead of cutting with a blade to prevent smearing. The SEM images show a smooth topography for the surface of either PGS samples and MI does not alter the morphology of PGS since all the crosslinked specimens show a similar morphology. This morphology also suggests that the pre-PGS samples are free of solvent (toluene) due to complete removal of solvent before the curing process, which is very crucial prior to use in bio-applications (also justified by the ^{1}H NMR results, Figure 5-11).

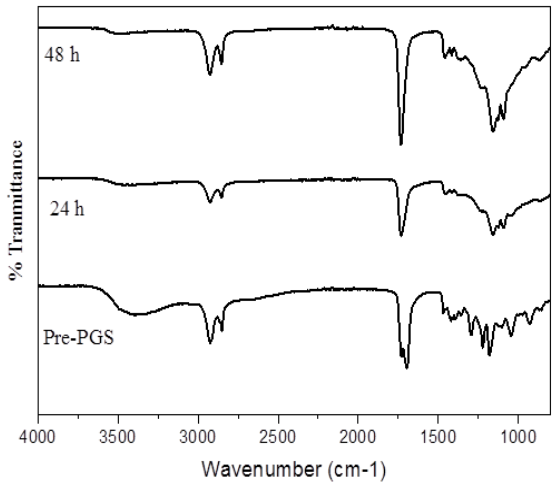

Figure 5-16 ATR-FTIR spectra of prepolymer and crosslinked PGS after 3 minutes of microwaving and then followed by 24-48 h of curing.

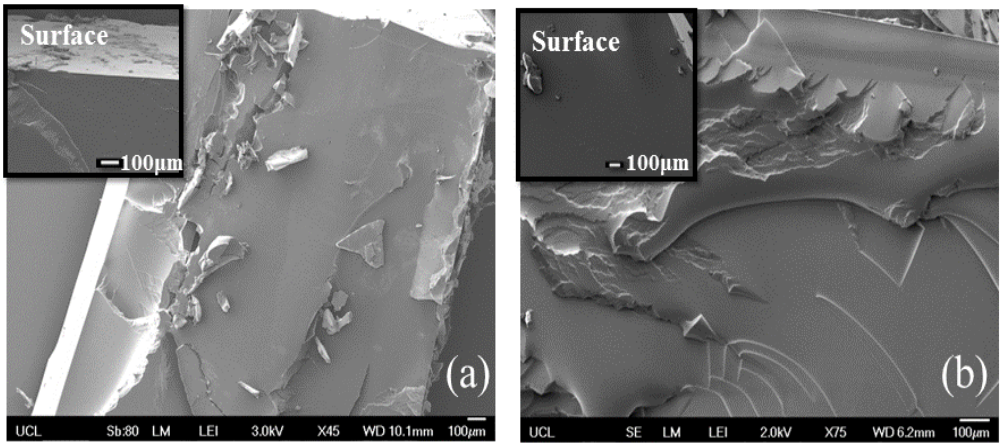

Figure 5-17 Cross section and surface (inserted) morphology of crosslinked PGS specimens where (a) 66.82%-MI, (b) 68.18%-CH after 24h curing in vacuum oven. These crosslinked specimens show similar morphology in microwave irradiation and conventional heating methods.

5.3.5 Optimization of curing time and its mechanical properties

To further discover the effect of branched pre-PGS on curing time and mechanical properties, similar DE (ca. 70% DE) of pre-PGS was used and further cured in the vacuum oven from 2-48 h. By reducing the curing time to 2 hr, PGS specimens prepared by MI (DE=66.82%) show faster toughening compared with CH samples (DE=68.18%) – can be seen in Figure 5-18. The PGSs samples cured with a shorter time were characterised by IR spectra, the ester linkage is found with a reduction of hydroxyl bond from time to time- as seen in Figure 5-18. This may be due to the branched pre-PGS samples, produced by MI, requiring a shorter curing time to form stiff polymer. On the other hand, the pre-PGS prepared by CH method needs at least 4 hr of curing time to produce a stiff polymer. It can be concluded that higher branching of pre-PGS achieved by MI facilitates the formation of crosslinked PGS in a very short curing time.

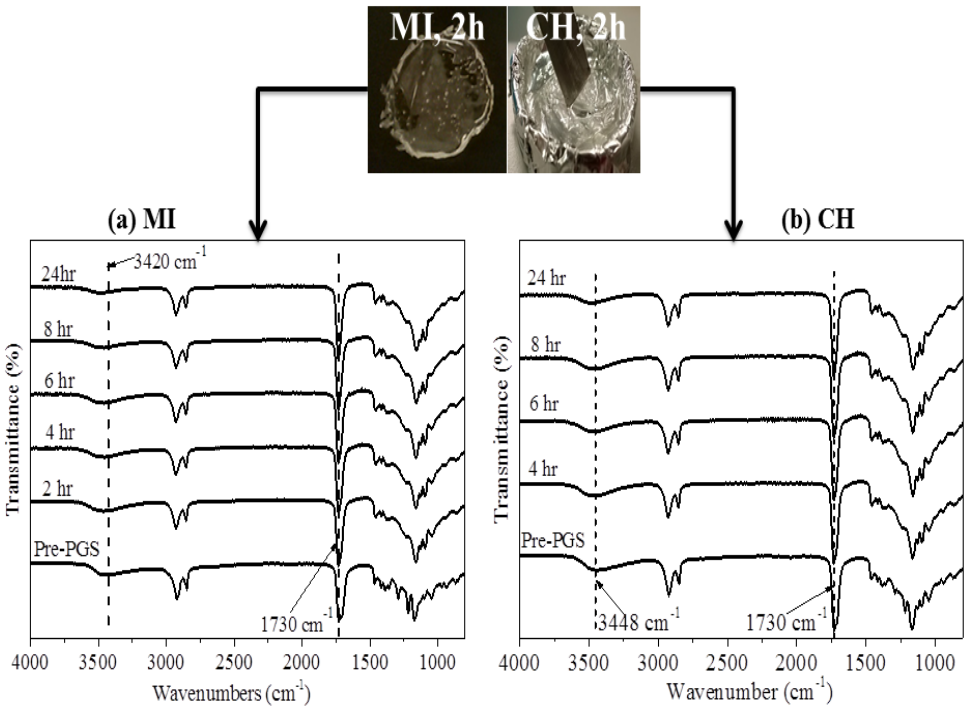

Figure 5-18 ATR-FTIR spectra of PGS (ca. 70% DE) that prepared by (a) single mode MI and (b) CH method before and after curing in the vacuum oven for 2-24 h.

The Young's modulus of the specimens (after 48 h curing) fabricated in this study by both MI and CH methods is at least 50% higher without changing the molar ratio of glycerol and sebacic acid as compared to the previous results.[8,166,183,184] This is probably due to our modified synthetic procedure in which the unreacted glycerol was removed from the bulk pre-PGS prior to the curing process. Consequently, the remaining sebacic acid probably only functions as a crosslinking agent and thus produces a stiffer polymer. This novel preparation approach proposes that PGS with a broad range of stiffness can be produced without an additional crosslinking agent, but by simply adjusting the degree of esterification and curing time. This highly toughened PGS may also improve the cytocompatibility of PGS.[9]

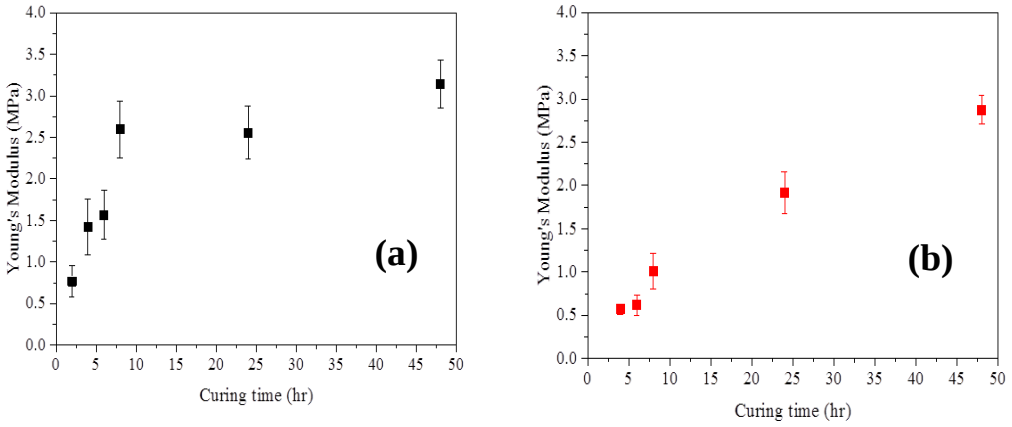

Figure 5-19 Young's modulus (MPa) of crosslinked PGS (ca. 70% DE) prepared by (a) MI and (b) CH method, respectively (n≥ 6). The pre-PGS samples were pre-polymerised at a predetermined degree of esterification before curing for 2-48 h in the vacuum oven.

The mechanical properties of crosslinked PGS (Figure 5-19**,** Figure 5-20 and Figure 5-21) that were prepared by both methods are clearly different. As the curing time increases, the Young's Modulus of these specimens is increased but at a different step (Figure 5-19). The Young's modulus of PGSs by MI after 8 h curing is equivalent to that achieved in 48 h by CH, thus MI reduces the curing time by a factor of six, similar results to that observed in the pre-polymerisation process. The Young's modulus of PGSs by MI after 8 h curing is increased from 0.77 ± 0.19 to 2.60 ± 0.34 MPa (a window of 1.83 MPa) and elongation at break is reduced from 53.41 ± 7.14 to 27.73 ± 1.87 %. On the other hand, PGSs synthesised by CH at a similar curing time have a smaller Young's modulus, ranging from 0.57 ± 0.06 MPa to 1.01 ± 0.21 MPa (a window of 0.44 MPa) and elongation at break is from 64.07 ± 10.71 to 48.72 ± 6.51 %. The ultimate tensile strength of these PGS samples fabricated is depicted in Figure 5-21, from 0.26 ± 0.07 to 0.46 ± 0.06 MPa for MI's samples and from 0.22 ± 0.03 to 0.35 ± 0.08 MPa for CH's samples. The Young's modulus of these PGS specimens prepared by MI method and followed by 48 h of curing time is slightly higher than the one prepared by CH method (i.e. 3.14 ± 0.28 MPa and 2.87± 0.17 MPa for MI and CH, respectively).

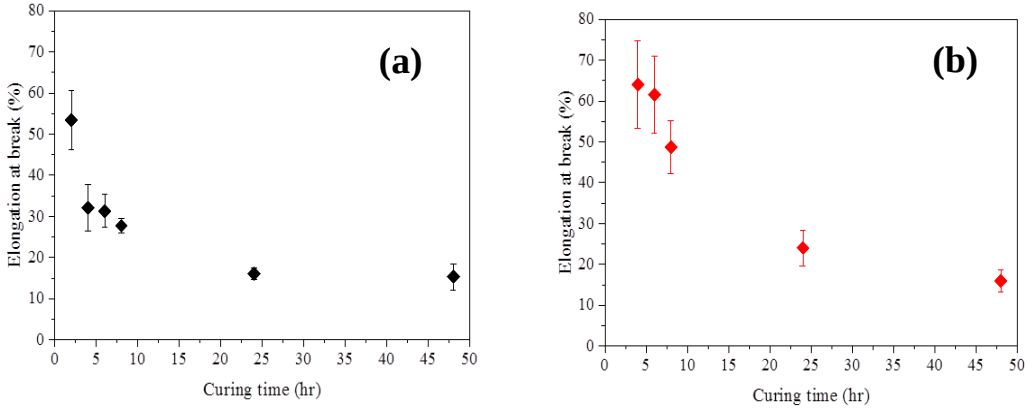

Figure 5-20 Elongation at break of crosslinked PGS (ca. 70% DE) prepared by (a) MI and (b) CH method, respectively (n≥ 6). The pre-PGS samples were pre-polymerised at a predetermined degree of esterification before curing for 2-48 h in the vacuum oven.

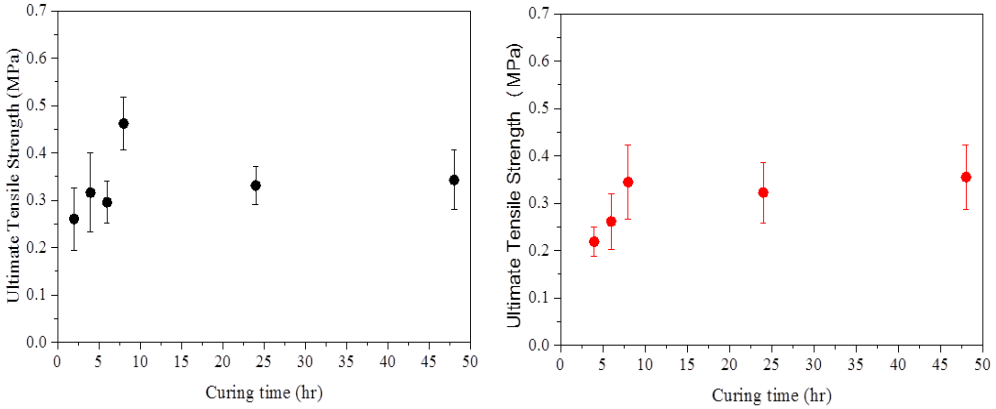

Figure 5-21 Ultimate tensile strength of PGS (ca. 70% DE) prepared by single mode MI (left) and CH (right) followed by a different curing period (2-24 h) (n≥ 6).

As stated in previous studies, the extent of crosslinking affects the properties of a polymer significantly.[185–187] A weak and soft polymer is produced at a low crosslink density. On the other hand, a stronger and stiffer polymer can be formed at higher crosslink density. These polymers would have different bio-applications. In this study, MI speeds up the curing process significantly and the CH method can produce PGS with similar mechanical properties only if the curing time is sufficiently long. Therefore, the Young's modulus of PGSs prepared by MI can be tuned easily, where a larger range of Young's modulus can be obtained (i.e. three times wider) with a short curing time as compared to

CH. This is because a higher degree of branching pre-PGS has been synthesised by MI rather than a linear pre-PGS by CH.

5.3.6 Degradation of PGS

As mentioned in Chapter 2.3.1, degradable polymers are widely studied either as implants or drug carriers because no surgical removals are needed. The surface erosion or degradation rate of PGS is highly important for its application. For instance, when using PGS as drug carriers, the controlled drug release is primarily dominated by diffusion and solubility of drugs, and followed by the degradation rate of the polymer.[188] Therefore, the degradation rate of the PGS could predict the drug release rate.

The surface erosion mechanism undergone by PGS is ideal for many drug delivery applications due to a slow water permeation rate and water-vulnerable drugs can be protected.[189] Degradation of PGS is a hydrolytic process where the ester bonds in the polymer chains react with water molecules, resulting in shorter chains via the surface erosion process. The degradation occurs within a region near the surface and provides linear changes in mechanical performance because the surface erosion happens much earlier than that in the bulk of the sample.[190] According to Wu *et al.*, initial porosity and pore size affected the degradation rate due to a variation of diffusion rate.[191] However, PGS samples produced herein have similar morphology (see SEM images, Figure 5-17), so it is not a dominating factor for the degradation rate of PGSs in this study.

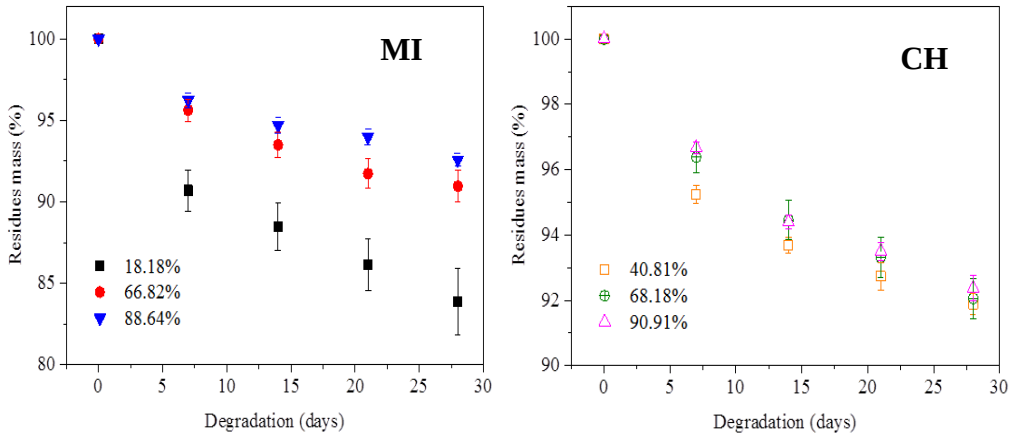

Figure 5-22 Degradation profile of PGS [pre-polymerised by MI and CH method and then cured for 24 h] in phosphate buffered solution at pH 7.4, 37 ˚C for 28 days (n≥ 5).

Degradation properties of PGS specimens were soaked in phosphate buffered saline (PBS) medium at pH 7.4, 37˚C for 28 days. Based on the literature, more than 70% of mass in the PGS samples were degraded *in vivo* and mass loss was reduced linearly.[93] Thus, the mass loss of PGS specimens were observed for 28 days as an preliminary results, demonstrating the effects of the heating methods on the degradation rate.

Firstly, the PGS specimens with a different degree of esterification (ca. 18-90%) but the same curing time of 24 h were investigated (Figure 5-22). The degradation rate of PGS samples prepared by both methods decreases fast initially and then reaches a linear mass loss. With an increment in DE of pre-polymers, the degradation rates of all samples are decreased. The residual mass of the PGS specimens by MI method (ca. 18.18% DE) after 28 days is 83.88 ± 2.02 % (16.12 % degraded) and the residues mass of PGS with 66.82 % DE is 90.96 ± 0.96 % (9.04 % degraded). For CH method, the residual mass of PGS samples are 91.89 ± 0.32 % for 40.81% DE and 92.56 ± 0.24% for 68.18% DE, i.e. these samples degrade less than 10 %. When reaching ca. 90% DE, the PGS samples degrade slowest (only 6.20-7.42 % degraded) and the residual mass are 92.58 ± 0.40 % and 93.80 ± 0.40 % for MI and CH, respectively.

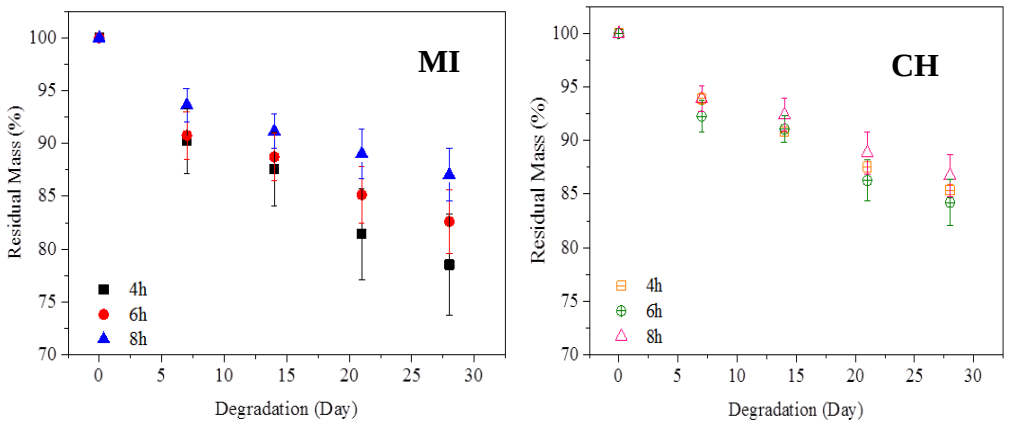

Figure 5-23 Degradation rate of crosslinked PGS at 70% DE (pre-polymerised by MI and CH method and then cured for 4-8 h) in phosphate buffered solution at pH 7.4, 37 ˚C for 28 days (n≥ 5).

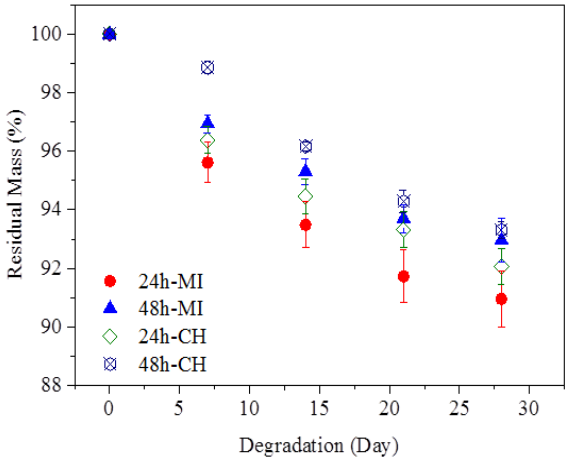

Figure 5-24 Degradation profile of PGS (ca. 70% DE)prepared by single mode MI and CH after 24-48 h curing process in phosphate buffered solution at pH 7.4, 37 ˚C for 28 days (n≥ 5).

Secondly, the PGS samples with similar DE (ca. 70 %) but different curing time were also tested. As illustrated in Figure 5-23, PGS specimens prepared by MI show a broader range of degradation profile compared to CH samples. After a long curing time (≥ 8h), MI samples show a similar degradation profile to the CH samples where both degrade to approximately 87 % (ca. 13% mass loss). Interestingly, when reducing the curing time to 4 and 6 h, the degradation rate of sample prepared by MI changes significantly while only little effects on the CH samples. For instance, after 4 h curing time, the residual mass of MI sample is 78.54 ± 4.76 % (21.46% degraded) compared to 85.37 ± 0.58 % of CH sample

(14.63 % degraded). On the other hand, by further increasing the curing time to 24-48h, the PGS samples by both methods show a slow and comparable degradation rate while the residual mass is above 90 %, shown in Figure 5-24.

Based on these degradation results, it can be found that the branched structure of PGS samples prepared by MI method provide a wider degradation rate window compared to the PGS samples prepared by CH with similar DE. In other words, the polymers prepared by MI show a degradation rate that ranged from 90.96 % to 78.54 % (a window of 14.42%), but those by CH are from 93.31 % to 84.24 % (a window of 9.07%). Thus, MI provides approximately 59% wider degradation window as compared to CH. The larger and controllable degradation rates enable more flexible drug delivery. A branched structure produced by MI method can give rise to a rapid hydrolytic cleavage due to more terminals which are attacked by water during degradation compared to a linear structure prepared by CH method.[192] In both methods, the increment in curing time or DE generally decreases the mass loss of PGS samples. This is because the pre-polymerisation and curing process both increase the number of ester bonds needed to be broken via surface erosion. Therefore, PGS with lower DE or shorter curing time degrades faster due to a lower number of ester bonds to be cleaved. On the other hand, the PGS prepared by both methods at similar DE but longer curing time (> 8h) shows a similar degradation rate (residual mass > 90%). This is due to the DE being able to reach a saturated point. As a result, the number of ester bonds to be broken is comparable. Therefore, the degradation rate does not alter much at this stage.

5.4 Conclusion

MI procedures have been demonstrated to prepare pre-PGS by introducing the low boiling point solvent which improve the reproducibility and reduce the evaporation of monomers. It also offered a well-control over temperature, homogeneous temperature medium and ease to manipulating the degree of

esterification. In addition, the degree of esterification of pre-PGS was finely tailored by collecting the condensed water which was crucial to control the mechanical properties and degradation rate.

Firstly, the pre-PGSs have been prepared by single mode and multimode MI. The single mode MI has been proven to be more energy efficient than multimode MI with a high degree of flexibility to tune PGSs Young's modulus and elongation at break. Secondly, the pre-PGSs were then compared in between single mode MI and CH method. MI dramatically sped up both pre-polymerisation and curing processes due to fast and selective heating mechanism. The degree of esterification of pre-PGS could also be easily controlled by single mode MI which strongly affected the polymer properties (e.g. degradation rate and mechanical strength). Moreover, the highly branched pre-PGSs were fabricated (proven by NMR and MALDI-TOF spectra) using single mode MI method without changing the molar ratio of glycerol and sebacic acid. In addition, by using this proposed strategy, the Young's Modulus of PGS (from 0.77 ± 0.19 to 3.14 ± 0.28 MPa) increased by 50% when compared to the reported literature.[8,166,183,184] These PGS samples prepared by single mode MI also reduced the curing time where a stiffer polymer was produced after 2 h curing in the vacuum oven while at least 4 h were required for CH sample. In addition, pre-polymer samples (DE = 66.82 %) of the single mode MI method cured for only 8 h showed Young's Modulus comparable to the one prepared by CH method and cured for 48 h.

For the degradation test, degree of esterification and curing time affected the degradation rate significantly. This is because these two factors strongly control the degradation rate of PGSs due to the increment of ester linkage that needed to be cleaved. The highly branched pre-PGS fabricated by single mode MI provided 59% wider window for degradation compared to the linear chain yielded by CH.

In total, the new microwave approach provided a higher degree of freedom to tune mechanical properties (threefold) and degradation rate (59%) in order to

meet demands of various applications such as drug delivery vectors which highly depend on the degradation rate of the polymer. This performance of the PGS polymer will be further optimised in the chapter 7.

6. Enhanced Biocompatibility of Poly(glycerol sebacate) Using β-Tricalcium Phosphate Particles via Microwave Synthesis

As mentioned in chapter 2.3.5, the main drawback of the poly(glycerol sebacate), PGS, is the cytotoxicity issue which is closely related to the degraded acid. By controlling the degree of crosslinking, the cytotoxicity can be minimized since the degradation rate is reduced. However, this may affect the hydrophilicity of the PGS which is preferable for cell adhesion and proliferation. In this chapter, β-tricalcium phosphate (β-TCP) particles will be used to mitigate this problem where the presence of these particles can reduce the degradation rate without reducing the hydrophilicity of PGS.

6.1 Introduction

As a synthetic polymer, biocompatibility of PGS is still an issue which is the bottleneck of this polymer. The cytotoxicity of the PGS strongly relies on its degradation rate, the carboxylic acids produced by aqueous hydrolysis of the PGS and decreases the local extracellular pH value to below physiological values.[167] The increment in the acidity of the surrounding environment can easily provoke cell death. Therefore, many studies have been performed to improve the biocompatibility of PGS which is challenging as determined by a group of factors, e.g. degradation rate, surface hydrophilicity, degree of crosslinking and swelling effect. Adding particles such as bioglass,[101] silica,[103,104] or cellulose[105] in the polymer matrix was proved to increase the degree of crosslinking and reduce the degradation rate, which would dominate cell viability on polymer matrix.

On the one hand, the surface state of a polymer plays a critical role in its bio-application, which can affect the cell proliferation. Specifically, polymer's biological performance can be enhanced by changing its surface topographical (i.e. roughness) or chemical/physical characteristics (i.e. hydrophilicity).[193] PGS surface could be hydrophobic or hydrophilic which depends on the experimental

conditions. When increasing the molar ratio of sebacic acid to glycerol, the surface becomes more hydrophobic, probably due to the reduced amount of hydroxyl backbone which reacts with carboxylic acids to form the ester linkage.[194,195] Therefore, there is a dilemma between a hydrophilic surface and a high degree of crosslinking, and both are highly desirable for a biopolymer.

On the other hand, calcium phosphate ceramics are generally used to improve the biocompatibility of other biomaterials by coating a layer of calcium phosphate on the surface of bioinert or bioactive material, since they are low toxicity, excellent biocompatibility and osteoconductive biomaterials.[196] Among these calcium phosphates, β-tricalcium phosphate (β-TCP) is more attractive due to its high biocompatibility, biological safety, ease of sterilization, and long shelf life.[67] More importantly, β-TCP has proven its osteogenic properties pre-clinically.[68]

Given advantages of both PGS and β-TCP, PGS has been modified with β-TCP particles by microwave synthesis approach herein, which has recently shown a great potential to synthesise materials due to its fast reaction rate, high reproducibility, improved product selectivity and yields.[112,170,197] Such biocomposites alter the morphology, degree of crosslinking and hydrophilicity of PGS, leading to a dramatically enhanced biocompatibility. The prepared samples were also investigated in cell viability, which further proves the advance of the new biocomposite. This work was in collaboration with Dr Mustafa Alqaysi and Nazanin Owji from Eastman Dental Institute UCL, where they provided the cell viability data.

6.2 Methodology

6.2.1 Material synthesis

After successfully preparing the β-tricalcium phosphate particles and poly(glycerol sebacate), the composite of these two biomaterials were synthesised

via preparation. In the beginning, the PGS was prepared following the methods in chapter 5 and then put into the precursor of β-TCP to form these particles.

For the PGS synthesis, equimolar of glycerol (99%, Sigma Aldrich) and sebacic acid (>99%, Sigma Aldrich) were mixed in a round bottom flask and heated in Discover SP microwave for 12 minutes (4 x 3 mins per cycle) under nitrogen gas. A cooling interval was introduced after every single cycle to minimize the overheating of monomers and increase the microwave efficiency. The pre-polymer was then cured in a vacuum oven at 120 ˚C for 8 h.

For preparation, calcium acetate monohydrate (≥99%, Sigma Aldrich) and phosphoric acid (≥98%, Acros Organics) were weighed and dissolved each in 20 mL of methanol (≥99.8%, Sigma Aldrich). The acid solution was added drop-wisely into the calcium solution and then transferred to a sealed PTFE vessel. The prepared PGS was then added into the vessel, followed by the irradiation in a microwave (MARS, CEM Company). The reaction mixture was ramped for 25 mins to the pre-set temperature ranged from 120-180 ˚C for 5-60 mins, where 60 mins were required for all temperatures except 180 ˚C at which only 5 mins was needed. PGS/β-TCP biocomposites were then removed from the vessel and washed with deionised water several times. Lastly, the biocomposite was dried in the drying oven at 60 ˚C overnight, denoted as PGS/β-TCP120, PGS/β-TCP150 and PGS/β-TCP180, depending on the reaction temperature.

6.2.2 Characterisation

Fourier Transform Infrared Spectroscopy

The functional groups of the prepared biocomposite were confirmed using a Perkin-Elmer 1605 FT-IR spectrometer in attenuated total reflection (ATR) mode with a frequency range of 400-4000 cm^{-1} at 4 cm^{-1} resolution.

X-ray Diffraction Spectroscopy

The synthesised calcium phosphate particles by microwave approach at different temperature were identified using Powder X-ray Diffractometer (Bruker D8 Advance Diffractometer, Bruker, UK) with a CuK_{α} (λ = 0.1541784 nm) radiation

source. Diffraction patterns were collected from 10˚ to 80˚ and a maximum step size of 0.05˚ with 5 seconds per step was applied. These diffraction patterns were compared with the standard spectra from the JCPDS database.

Raman Spectroscopy

Raman spectra data of the synthesised PGS/β-TCP biocomposites were acquired using a Renishaw Raman Microscope with a helium-neon laser at a wavelength of 514.5 nm and 10 scan numbers.

Surface morphology

In order to observe the morphology of prepared PGS/β-TCP composite, SEM (XL 30, Philips, Eindhoven, Netherlands) was operated at 5-10 kV and a working distance of 10 mm. Due to low conductivity of the samples, a layer of Au was coated on the surface of the samples before the SEM observation.

Sol/gel content analysis

The degree of crosslinking of the specimens was determined by sol (uncrosslinked network) and gel (crosslinked network) content analysis. The specimens were weighed (W_i) and then submerged in tetrahydrofuran for 24 h. The swollen samples were dried overnight and the final weight (W_f) was measured. The percentage of sol content (%) was calculated using Equation 6-2 and 6-2:

$$Sol\ (\%) = \frac{W_f - W_i}{W_i}\ x100\% \qquad \text{Equation 6-1}$$

$$Gel\ (\%) = 100\% - Sol(\%) \qquad \text{Equation 6-2}$$

Where $W_{initial}$ is the initial weight of the specimens and W_{final} is the residual mass of the specimens at the pre-set time. Gel (%) content was the residuals percentage.

Hydration properties

Hydration properties of specimens were evaluated from the swelling ratio and contact angle measurement. For the swelling study, samples were weighed (W_i) and then submerged in phosphate buffer saline (PBS) at 37 ˚C for 48 h. The

excess water was drained and the weight of the swollen sample (W_s) was measured. The swelling ratio was calculated using Equation 6-3-3:

$$Swelling\ ratio = \frac{W_s}{W_i} \qquad \text{Equation 6-3}$$

Surface hydrophilicity was determined by water contact angle analysis. The contact angle measurements of the samples were obtained with a goniometer (Cam 200, KSV Instruments Ltd). A drop of 10 μL size of water was dripped onto the sample surface. The mean value of the contact angles was calculated by the Cam2008 software (KSV Instruments Ltd) on three specimens.

6.2.3 Degradation study

Five or more specimens with a dimension of 5 x 5 mm^2 were stored in the standard phosphate buffer saline (PBS, 1X) at 37 ˚C. The samples were collected after 7, 14, 21 and 28 days. After degradation, the sample was washed thoroughly with deionised water to remove traces of soluble degradation products, salts or other impurities and dried under vacuum conditions at 60 ˚C until constant weight. The percentage of mass loss (%) was calculated using Equation 6-4:

$$Mass\ loss\ (\%) = \frac{W_{initial} - W_{final}}{W_{initial}}\ x100\% \qquad \text{Equation 6-4}$$

Where $W_{initial}$ is the initial weight of the biocomposites or PGS and W_{final} is the residual mass of the biocomposites or PGS at the pre-set time.

6.2.4 Cell Culture Study

The cell culture study was collaborated with Mustafa Alqaysi and Nazanin Owji from Eastman Dental Institute. Human mesenchymal stem cells (hMSCs) (passage 3) were used for this cell culture studies. Initially, cells were incubated for growing at standard condition (37°C, 95% air, 5% CO_2, 95% relative humidity) in Dulbecco's modified Eagle medium (DMEM, Gibco, Life

Technologies, Paisley, UK) supplemented with 10% fetal bovine serum (Gibco) and 1% penicillin/streptomycin (PAA Laboratories, GE Healthcare, Chalfont St. Giles, UK). When cell confluency percentage reached 80%, they were trypisinsed and ready for seeding on the prepared samples. PGS and its biocomposites were sterilised by UV light exposure for 20 minutes before the seeding process.

A triplicate of specimens was used for this study. hMSCs were initially seeded at density of 15000 cells/polymer in 24 well plates. Seeding was undertaken by pipetting out the intended cell density in 10 uL of culture media on the polymer. Then they were kept in the incubator for 1 hour to ensure cell attachment on the polymers. 1 ml of culture media was added to each polymer. Culture media was changed every three days.

A Cell Counting Kit (CCK) assay was carried out in three-time points (day 1, 4 and 7). At each time point 10% of the assay reagent was added to the sample and incubated for 1 hour. Subsequently, fluorescence measurement was taken for each well plate and this measurement was repeated three times by using wavelength detector (Infinite® M200, Tecan) at 450 nm wavelength.

Blank wells were used in a control experiment. A calibration curve was obtained by seeding the cells in different cell densities and fluorescence was measured for each cell density. Fluorescence absorbance was correlated with cell number which generated a calibration curve and an equation that was accordingly used for indirect cell counting.

6.3 Results and Discussion

Calcium phosphate particles prepared by microwave at different reaction temperatures and times were characterised by X-ray diffraction (XRD) spectroscopy, as illustrated in Figure 6-1. The phase of the synthesised calcium phosphate matches with the standard diffraction pattern of β-TCP (JCPDS #09-0169).[198] The phase of the calcium phosphates does not alter with the reaction temperature and reaction time in the microwave. This is because the formation of β-TCP relies on the solvent species in which the solubility of both calcium and

phosphate precursors affects the final phase of the calcium phosphates.[135] The characteristic Raman peaks associated with β-TCP are often observed at a few regions: symmetric P-O stretching vibrations (ν_1:960 cm^{-1}), anti-symmetric P-O bending vibrations (ν_4: 650-400 cm^{-1}), and anti-symmetric P-O stretching vibration (ν_3: 1010-1090 cm^{-1}).[199,200] From the Raman spectra of β-TCP (Figure 6-2), the peaks are also comparable with the literature, showing the symmetric P-O bending (ν_2), anti-symmetric P-O bending (ν_4) and symmetric P-O stretching (ν_1) around 400-460 cm^{-1}, 560-610 cm^{-1} and 950-970 cm^{-1}, respectively.[200]

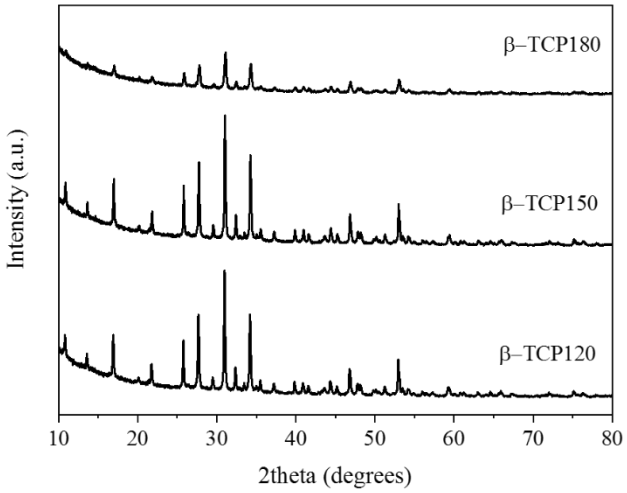

Figure 6-1 XRD of β-TCP particles prepared at different reaction temperature and reaction time, where the reaction time is 60 minutes at 120˚C and 150 ˚C, while only 5 minutes at 180 ˚C. These diffraction patterns are matched with standard peak in β-TCP (JCPDS #09-0169).

For PGS, ATR-FTIR analysis (Figure 6-3) was used to confirm the formation of ester bonds, indicated by an intense peak at 1735 cm^{-1}. The two absorption peaks around 2928 and 2855 cm^{-1} are attributed to the methylene group and the broad peak observed around 3400-3600 cm^{-1} is due to hydrogen bonded hydroxyl groups.[101] For the Raman spectra of PGS, there are no significant peaks found at the range between 200-1000 cm^{-1}(Figure 6-2).

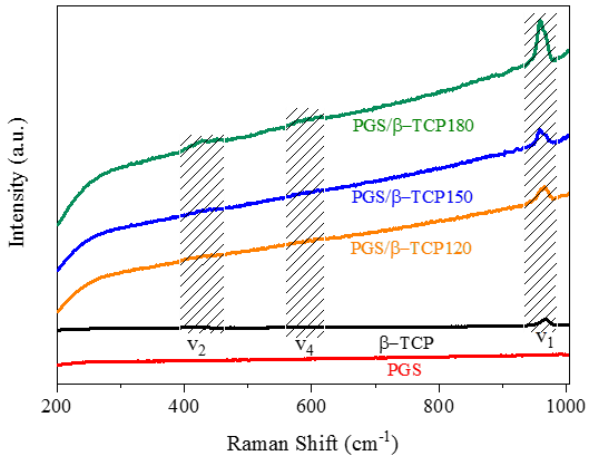

Figure 6-2 Raman spectra of PGS/β-TCP biocomposite prepared at 120-180 ˚C with 5-60 mins in the microwave, compared with single material of PGS and β-TCP.

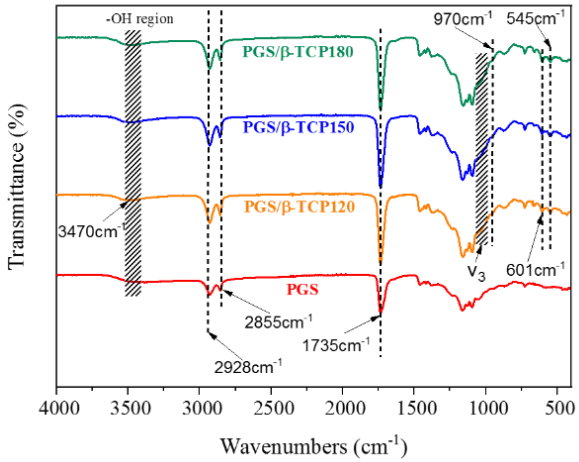

Figure 6-3 IR spectra of the PGS/ β-TCP biocomposites and further compared with PGS.

The prepared biocomposites (i.e. PGS/β-TCP120, PGS/β-TCP150 and PGS/β-TCP180) were then characterised by Raman (Figure 6-2) and ATR-FTIR (Figure 6-3) spectroscopy. Similar to the PGS, ester linkage at 1735 cm^{-1}, methylene group at 2928 and 2855 cm^{-1}, and broad hydroxyl group at around 3400- 3600 cm^{-1} are observed. Apart from IR spectroscopy, these biocomposites were characterised using Raman spectroscopy. Additional peaks corresponded to the P-

O bond of the β-TCP are also found in these biocomposites. Based on the Raman spectra of the PGS/β-TCP biocomposite, the peaks around 400-460 cm^{-1}, 560-610 cm^{-1} and 950-970 cm^{-1} correspond to symmetric P-O bending (ν_2), anti-symmetric P-O bending (ν_4) and symmetric P-O stretching (ν_1), respectively.[200] Both IR and Raman spectra prove that the β-TCP particles are incorporated within PGS.

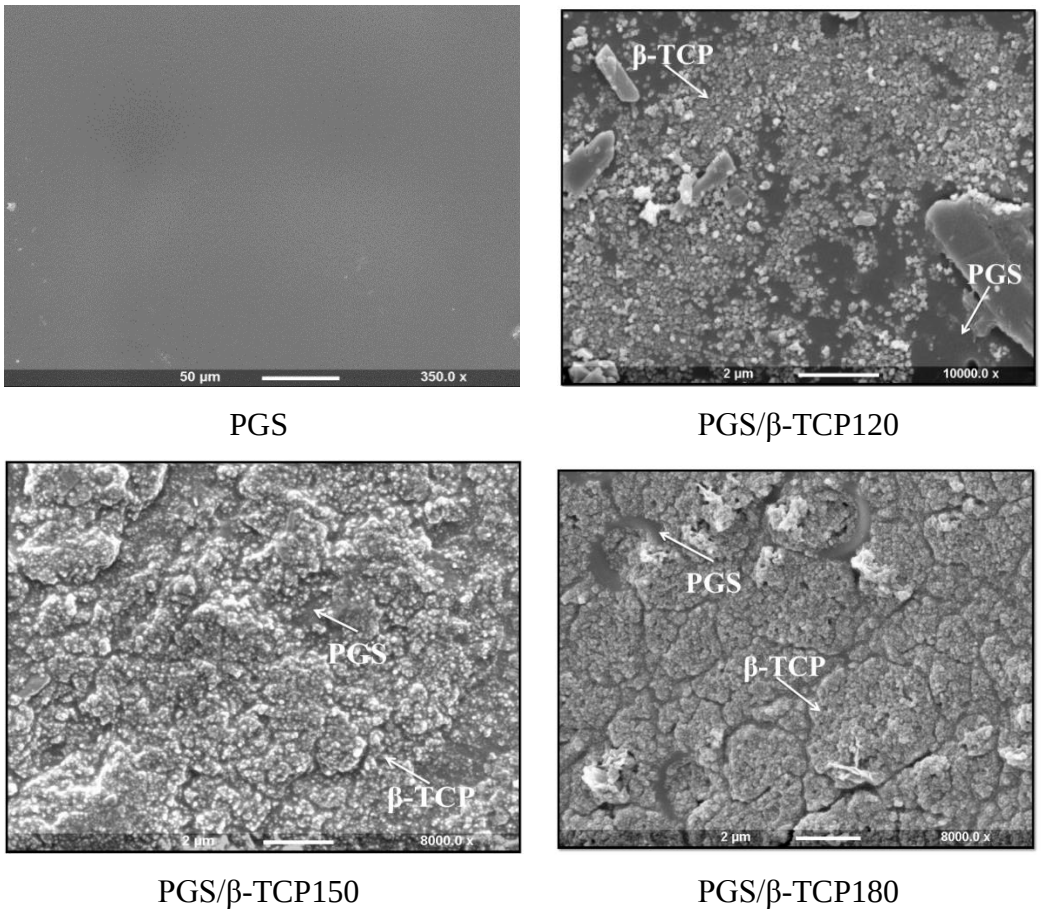

PGS PGS/β-TCP120

PGS/β-TCP150 PGS/β-TCP180

Figure 6-4 SEM images of the PGS and its biocomposites prepared at different microwave temperature. PGS was incorporated with β-TCP particles and varied with the smooth surface of PGS.

SEM images of the PGS and its biocomposites (Figure 6-4 a-d) reveal the spherical β-TCP particles with a dimension of 50-190 nm distributed on the surface of PGS (Figure 6-5). The surface condition the biocomposites changes significantly when compared to PGS. The surface of PGS is generally smooth (Figure 6-4) and the presence of β-TCP particles results in an uneven/rough

surface as illustrated in Figure 6-4. Furthermore, higher temperature allows more particles to be attached in the PGS. As seen in the Figure 6-4(b), PGS/β-TCP prepared at low temperature (120˚C) has lesser β-TCP particles while agglomerated on its surface. On the other hand, PGS/β-TCP150 and PGS/β-TCP180 biocomposites have much better incorporation of the β-TCP particles into PGS (Figure 6-4 (c-d)). However, when comparing PGS/β-TCP150 and PGS/β-TCP180 biocomposites, β-TCP particles tend to agglomerate in the PGS polymer when the temperature is higher than 150 ˚C. On the other hand, PGS/β-TCP150 demonstrates a more homogeneous layer of β-TCP particles on the surface of the biocomposite (refer Figure 6-5).

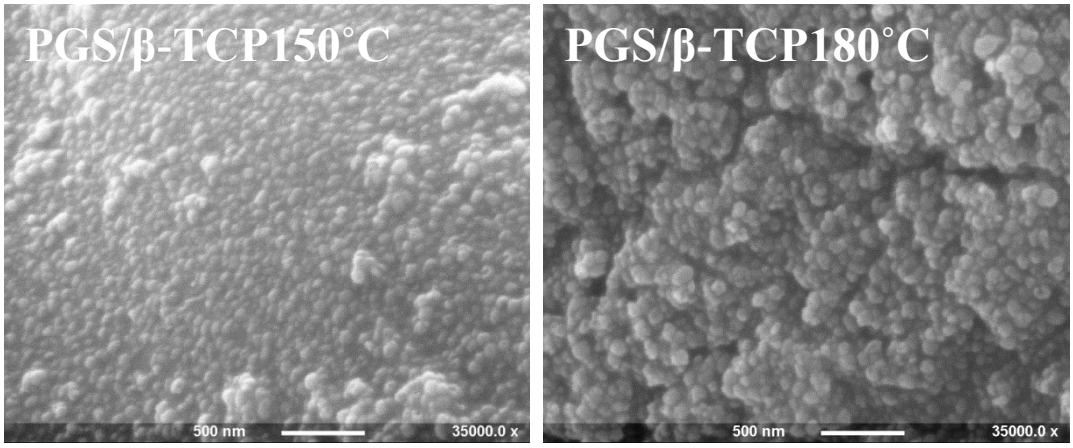

Figure 6-5 SEM images of PGS/β-TCP biocomposites prepared at 150 ˚C and 180 ˚C with 5-60 mins in the microwave.

Based on the XRD patterns, IR spectra, Raman spectra and SEM images, the biocomposites of PGS/ β-TCP were prepared successfully, where the presence of these β-TCP particles alters the morphology and surface conditions of the PGS. These altered surfaces would have different surface properties, changing their biocompatibility.

6.3.1 β-TCP particles improved surface properties of biocomposites

As mentioned above, the surface hydrophilicity of a biomaterial is crucial to cell adhesion and proliferation. Therefore, the surface of the biocomposites was

investigated by measuring the swelling ratio and contact angle. Figure 6-6 illustrates the swelling data for the PGS and its biocomposites. The swelling ratio of PGS/β-TCP150 increases by 8% to 1.16 ± 0.03 as compared to PGS which is only 1.07 ± 0.01, and followed by PGS/β-TCP180 which is 1.14 ± 0.01. PGS/β-TCP120 has comparable swelling ratio with PGS, also proving the lower incorporation of β-TCP particles in the PGS as seen in its SEM image (Figure 6-4). The incorporation of β-TCP particles stimulates the water uptake owing to the changes in the surface. The uneven surface increases surface area-to-volume ratios of the biocomposites and this also increases the amount of the absorbed water, which can affect the degradation rate.[201] Moreover, for PGS/β-TCP180, the agglomeration of β-TCP particles reduces the surface area-to-volume ratio, leading to lower swelling ratio when compared to PGS/β-TCP150.

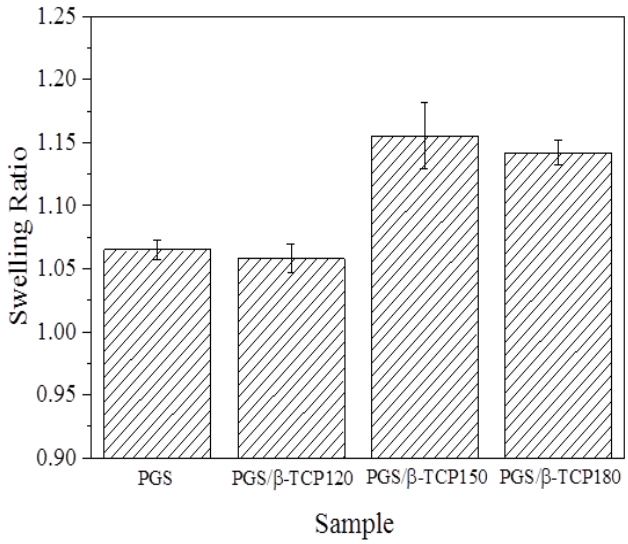

Figure 6-6 Swelling ratio of the PGS and its biocomposites at different reaction temperature and time in the microwave.

The contact angle of these specimens was also examined. As shown in Table 6-1, the contact angle of the PGS implies that the PGS surface appears to be hydrophilic. PGS/β-TCP150 and PGS/β-TCP180 exhibit a 14 % lower in contact angle compared with PGS (76.70 ± 2.30 °), indicating these biocomposites have a better hydrophilic surface. On the other hand, PGS/β-TCP120 has a comparable contact angle to PGS due to two separate phases instead of a composite. The

adding of the particles in the polymer can increase the degree of crosslinking but affects the hydrophilicity of the PGS.[194,195] In this study, the incorporation of β-TCP particles improves the hydrophilicity since these particles are hydrophilic.[202,203] These β-TCP particles can interact with water, like the hydroxyl backbone of PGS and create a hydrophilic surface, which is in agreement with a previous study.[204] On the other hand, the changes in the contact angle can be explained by Wenzel's equation: a larger surface area or a rough surface can reduce the contact angle of a hydrophilic surface since it increases the polar interaction with a water droplet, leading to a lower contact angle.[205,206] These properties could affect the degradation kinetics and cellular responses as water molecules at the interfaces affect cell adhesion and proliferation.[104]

Table 6-1 Contact angle of the PGS and its composite prepared at different reaction temperature and time in microwave.

Sample	Contact angle (˚)
PGS	76.70 ± 2.30
PGS/β-TCP120	72.95 ± 9.80
PGS/β-TCP150	65.65 ± 7.34
PGS/β-TCP180	65.95 ± 4.11

6.3.2 β-TCP particles enhanced degree of crosslinking of biocomposites

Other than the surface properties, the degree of crosslinking of bulk materials was determined via sol-gel content. Theoretically, the crosslinked part swells and the un-crosslinked part leaches out from the polymer in THF solution. Therefore, the remaining dry weight of the crosslinked network is used to determine the gel content of the biocomposite network. Figure 6-7 shows that sol content (un-crosslinked monomer) decreases when incorporating the PGS with β-TCP particles. For instance, the sol content of all biocomposites decreases by at least 66% as compared to PGS sample, which is 26.43 ± 4.10 %. All the biocomposites show a higher degree of crosslinking where the gel content is 91.07 ± 2.35 %,

91.75 ± 0.98 % and 93.41 ± 0.97% for the PGS/β-TCP 120, PGS/β-TCP150 and PGS/β-TCP180, respectively. This is because the incorporation of β-TCP particles in the polymer matrix can increase the degree of crosslinking.[103,104,101] This may be due to the electrostatic interaction between 'Ca^{2+} site bridging' mechanisms, i.e. negatively charged of unreacted carboxylic site ($-COO^-$) or the unreacted ($-OH^-$) presented on the surface of PGS binds to Ca^{2+} of β-TCP.[101]

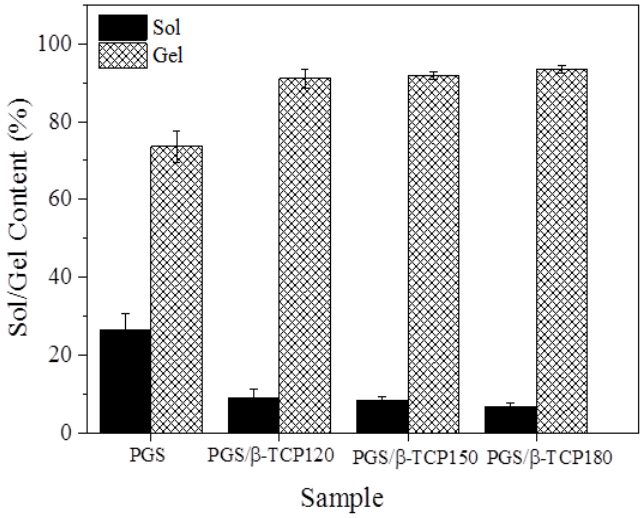

Figure 6-7 Effects of β-TCP particles on the degree of crosslinking which are determined by the sol-gel content. The presence of β-TCP particles increases the gel (crosslinked) content.

Degradation properties of biomaterials have significant effects on their application in tissue engineering as it should match with the rate of new tissue regeneration. Under physiological conditions, PGS degrades due to surface erosion via cleaving the ester linkage. The surface erosion is advantageous over bulk degradation since this type of erosion exhibits gradual loss in geometry in relation to mass loss.

Degradation of the PGS and PGS/β-TCP biocomposites were investigated under physiological conditions (PBS, 37 ˚C) for 4 weeks (Figure 6-8). From the results, apparently, the mass loss of the biocomposites reduces significantly when compared with PGS. After 7 days, the mass loss of PGS is the highest which is 8.84 ± 0.94% and maximum 3% for the biocomposites The similar trend is

observed after 28 days where the residual mass of PGS is less than 83% compared to all biocomposites (> 92%), indicating the biocomposite degrades slower than the PGS. On the other hand, the morphology of these degraded samples after 28 days was observed using SEM to examine the effect of degradation on their surface morphology. The images show that many evenly distributed β-TCP particles are still found on the surface of biocomposites, especially for those two prepared at higher temperature (i.e. PGS/β-TCP150 and PGS/β-TCP180) - as shown in (Figure 6-8), indicating such biocomposites undergo the same surface erosion mechanism which is mainly dominated by hydrolysis of PGS and these β-TCP particles are relatively incorporated into the polymer matrix.

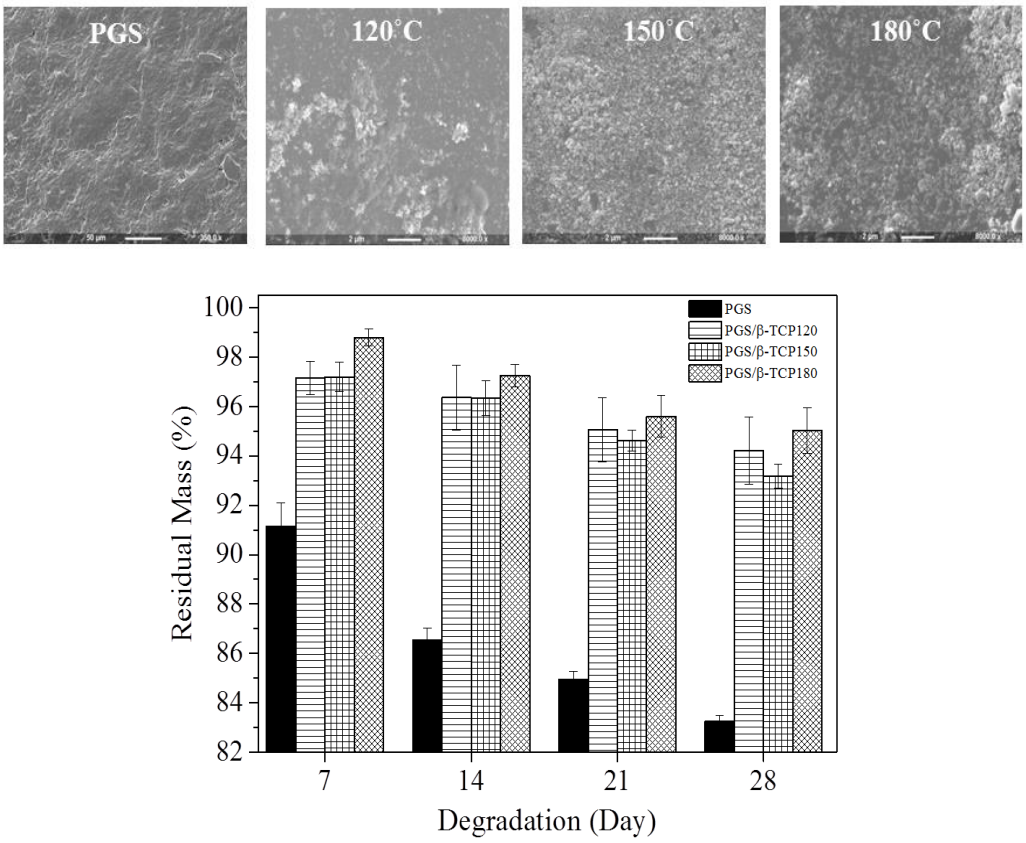

Figure 6-8 Degradation rates of the PGS and PGS/β-TCP biocomposites at day 7, 14, 21 and 28 days. The SEM images depicts the degraded samples at day 28 where lots of β-TCP particles still can be observed from the biocomposite surface.

The degradation rate of the biocomposites is slower than PGS owing to a higher degree of crosslinking as observed by the sol/gel analysis. Increase in the gel content indicates a higher degree of crosslinking, and the degradation rate is always inversely proportional to the degree of crosslinking. Therefore, PGS with highest sol content degrades faster than the biocomposites. This is because the incorporation of β-TCP particles into PGS can retard the degradation of the polyester backbone and enhance physiological stability by increasing the degree of crosslinking. Furthermore, swelling ratio also plays a critical role in the degradation rate. Higher swelling ratio allows more water to be absorbed and results in a faster degradation rate.[201] Therefore, PGS/β-TCP 150 with the highest swelling ratio shows the fastest mass loss among these biocomposites.

The short term degradation of these biocomposites is mainly dominated by the hydrolysis of PGS, but long term degradation is complex and requires further investigation which involves the degradation of the β-TCP particles where β-TCP is a weakly water soluble inorganic salt and it could be dissolved slowly from the composite after a long period. For instance, only 5% of mass loss from TCP was observed from its composite after 15 weeks.[104,207]

6.3.3 β-TCP particles enhanced *in vitro* bioactivity

After investigating the properties of the biocomposites, PGS/β-TCP150 and PGS/β-TCP180 were selected to study their biocompatibility owing to their improved hydrophilicity, and reduced degradation rate. Figure 6-9 presents cell proliferation data over three-intervals (at day 1, 4, and 7). Initially cells were seeded at a density of 15000 cells/biocomposite. Overall, there is a continuous cellular growth over time in all samples. At day 1, the control sample (blank) exhibits the highest proliferation rate at around 27800 ± 2400 cells, being statistically different from the PGS samples (the statistic value to show the significant differences between samples when p is less than 0.05). Both PGS/β-TCP150 and PGS/β-TCP180 show higher cell viability (around 16500-18000 cells per biocomposite) in comparison to the PGS samples that are less than

10000 cells per sample which is in agreement with the previous study.[101] Both of the biocomposites increase 65% of cell proliferation rate when compared with PGS. At day 4, a similar trend is found where the highest cellular proliferation is noticed in the control experiment (blank), followed by the PGS/β-TCP (around 26000- 26400 cells per biocomposite) and the worst is the PGS samples, which is only 18795 ± 561 cells per sample, which again shows an increase of 38% difference when compared to the PGS. At day 7, cell proliferation figures of all the samples are about double of that on day 1. PGS/β-TCP150 and PGS/β-TCP180 illustrate better proliferation rate than PGS samples than PGS which is at least 24% increase in cell viability than PGS sample (30637 ± 722 cells per sample). One can summarise that the biocomposites are much better than PGS for cell viability and proliferation.

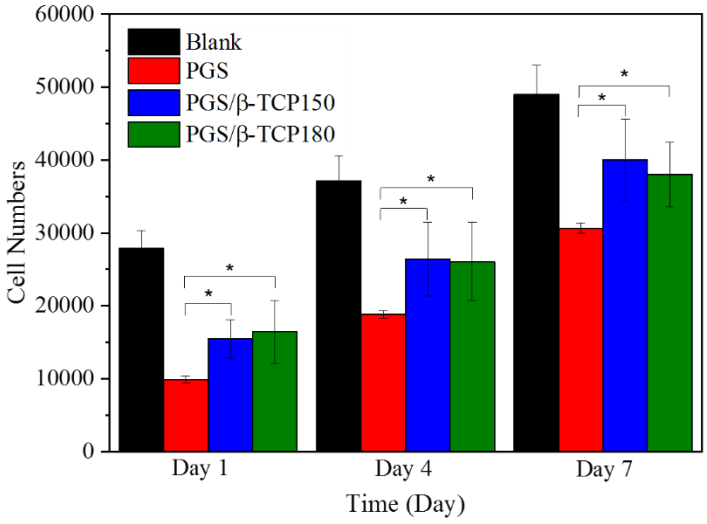

Figure 6-9 Cell viability study of the PGS and PGS/β-TCP composites with the control (blank well without any sample) where the measurements were taken at day 1, 4 and 7. The composites did not show the significant different between each other ($p > 0.05$), but the PGS and the composites exhibited significant difference higher cell viability after 7 days ($p < 0.05$).

The bioactivity studies display the biocomposites show promising results that are slightly less active in comparison to the control. This can be interpreted by relating the biocomposite degradation rate with cell bioactivities; a slower degradation rate may provoke cellular metabolic and proliferative activities. In

other words, the cell viability is inversely related to the degradation rate.[104,208,209] The sebacic acids degraded from the hydrolysis process of PGS could lower the local pH and produce an acidic environment which is unfavourable for the cell viability.[101,162] Secondly, the hydrophilic surface and better swelling effect are preferable for cell proliferation as proved in the reported literatures,[210,211,212,213] therefore the improved hydrophilic surface of biocomposites shows better cell viability. As such the PGS/β-TCP150 and PGS/ β-TCP180 show the improved cell viability after 7 days among these biomaterials due to slower degradation rate, smaller contact angle and larger swelling effect.

It can be summarised that the incorporation of β-TCP particles not only reduces the degradation rate, but also improves the surface hydrophilicity and swelling effect. The improved properties dramatically enhance the biocompatibility of PGS which could not be achieved by a single PGS biomaterial. This is because the hydrophilicity and degree of crosslinking of PGS always conflict with each other. For instance, to decrease the degradation rate, the degree of crosslinking of PGS needs to be increased, while this reduces the free hydroxyl bonds in the backbone of PGS and then affects the hydrophilicity of the polymer, although it is beneficial for cell proliferation. Another benefit of composing β-TCP into a polymer is to promote the new bone ingrowth and to buffer the drop in pH during the degradation process, as suggested by Roy *et al*. [214]

6.4 Conclusion

In this work, PGS/β-TCP biocomposites have been successfully fabricated by a fast microwave synthesis approach. The degree of crosslinking, hydrophilicity, and morphology of the biocomposites have been altered with the presence of these biocompatible β-TCP particles with a size of 50-190 nm. Specifically, these β-TCP particles improved the degree of crosslinking by decreasing the sol content by at least 66% and enhanced the hydrophilicity as indicated by the smaller contact angle. Such biocomposites increased the swelling ratio of the

biopolymer by 8%. The degradation rate of these biocomposites also changed notably where less than 8% was degraded at 28 days while 17 % loss for pure PGS polymer in the PBS solution. Many β-TCP particles were observed at 28 days indicating these β-TCP particles relatively evenly incorporated into the polymer matrix. As a result, both biocomposite (i.e. PGS/β-TCP150 and PGS/β-TCP180) showed higher cell viability after day 7, increasing by at least 24% compared to PGS polymer. It can be concluded that a slower degradation rate (higher degree of crosslinking), hydrophilic surface and higher swelling effect support the attachment and proliferation of cells, resulting in the best biocompatibility of the new biocomposite, which would meet the requirement of a drug carrier or an implant.

7. Single-step Synthesis of Poly(glycerol sebacate)

The pre-polymer of poly(glycerol sebacate) (pre-PGS) with measurable degree of esterification by MI and further PGS by curing of the pre-PGS with controlled degradation rate has been discussed in chapter 5. However, the two steps for PGS synthesis is dispensable and it is very challenging to prepare it by one step method even without any solvent or catalysts. In this chapter, for the first time crosslinked poly(glycerol sebacate) (PGS) has been fabricated by the microwave approach in one step and it is not necessary to either remove the solvent or cure in the vacuum oven.

7.1 Introduction

Poly(glycerol sebacate) [PGS] was widely investigated to discover its potentials to different bio-applications. Different approaches have been performed to control the properties of PGS, especially on its flexibility and degradation rate. The reported literature has been focused on three major aspects: (i) develop better methods to control its properties, (ii) integrate with other materials to improve its biocompatibility (i.e. silica, bioglass and carbon nanotube), and (iii) load different drugs on this polymer and further control the drugs' release profile.[103,104,106,101] Till now, more than 300 publications have been published, proving the superior potential of this polymer to act as an implant or a drug carrier.

Synthesis of this polyester is simple which undergoes polyesterification in the presence of inert gas and then curing in the vacuum oven. However, the synthesis process is time and energy consuming, and the properties can hardly be controlled under these circumstances. Li *et al.* proposed a method to control the degree of esterification (DE) of PGS by quantifying the remaining carboxyl groups and measuring the mass loss because of water evaporation.[166] Nonetheless, this method did not provide a continuous on-line monitoring of DE and the reaction time is lengthy (> 24 h). Therefore, a better method to prepare pre-

polymer of poly(glycerol sebacate) [pre-PGS] with controlled DE has been described in chapter 5. The reaction rate was improved by at least sixfold and different polymer structures of pre-PGS were produced by altering the heating source.

However, the use of solvent in the reaction may not be preferable since an additional step is required to remove it. To solve this problem, a single-step synthesis of PGS by microwave irradiation (MI) has been proposed. By introducing high microwave power with a short time, it supplies sufficient energy for the esterification process. The cooling intervals were also applied to mitigate the overheating issue. Apart from that, the mass loss indicating the removal of water during the reaction was measured. It is hypothesised that the mass loss by monomers could be minimized when the reaction temperature was monitored properly. The properties of the prepared PGS were studied by IR spectra to examine the presence of ester bond, NMR spectra to identify the polymer structure and lastly thermal analysis to track the melting and crystallisation temperature of the prepared PGS.

7.2 Methodology

7.2.1 Material synthesis

The equimolar of glycerol (99%, Sigma Aldrich) and sebacic acid (> 99% Sigma Aldrich) were measured and pre-mixed in a round bottom flask. The flask was then put into a single mode microwave (CEM Discover SP) which was connected to a Drechsel bottle. The mixture was purged with nitrogen gas for a few minutes. The mixture was then irradiated for 30 seconds at a Fixed-power mode (300W) with a temperature limit of 130 ˚C. It was then cooled to room temperature. The heating and cooling cycle was repeated until an elastomer was obtained. The produced pre-polymer and final polymer were collected at different MI time and then characterised.

7.2.2 Characterisation

Fourier Transform Infrared Spectroscopy

The chemical bonds were confirmed using a Perkin-Elmer 1605 FT-IR spectrometer in attenuated total reflection (ATR) mode with the frequency range 400-4000 cm^{-1} at 4 cm^{-1} resolution. PGS samples including pre-polymer (pre-PGS) and crosslinked PGS were placed on the ATR crystal, and then compressed using a flat axial screw. Spectra were then compared with the literature to distinguish the characteristic bonds of the samples.

Differential Scanning Calorimetry (DSC)

The thermal properties of pre-PGS and PGS were studied by using a differential scanning calorimetry (Perkin Elmer Diamond DSC instrument). 5-15 mg of polymer was encapsulated in standard aluminium pans. The heating rate was 10 ˚C/min from -50 to 200 ˚C. The endothermic/exothermic peaks were integrated with the DSC software.

NMR spectroscopy

NMR spectra were recorded using a Bruker Avance III 600 MHz NMR spectrometer equipped with a 5 mm cryoprobe (^1H 600.13 MHz). NMR spectra of the pre-polymers (pre-PGS) were obtained in acetone-d6. All chemical shifts (δ) were given in ppm, where the residual C_3H_6O peak was used as an internal reference for ^1H NMR (δ_H = 2.09 ppm). The resulting data were processed and analysed using ACD/NMR Processor software.

7.3 Results and Discussion

The pre-PGS and crosslinked PGS were prepared successfully by the MI method without adding any solvent or catalysts. More interestingly, no curing process was needed to yield a crosslinked PGS. By applying high microwave power (300W) with sufficient cooling interval, the crosslinked PGS was produced after 43 minutes of irradiation time (86 cycle x 30 second/cycle) in microwave. As shown in Figure 7-1, the physical appearance of the PGS changes with the reaction time, transforming from wax form (after 15 minutes of MI) into viscous

liquid (after 30 minutes of MI), and lastly becoming the elastomer (after 43 minutes of MI). This physical change is comparable with the reported literature where the polymer appearance strongly relies on the degree of the esterification (DE).[166] Other than its physical appearance, mass loss of the reactants was also monitored (Figure 7-1). The mass loss is proportional to the MI time. When the irradiation time increases, the mass loss also increases. Initially, the mass loss is higher and more than 50% (0.28 g) of the mass loss is observed after 15 minutes in the microwave. The mass loss becomes lower and an elastomer is obtained with 0.51 g of mass loss. The notable reduction in the mass loss could be due to the limited amount of free hydroxyl group remaining in the system. The mass loss observed during the reaction is mainly due to the evaporation of water, a side product of the formation of PGS, and this may be used to tailor the degree of esterification.[89] However, the total of mass loss in this work is slightly higher than the theoretical value, which is 0.49 g of water should be produced in order to achieve a fully crosslinked PGS. The difference between the theoretical and experimental values may be due to the loss of some monomers during the MI process.

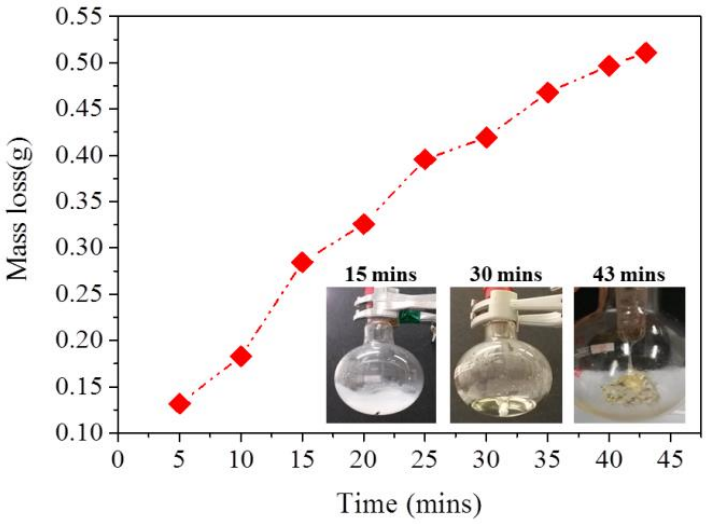

Figure 7-1 Mass loss of precursor mixture after microwaving for 43 minutes.

The chemical bonds in the prepared pre-PGS and crosslinked PGS were then analysed with ATR-FTIR. As shown in Figure 7-2, the mixture of the precursors shows a broad peak around 3290 cm^{-1} and 1693 cm^{-1}, corresponding to the -OH

in glycerol and C=O symmetric stretch in sebacic acid, respectively. After the MI, a new ester C=O stretching bond is found at 1734 cm^{-1} and its intensity increases with the reaction time which indicates the DE is proportional to the heating time. Conversely, the intensity of both C=O bond (1693 cm^{-1}) in the sebacic acid and –OH group (3290 cm^{-1}) in the glycerol reduces with the reaction time because these two bonds react to form the ester. On the other hand, the peaks at 2855 cm^{-1} and 2928 cm^{-1} correspond to C-H stretching of the polymer backbone.[8,166] Additional peaks around 1040 cm^{-1}, 1100-1300 cm^{-1}, 1420 cm^{-1}, 1464 $cm^{-1}$are attributed to C-C-O stretching, O=C-O stretching, O-H bending and CH_2 deformation.[215,216] More importantly, a similar phenomenon described in chapter 5 is observed in this IR spectra; the –OH bond shifts to a higher wavenumber (3460 cm^{-1}) because more secondary –OH is consumed than primary –OH during the esterification process.[175]

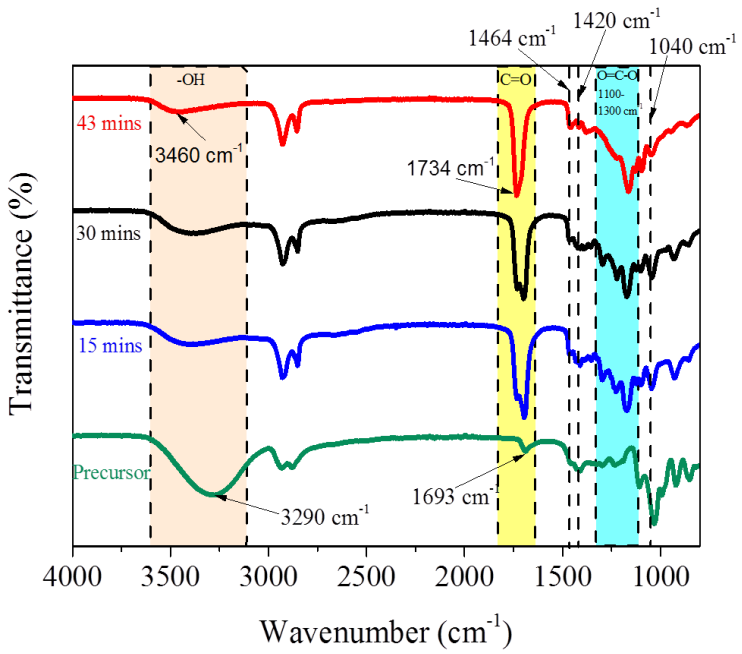

Figure 7-2 ATR-IR spectra of precursor, pre-PGS and crosslinked PGS.

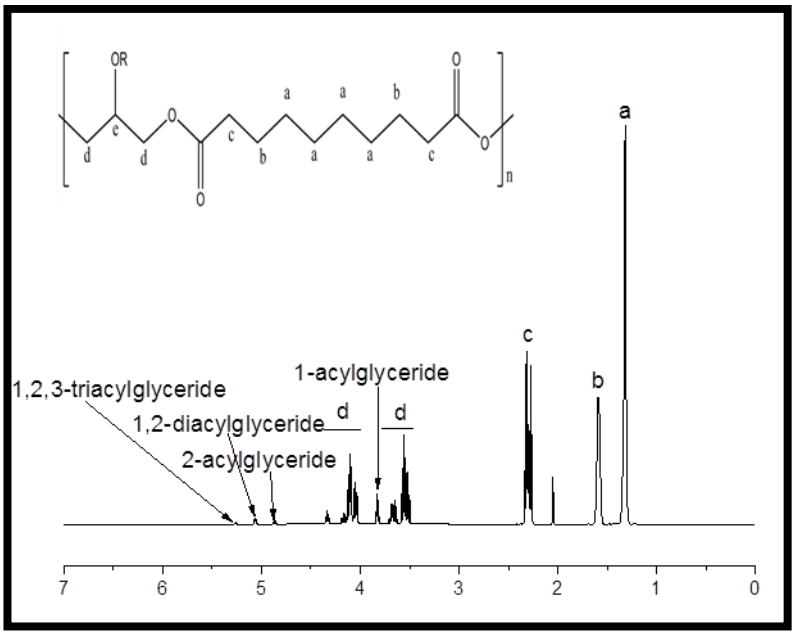

Figure 7-3 ^{1}H NMR spectrum of pre-PGS after 30 minutes of microwaving.

^{1}H NMR spectrum of the pre-PGS (Figure 7-3) prepared by microwave (30 mins) was recorded, using acetone-d6 (δ2.09 ppm) as the deuterated solvent while it is difficult to analyse the crosslinked PGS because this polymer cannot be dissolved in the deuterated solvent. There are six different protons (H_{a-e}**)** which can be assigned to the repeating units of pre-PGS, where the chemical shifts at δ1.32 ppm (H_a), δ1.59 ppm (H_b) and δ2.32 ppm (H_c) refer to –CO-CH_2-CH_2-CH_2- group in the pre-polymer from the precursor sebacic chain, while the additional shifts at δ 3.50-5.50 ppm identified in the spectrum ascribe to the H_d and H_e in pre-PGS molecular chain from glycerol.[176,177,178] The deshielded methylene (-CH_2-) protons of the glycerol show between 3.5-4.4 ppm, while the methine (-CH-) protons of the glycerol locate around 4.8-5.4 ppm. On the other hand, the polymer structure can be predicted by integrating the peak area. The relative ratio of H_b/H_a is a constant (i.e. 0.5) because these protons are the polymer backbone and do not react during the esterification. In addition, the relative ratio of H_e/H_a corresponding to 1,2,3-triacylglyceride (δ 5.27 ppm) is 0.0326, demonstrating branched polymer forms after 30 mins in microwave. This is because all three –OH group from glycerol have reacted with carboxylic acid to form a 1,2,3-triacylglyceride. Surprisingly, this calculated H_e/H_a ratio of the pre-PGS is higher than the one shown in chapter 5, which is only 0.0132. This might be due to the

absence of solvent in the system and most of the applied microwave was absorbed by the glycerol to activate both primary and secondary hydroxyl groups. Generally, the $–CH_2$-OH (primary hydroxyl) mainly serves as the chain propagation and –CH-OH (secondary hydroxyl) contributes to the branching and crosslinking reaction.[217] The activation of both hydroxyl groups in glycerol to react with sebacic acid could produce a branched and linear structure of polymer simultaneously.

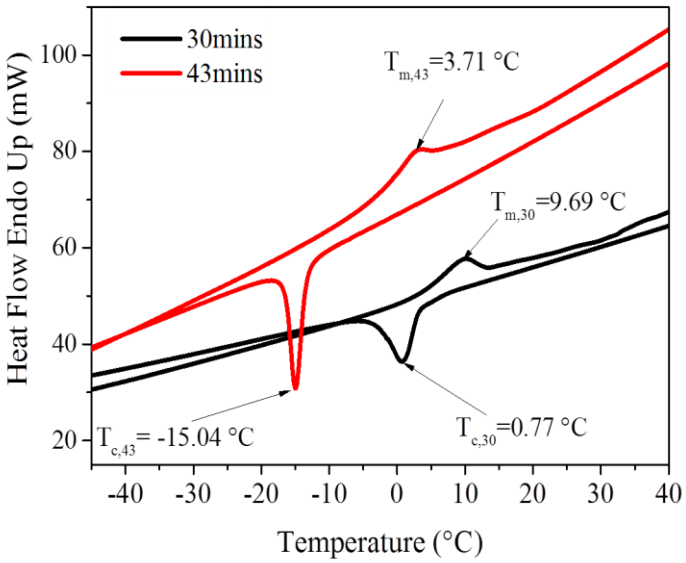

Figure 7-4 Thermal analysis of pre-PGS and crosslinked PGS prepared by MI after 30 and 43 minutes.

PGS is a partially semi-crystalline polymer and its thermal properties depend on glass to rubber transition temperature (T_g) of the amorphous phase and melting temperature (T_m) of the crystalline phase. In other words, T_m is the melting temperature of the crystalline domain of a polymer while the T_g is the transition temperature of the amorphous domain. In this study, the phase transformation of polymers collected at 30 mins and 43 mins MI time was investigated using DSC. The thermal profile of pre-PGS and PGS are different, indicating the polymer is crosslinked. As shown in Figure 7-4, a weak endothermic peak at 9.69 ˚C (ΔH= 25.019 J/g) and 3.71 ˚C (ΔH= 11.038 J/g), for the samples that were prepared by microwave for 30 and 43 minutes, respectively. These are the melting points of

pre-PGS (30 mins MI) and PGS (43 mins MI) and are in agreement with the previously reported literature.[218] During the cooling cycle, an exothermic crystallise peak is also observed. For crystallisation temperature, pre-PGS is at 0.77 ˚C (ΔH= -34.789 J/g) and crosslinked PGS is around -15.04 ˚C (ΔH= -26.018 J/g). As the curing time or temperature increases, a reduction in peak magnitude and crystallisation temperature, which is in consistency with the previous study.[218] This indicates the crystallinity of the PGS changes with the curing time. As mentioned in Chapter 5, a highly branched pre-PGS were formed in microwave. A branched polymer tends to increase the size of side groups compared to a linear polymer and this also decreases T_m as the reaction time increases. The branched structure creates a lesser perfection of molecular packing and decreases its crystallinity.[59] In addition, the large side groups hinder the movement of the main chains which lowers the T_m.[59] In addition, no T_g was detected since the T_g could be around -80 ˚C and this is beyond the machine limit.[7] Thus, the produced crosslinked PGS retains its rubbery properties at body temperature (37 ˚C).

7.4 Conclusion

In this chapter, crosslinked PGS has been prepared successfully by single-step microwave synthesis without adding any solvent or catalysts. In other words, an elastomer was obtained after 43 minutes of irradiation and no curing step was needed when using this facile energy approach. It was also found that high microwave power (300 W) with short reaction time was crucial to prepare this polymer. The reaction temperature was monitored to minimize the evaporation of monomers and improve the reproducibility of the PGS. The mass loss profile during the esterification process was monitored and was found to be proportional to the MI time. The prepared pre-PGS and crosslinked PGS were characterised by IR spectra, ^{1}H NMR spectra and thermal analysis. The presence of the ester linkage at 1734 cm^{-1} confirmed the esterification process. Based on ^{1}H NMR, both primary and secondary hydroxyl groups were activated by microwave to

form linear and branched polymers. On the other hand, the melting and crystallisation temperature of the pre-PGS and crosslinked PGS was also measured. No glass transition temperature was observed, indicating the produced PGS retains its rubbery properties at body temperature. Both crystallisation and melting temperature decreased with increment in degree of crosslinking due to limited mobility of the chains.

8. Overall Conclusion and Future Work

8.1 Conclusion

The thesis aimed to synthesise a biocomposite composed of two key components calcium phosphates (CaP) and poly(glycerol sebacate) [PGS] with controlled properties, further investigating the biomaterials' properties.

Chapters 2 and 3 describe types and function of biomaterials (i.e. CaP and PGS), fundamentals of the microwave and also the characterisation methods. The phase and morphology control of CaP materials were synthesised by microwave and reported in chapter 4. Three interesting CaP phases (β-TCP, DCPA and HA) were for the first time successfully prepared under mild processing conditions by microwave (> 80% of yields). The phase and morphology control of CaP particles strongly relied on the solvent species where the used precursors had different solubility in the solvents and these solvents had variable interaction potential with the microwave, resulting in one-dimensional and three-dimensional growth of the particles. For example, β-TCP was prepared in methanol solvent with spherical, DCPA was produced in ethanol solvent with plate-like shape and HA was synthesised in water solvent with long rod shape. Additionally, varied specific surface area and pore size of CaP were produced. The increment in the specific surface area provided more binding sites to the BSA molecules. For instance, DCPA particles with highest specific surface area allowed 50 wt% of BSA loading, followed by β-TCP (41 wt%) and lastly HA particles (15 wt%). The mesopores formed in the DCPA and β-TCP particles also demonstrated a controlled release profile; larger pore size in the β-TCP particles increased the adsorption of BSA molecules and allowed a higher release amount of BSA molecules. Thus, these CaP particles provide a platform to readily control both the drug delivery profile and loading capacity of proteins.

In chapter 5, poly(glycerol sebacate), PGS, with a controlled degree of esterification (DE) was synthesised via a modified microwave approach. By

introducing low boiling point solvent (toluene), the reproducibility was improved, and the evaporation of monomers was minimised because of the homogeneous temperature medium. DE of the pre-polymer of PGS (pre-PGS) was tailored by collecting the condensed water to monitor the degree of polymerisation. Initially, the preparation of pre-PGS was studied by single mode and multimode microwave. One can see that single mode offers more flexibility to tune PGS Young's modulus and the reaction time is shorter to obtain a similar amount of water to achieve the same degree of DE. The experimental conditions in the single mode microwave were then optimised and compared with conventional heating. Interestingly, the microwave not only sped up the pre-polymerisation and curing time by sixfold, but also produced highly branched pre-PGS without changing the molar ratio of reactants. The polymer structure was confirmed by ^{1}HNMR and MALDI-TOF. In terms of mechanical properties, the PGS prepared by microwave only required 8 h to achieve similar mechanical properties to that prepared by CH 48 h. The highly branched pre-PGS by MI also reduced the curing time where a stiffer polymer was obtained after 2 h curing in the vacuum oven. The degradation rate of PGS prepared by the microwave provided a 59% wider degradation window due to its branching structure. It can be concluded that the microwave approach provides a higher degree of freedom to tune mechanical properties (threefold) and degradation rate (59% wider) in order to meet demands of various applications such as drug delivery vectors which highly depend on the degradation rate of the polymer.

Following on the success of preparation of these two biomaterials, a hybrid of PGS/β-TCP was prepared to overcome the cytotoxicity issue of PGS. In this session, the β-TCP particles were incorporated into PGS by microwave synthesis, leading to improved degree of crosslinking, hydrophilicity and morphology of PGS and resulting in enhancement in biocompatibility. It was revealed that these particles tended to increase the degree of crosslinking and the hydrophilicity of PGS. The sol content was decreased by at least 66%, and the contact angle was reduced by 14 % with an 8% increase in swelling ratio due to the incorporation of β-TCP into PGS. The degradation rate was also reduced and less than 18% was

degraded after 28 days in the PBS solutions. More importantly, the cell viability was increased by at least 24% as compared to PGS in 7 days. The slow degradation rate with hydrophilic surface supports cell attachment and proliferation without any additional factors, providing a much better biocompatibility.

Lastly, the synthesis of PGS by microwave was further improved since the presence of organic solvent is unfavourable and additional steps were needed to remove the solvent. A single-step synthesis of PGS has been developed without adding any solvent or catalysts. Importantly, no curing step was needed and an elastomer was obtained after 43 minutes of microwave heating. To the best of my knowledge, this is the first report to prepare PGS polymer by such a facile and efficient approach. It is found that a high microwave power (300W) with sufficient cooling time was crucial to prepare PGS successfully. On the other hand, the reaction temperature was monitored to avoid the evaporation of monomers. The mass loss profile during the synthesis was also recorded. The prepared pre-PGS and PGS were characterised by IR spectra, ^{1}H NMR spectra and thermal analysis. The ester linkage was confirmed, indicating both primary and secondary hydroxyl groups reacted to form linear and branch polymers. The melting and crystallisation temperature of pre-PGS and PGS were comparable with the reported literature.

Overall, an advanced microwave approach has been developed to prepare these biomaterials with controllable properties, demonstrating their strong potential in bioapplication. Furthermore, the fast and energy efficient approach can be applied in other biopolymers' or bioinorganic synthesis.

8.2 Future Work

The thesis achieved the main goals set up by preparing CaP, PGS and the biocomposites of these two materials successfully using a microwave-assisted method. Despite these successes, the research is only a starting point prior to any

clinical applications and therefore there are many possible follow-up investigations which could be pursued in order to meet the target of robust and efficient biomaterials suitable for clinical use, which could be carried out in the project due to time limitation.

Chapters 4, 5, 6 and 7 detailed a rapid and efficient microwave method to prepare CaP and PGS. More importantly, a superior control of material properties including the phase, morphology, and mechanical properties, has been demonstrated. However, many further investigations should be conducted to understand the reaction mechanism of the particles nucleation and growth by microwave.

Furthermore, for CaP particles, the particle size distribution and porosity of the particles could be studied by altering the experimental conditions (i.e. solvent species and microwave conditions) since these factors affect the protein loading and release profile significantly. Additionally, β-TCP is biodegradable ceramics, therefore, an interesting further work would be to carry out to understand the comprehensive effect of microwave reaction parameters (i.e. microwave power and dual-solvent system) upon nano-material characteristics and its efficiency as a drug carrier. Furthermore, delivery testing of CaP biomaterials could be extended based on the preliminary standard protein works in this thesis to specific growth factors such as transforming growth factor-β and Fibroblast growth factor.

In chapter 5, it was demonstrated that highly branched poly(glycerol sebacate) by microwave synthesis has high potential as a drug carrier. This polymer is biodegradable in a manner that is readily degraded over times. The control over polymer structure in this study showed great promise for controlled delivery therapeutic agents, however, this was not tested. With this in mind, it would be interesting to investigate the effect of polymer structure on the protein loading and release profile. On the other hand, a sizeable project would be to investigate the experimental conditions, including the molar ratio of reactants and microwave temperature on the fabrication of PGS. This may produce a different polymer

structure which could provide more binding sites as the drug carriers. On the other hand, it would be useful to study the dissolution or diffusion of drugs using the prepared PGS since the release profile is dominated by the degradation of PGS.

Chapter 6 introduced the synthesis of biocomposite which is a great candidate for other applications. More tests could be performed, including the mechanical properties and thermal analysis. Furthermore, the synthesis approach could be further compared with other methods, such as physical mixing. On the other hand, an attractive project would be to grow other CaP phases or mixture of CaP phases on the PGS surface. The comparisons of these phases towards their application could be useful, for instance, a different CaP layer of drug-loaded materials with different resorbability rates may allow the controlled release of certain therapeutics at predetermined times. On the other hand, porous PGS/β-TCP composites would be interesting. Microwave coupled with a template can be used to produce this porous structure which may be useful for cell attachments or as drug carriers.

The single step synthesis of PGS only showed some preliminary interesting results and further investigations would be necessary to reveal the properties of the prepared PGS such as its mechanical properties and degradation rate. On the other hand, the microwave conditions on preparing the PGS can be optimised, revealing the effect of microwave on preparing the polymer. On the other hand, the biocomposite of CaP and PGS could be prepared using this method since it would be interesting if a composite with improved bio-properties could be prepared with a short reaction time. In addition, a porous PGS could be prepared by modifying the current methods. For instance, the precursors of the PGS can be added into a salt template and irradiated until a crosslinked PGS is obtained.

Lastly, to implement the materials clinically, many further *in vitro* and *in vivo* tests are required. Preliminary work in this regard was inconclusive and *in vivo* test could be necessary to study the real interaction between materials and living

body. In addition, the microwave method can potentially be expanded to prepare other polyester or hydrogel since the highly branched polymers provide different properties which could be useful for other applications.

Bibliography

(1) Hench, L. L.; Polak, J. M. Third-Generation Biomedical Materials. *Science (80-.).* **2002**, *295* (5557), 1014–1017.

(2) Holzapfel, B. M.; Reichert, J. C.; Schantz, J.-T.; Gbureck, U.; Rackwitz, L.; Nöth, U.; Jakob, F.; Rudert, M.; Groll, J.; Hutmacher, D. W. How Smart Do Biomaterials Need to Be? A Translational Science and Clinical Point of View. *Adv. Drug Deliv. Rev.* **2013**, *65* (4), 581–603.

(3) LeGeros, R. Z. Calcium Phosphate-Based Osteoinductive Materials. *Chem. Rev.* **2008**, *108* (11), 4742–4753.

(4) Lobo, S. E.; Livingston Arinzeh, T. Biphasic Calcium Phosphate Ceramics for Bone Regeneration and Tissue Engineering Applications. *Materials (Basel).* **2010**, *3* (2), 815–826.

(5) Uskoković, V.; Uskoković, D. P. Nanosized Hydroxyapatite and Other Calcium Phosphates: Chemistry of Formation and Application as Drug and Gene Delivery Agents. *J. Biomed. Mater. Res. B. Appl. Biomater.* **2011**, *96* (1), 152–191.

(6) Dorozhkin, S. V; Epple, M. Biological and Medical Significance of Calcium Phosphates. *Angew. Chem. Int. Ed. Engl.* **2002**, *41* (17), 3130–3146.

(7) Wang, Y.; Ameer, G.; Sheppard, B.; Langer, R. A Tough Biodegradable Elastomer. *Nat. Biotechnol.* **2002**, *20*, 602–606.

(8) Aydin, H. M.; Salimi, K.; Rzayev, Z. M. O.; Pişkin, E. Microwave-Assisted Rapid Synthesis of Poly(glycerol-Sebacate) Elastomers. *Biomater. Sci.* **2013**, *1* (5), 503.

(9) Park, J.; Lakes, R. S. *Biomaterials: An Introduction*; Springer Science & Business Media, 2007.

(10) Manivasagam, G.; Dhinasekaran, D.; Rajamanickam, A. Biomedical Implants : Corrosion and Its Prevention - A Review. *Recent Patents Corros. Sci.* **2010**, *2*, 40–54.

(11) Aramwit, P. *Introduction to Biomaterials for Wound Healing*; Ågren, M., Ed.; Elsevier Ltd, 2016.

(12) Kenny, S. M.; Buggy, M. Bone Cements and Fillers : A Review. *J. Mater. Sci. Mater. Med.* **2003**, *14*, 923–938.

(13) Ikada, Y. Challenges in Tissue Engineering. *J. R. Soc. Interface* **2006**, *3*, 589–601.

(14) Horcajada, P.; Chalati, T.; Serre, C.; Gillet, B.; Sebrie, C.; Baati, T.; Eubank, J. F.; Heurtaux, D.; Clayette, P.; Kreuz, C.; et al. Porous Metal-Organic-Framework Nanoscale Carriers as a Potential Platform for Drug Deliveryand Imaging. *Nat. Mater.* **2010**, *9* (2), 172–178.

(15) Dhar, S.; Gu, F. X.; Langer, R.; Farokhzad, O. C.; Lippard, S. J. Targeted Delivery of Cisplatin to Prostate Cancer Cells by Aptamer Functionalized Pt(IV) Prodrug-PLGA-PEG Nanoparticles. *Proc. Natl. Acad. Sci.* **2008**,

105 (45), 17356–17361.

(16) Kearney, C. J.; Mooney, D. J. Macroscale Delivery Systems for Molecular and Cellular Payloads. *Nat. Mater.* **2013**, *12* (11), 1004–1017.

(17) Arcos, D. Bioceramics for Drug Delivery. *Acta Mater.* **2013**, *61*, 890–911.

(18) Grangiep, J. L.; Puygrenierb, M.; Gautierb, J. C.; Couvreu, P. Nanoparticles as Carriers for Growth Hormone Releasing Factor. *J. Control. Release* **1991**, *15*, 3–13.

(19) Grimandi, G.; Faivre, A.; Takahashi, S.; Daculsi, G. Apatite as Carrier for Growth Hormone : In Vitro Characterization of Loading and Release. *J. Biomed. Mater. Res.* **1997**, *34*, 165–170.

(20) Tabata, Y. Nanomaterials of Drug Delivery Systems. *300*, 81–100.

(21) Nguyen, A. H.; McKinney, J.; Miller, T.; Bongiorno, T.; McDevitt, T. C. Gelatin Methacrylate Microspheres for Controlled Growth Factor Release. *Acta Biomater.* **2015**, *13*, 101–110.

(22) Yamamoto, M.; Ikada, Y.; Tabata, Y. Controlled Release of Growth Factors Based on Biodegradation of Gelatin Hydrogel. *J. Biomater. Sci. Polym. Ed.* **2001**, *12* (1), 77–88.

(23) Seo, B. B.; Koh, J. T.; Song, S. C. Tuning Physical Properties and BMP-2 Release Rates of Injectable Hydrogel Systems for an Optimal Bone Regeneration Effect. *Biomaterials* **2017**, *122*, 91–104.

(24) Holland, T. A.; Tabata, Y.; Mikos, A. G. Dual Growth Factor Delivery from Degradable Oligo(poly(ethylene Glycol) Fumarate) Hydrogel Scaffolds for Cartilage Tissue Engineering. *J. Control. Release* **2005**, *101* (1–3 SPEC. ISS.), 111–125.

(25) Zhu, X. D.; Fan, H. S.; Xiao, Y. M.; Li, D. X.; Zhang, H. J.; Luxbacher, T.; Zhang, X. D. Effect of Surface Structure on Protein Adsorption to Biphasic Calcium-Phosphate Ceramics in Vitro and in Vivo. *Acta Biomater.* **2009**, *5* (4), 1311–1318.

(26) Blom, E. J.; Klein-Nulend, J.; Klein, C. P.; Kurashina, K.; van Waas, M. a; Burger, E. H. Transforming Growth Factor-beta1 Incorporated during Setting in Calcium Phosphate Cement Stimulates Bone Cell Differentiation in Vitro. *J. Biomed. Mater. Res.* **2000**, *50* (1), 67–74.

(27) Laffargue, P.; Fialdes, P.; Frayssinet, P.; Rtaimate, M.; Hildebrand, H. F.; Marchandise, X. Adsorption and Release of Insulin-like Growth Factor-I on Porous Tricalcium Phosphate Implant. *J. Biomed. Mater. Res.* **2000**, *49* (3), 415–421.

(28) Jayasuriya, A. C.; Shah, C. Controlled Release of Insulin-like Growth Factor-1 and Bone Marrow Stromal Cell Function of Bone-like Mineral Layer-Coated Poly(lactic-Co-Glycolic Acid) Scaffolds. *J. Tissue Eng. Regen. Med.* **2008**, *2*, 43–49.

(29) Sokolsky-papkov, M.; Agashi, K.; Olaye, A.; Shakesheff, K.; Domb, A. J. Polymer Carriers for Drug Delivery in Tissue Engineering ☆. *Adv. Drug Deliv. Rev.* **2007**, *59*, 187–206.

(30) Huang, X.; Yang, D.; Yan, W.; Shi, Z.; Feng, J.; Gao, Y.; Weng, W.; Yan, S. Osteochondral Repair Using the Combination of Fibroblast Growth Factor and Amorphous Calcium Phosphate/poly(l-Lactic Acid) Hybrid Materials. *Biomaterials* **2007**, *28* (20), 3091–3100.

(31) Ishihara, M.; Obara, K.; Nakamura, S.; Fujita, M.; Masuoka, K.; Kanatani, Y.; Takase, B.; Hattori, H.; Morimoto, Y.; Ishihara, M.; et al. Chitosan Hydrogel as a Drug Delivery Carrier to Control Angiogenesis. *J. Artif. Organs* **2006**, *9* (1), 8–16.

(32) Zhang, Y.; Zhang, M. Calcium Phosphate/chitosan Composite Scaffolds for Controlled in Vitro Antibiotic Drug Release. *J. Biomed. Mater. Res.* **2002**, *62* (3), 378–386.

(33) Lim, S. T.; Martin, G. P.; Berry, D. J.; Brown, M. B. Preparation and Evaluation of the in Vitro Drug Release Properties and Mucoadhesion of Novel Microspheres of Hyaluronic Acid and Chitosan. *J. Control. Release* **2000**, *66*, 281–292.

(34) Perni, S.; Martini-Gilching, K.; Prokopovich, P. Controlling Release Kinetics of Gentamicin from Silica Nano-Carriers. *Colloids Surfaces A Physicochem. Eng. Asp.* **2018**, *541* (March 2017), 212–221.

(35) Zhou, X.; Weng, W.; Chen, B.; Feng, W.; Wang, W.; Nie, W.; Chen, L.; Mo, X.; Su, J.; He, C. Mesoporous Silica Nanoparticles/gelatin Porous Composite Scaffolds with Localized and Sustained Release of Vancomycin for Treatment of Infected Bone Defects. *J. Mater. Chem. B* **2018**, *6* (5), 740–752.

(36) Unagolla, J. M.; Jayasuriya, A. C. Drug Transport Mechanisms and in Vitro Release Kinetics of Vancomycin Encapsulated Chitosan-Alginate Polyelectrolyte Microparticles as a Controlled Drug Delivery System. *Eur. J. Pharm. Sci.* **2018**, *114*, 199–209.

(37) Ye, F.; Guo, H.; Zhang, H.; He, X. Polymeric Micelle-Templated Synthesis of Hydroxyapatite Hollow Nanoparticles for a Drug Delivery System. *Acta Biomater.* **2010**, *6* (6), 2212–2218.

(38) Yang, Q.; Wang, S.; Fan, P.; Wang, L.; Di, Y.; Lin, K.; Xiao, F. S. pH-Responsive Carrier System Based on Carboxylic Acid Modified Mesoporous Silica and Polyelectrolyte for Drug Delivery. *Chem. Mater.* **2005**, *17* (24), 5999–6003.

(39) Konishi, M.; Tabata, Y.; Kariya, M.; Suzuki, A.; Mandai, M.; Nanbu, K.; Takakura, K.; Fujii, S. In Vivo Anti-Tumor Effect through the Controlled Release of Cisplatin from Biodegradable Gelatin Hydrogel. *J. Control. Release* **2003**, *92* (3), 301–313.

(40) Avgoustakis, K.; Beletsi, A.; Panagi, Z.; Klepetsanis, P.; Karydas, A. G.; Ithakissios, D. S. PLGA-mPEG Nanoparticles of Cisplatin: In Vitro Nanoparticle Degradation, in Vitro Drug Release and in Vivo Drug Residence in Blood Properties. *J. Control. Release* **2002**, *79* (1–3), 123–135.

(41) Aryal, S.; Hu, C. J.; Zhang, L. Polymer-Cisplatin Conjugate Nanoparticles

for Acid-Responsive Drug Delivery. *ACS Nano* **2010**, *4* (1), 251–258.

(42) Koo, O. M.; Rubinstein, I.; Onyuksel, H. Role of Nanotechnology in Targeted Drug Delivery and Imaging: A Concise Review. *Nanomedicine* **2005**, *1* (3), 193–212.

(43) Janes, K. A.; Fresneau, M. P.; Marazuela, A.; Fabra, A.; Alonso, M. J. Chitosan Nanoparticles as Delivery Systems for Doxorubicin. *J. Control. Release* **2001**, *73* (2–3), 255–267.

(44) Sun, H.; Guo, B.; Cheng, R.; Meng, F.; Liu, H.; Zhong, Z. Biodegradable Micelles with Sheddable Poly(ethylene Glycol) Shells for Triggered Intracellular Release of Doxorubicin. *Biomaterials* **2009**, *30* (31), 6358–6366.

(45) Min, K. H.; Lee, H. J.; Kim, K.; Kwon, I. C.; Jeong, S. Y.; Lee, S. C. The Tumor Accumulation and Therapeutic Efficacy of Doxorubicin Carried in Calcium Phosphate-Reinforced Polymer Nanoparticles. *Biomaterials* **2012**, *33* (23), 5788–5797.

(46) Musumeci, T.; Ventura, C. A.; Giannone, I.; Ruozi, B.; Montenegro, L.; Pignatello, R.; Puglisi, G. PLA/PLGA Nanoparticles for Sustained Release of Docetaxel. *Int. J. Pharm.* **2006**, *325*, 172–179.

(47) Qi, C.; Zhu, Y. J.; Zhao, X. Y.; Lu, B. Q.; Tang, Q. L.; Zhao, J.; Chen, F. Highly Stable Amorphous Calcium Phosphate Porous Nanospheres: Microwave-Assisted Rapid Synthesis Using ATP as Phosphorus Source and Stabilizer, and Their Application in Anticancer Drug Delivery. *Chem. - A Eur. J.* **2013**, *19* (3), 981–987.

(48) Chan, J. M.; Zhang, L.; Yuet, K. P.; Liao, G.; Rhee, J. W.; Langer, R.; Farokhzad, O. C. PLGA-Lecithin-PEG Core-Shell Nanoparticles for Controlled Drug Delivery. *Biomaterials* **2009**, *30* (8), 1627–1634.

(49) Yang, P.; Quan, Z.; Li, C.; Kang, X.; Lian, H.; Lin, J. Bioactive, Luminescent and Mesoporous Europium-Doped Hydroxyapatite as a Drug Carrier. *Biomaterials* **2008**, *29* (32), 4341–4347.

(50) Qiu, X.; Leporatti, S.; Donath, E.; Möhwald, H. Studies on the Drug Release Properties of Polysaccharide Multilayers Encapsulated Ibuprofen Microparticles. *Langmuir* **2001**, *17* (17), 5375–5380.

(51) Andersson, J.; Rosenholm, J.; Areva, S.; Lindén, M. Influences of Material Characteristics on Ibuprofen Drug Loading and Release Profiles from Ordered Micro- and Mesoporous Silica Matrices. *Chem. Mater.* **2004**, *16* (21), 4160–4167.

(52) Holowka, E. P.; Bhatia, S. K. Controlled-Release Systems. In *Drug Delivery: Materials Design and Clinical Perspective*; 2014; pp 7–58.

(53) Santos, V. dos; Brandalise, R. N.; Savaris, M. Chapter 4 Ceramic Biomaterials and Chapter 5 Polymeric Biomaterials. In *Engineering of Biomaterials*; 2017; pp 29–50.

(54) Uskoković, V.; Desai, T. a. Phase Composition Control of Calcium Phosphate Nanoparticles for Tunable Drug Delivery Kinetics and

Treatment of Osteomyelitis. II. Antibacterial and Osteoblastic Response. *J. Biomed. Mater. Res. A* **2013**, *101* (5), 1427–1436.

(55) LeGeros, R. Z. Properties of Osteoconductive Biomaterials: Calcium Phosphates. *Clin. Orthop. Relat. Res.* **2002**, *395* (395), 81–98.

(56) Dorozhkin, S. V. Calcium Orthophosphate-Based Biocomposites and Hybrid Biomaterials. *J. Mater. Sci.* **2009**, *44* (9), 2343–2387.

(57) Dorozhkin, S. Calcium Orthophosphate-Based Bioceramics. *Materials (Basel).* **2013**, *6*, 3840–3942.

(58) Bohner, M. Calcium Orthophosphates in Medicine: From Ceramics to Calcium Phosphate Cements. *Injury* **2000**, *31*, 37–47.

(59) Park, J.; Lakes, R. S. Chapter 6 Ceramic Implant Materials and Chapter 7 Polymeric Implant Materials. In *Biomaterials: An Introduction*; 2007; pp 140–206.

(60) Uskoković, V.; Desai, T. A. Phase Composition Control of Calcium Phosphate Nanoparticles for Tunable Drug Delivery Kinetics and Treatment of Osteomyelitis. I. Preparation and Drug Release. *J. Biomed. Mater. Res. A* **2013**, *101A* (5), 1416–1426.

(61) Valletregi, M. Calcium Phosphates as Substitution of Bone Tissues. *Prog. Solid State Chem.* **2004**, *32* (1–2), 1–31.

(62) Dorozhkin, S. Calcium Orthophosphates in Nature, Biology and Medicine. *Materials (Basel).* **2009**, *2* (2), 399–498.

(63) V. Dorozhkin, S. Amorphous Calcium Orthophosphates: Nature, Chemistry and Biomedical Applications. *Int. J. Mater. Chem.* **2012**, *2* (1), 19–46.

(64) Tas, A. C. Monetite (CaHPO 4) Synthesis in Ethanol at Room Temperature. *J. Am. Ceram. Soc.* **2009**, *92* (12), 2907–2912.

(65) Verron, E.; Khairoun, I.; Guicheux, J.; Bouler, J.-M. Calcium Phosphate Biomaterials as Bone Drug Delivery Systems: A Review. *Drug Discov. Today* **2010**, *15* (13–14), 547–552.

(66) Suh, D. Y.; Boden, S. D.; Louis-ugbo, J.; Mayr, M.; Murakami, H.; Kim, H.; Minamide, A.; Hutton, W. C. Delivery of Recombinant Human Bone Morphogenetic Protein-2 Using a Compression-Resistant Matrix in Posterolateral Spine Fusion in the Rabbit and in the Non-Human Primate. *Spine (Phila. Pa. 1976).* **2002**, *27* (4), 353–360.

(67) Le, D.; Duval, L.; Lecomte, A.; Julien, M.; Guicheux, J.; Daculsi, G.; Layrolle, P. Interactions of Total Bone Marrow Cells with Increasing Quantities of Macroporous Calcium Phosphate Ceramic Granules. *J. Mater. Sci. Mater. Med.* **2007**, *18*, 1983–1990.

(68) Gao, P.; Zhang, H.; Liu, Y.; Fan, B.; Li, X.; Xiao, X.; Lan, P.; Li, M.; Geng, L.; Liu, D.; et al. Beta-Tricalcium Phosphate Granules Improve Osteogenesis in Vitro and Establish Innovative Osteo-Regenerators for Bone Tissue Engineering in Vivo. *Sci. Rep.* **2016**, *6* (23367), 1–14.

(69) Tas, A. C. Synthesis of Biomimetic Ca-Hydroxyapatite Powders at 37 3 C

in Synthetic Body Fluids. *Biomaterials* **2000**, *21*, 1429–1438.

(70) Raynaud, S.; Champion, E.; Bernache-Assollant, D.; Thomas, P. Calcium Phosphate Apatites with Variable Ca / P Atomic Ratio I . Synthesis , Characterisation and Thermal Stability of Powders. *Biomaterials* **2002**, *23* (3), 1065–1072.

(71) Rhee, S. Synthesis of Hydroxyapatite via Mechanochemical Treatment. *Biomaterials* **2002**, *23*, 1147–1152.

(72) Nasiri-tabrizi, B.; Honarmandi, P.; Ebrahimi-kahrizsangi, R.; Honarmandi, P. Synthesis of Nanosize Single-Crystal Hydroxyapatite via Mechanochemical Method. *Mater. Lett.* **2009**, *63* (5), 543–546.

(73) Bigi, A.; Boanini, E.; Rubini, K. Hydroxyapatite Gels and Nanocrystals Prepared through a Sol – Gel Process. *J. Solid State Chem.* **2004**, *177*, 3092–3098.

(74) Chen, J.; Wang, Y.; Chen, X.; Ren, L.; Lai, C.; He, W.; Zhang, Q. A Simple Sol-Gel Technique for Synthesis of Nanostructured Hydroxyapatite , Tricalcium Phosphate and Biphasic Powders. *Mater. Lett.* **2011**, *65* (12), 1923–1926.

(75) Bao, L. Y.; Groot, K. D.; Wijin, J. D.; Klein, C. P. A. T.; Meer, S. V. D. Morphology and Composition of Nanograde Calcium Phosphate Needle-like Crystals Formed by Simple Hydrothermal Treatment. *J. Mater. Sci. Mater. Med.* **1994**, *5*, 326–331.

(76) Jinawath, S.; Pongkao, D.; Suchanek, W.; Yoshimura, M. Hydrothermal Synthesis of Monetite and Hydroxyapatite from Monocalcium Phosphate Monohydrate. *Int. J. Inorg. Mater.* **2001**, *3*, 997–1001.

(77) Zhang, X.; Vecchio, K. S. Hydrothermal Synthesis of Hydroxyapatite Rods. *J. Cryst. Growth* **2007**, *308*, 133–140.

(78) Chaudhry, A. A.; Haque, S.; Kellici, S.; Boldrin, P.; Rehman, I.; Khalid, A.; Darr, J. A. Instant Nano-Hydroxyapatite : A Continuous and Rapid Hydrothermal Synthesis. *Chem. Commun.* **2006**, No. 200, 2286–2288.

(79) Wang, Y.; Zhang, S.; Wei, K.; Zhao, N.; Chen, J.; Wang, X. Hydrothermal Synthesis of Hydroxyapatite Nanopowders Using Cationic Surfactant as a Template. *Mater. Lett.* **2006**, *60*, 1484–1487.

(80) Han, J.; Song, H.; Saito, F.; Lee, B. Synthesis of High Purity Nano-Sized Hydroxyapatite Powder by Microwave-Hydrothermal Method. *Mater. Chemi* **2006**, *99*, 235–239.

(81) Reardon, P. J. T.; Huang, J.; Tang, J. Morphology Controlled Porous Calcium Phosphate Nanoplates and Nanorods with Enhanced Protein Loading and Release Functionality. *Adv. Healthc. Mater.* **2013**, *2* (5), 682–686.

(82) Reardon, P. J. T.; Handoko, A. D.; Li, L.; Huang, J.; Tang, J. Dimensionally and Compositionally Controlled Growth of Calcium Phosphate Nanowires for Bone Tissue Regeneration. *J. Mater. Chem. B* **2013**, *1* (44), 6170–6176.

(83) Shandilya, M.; Rai, R.; Singh, J. Review : Hydrothermal Technology for Smart Materials Review : Hydrothermal Technology for Smart Materials. *Adv. Appl. Ceram.* **2016**, *115* (6), 354–376.

(84) Webb, A. R.; Yang, J.; Ameer, G. a. Biodegradable Polyester Elastomers in Tissue Engineering. *Expert Opin. Biol. Ther.* **2004**, *4* (6), 801–812.

(85) Nair, L. S.; Laurencin, C. T. Biodegradable Polymers as Biomaterials. *Prog. Polym. Sci.* **2007**, *32*, 762–798.

(86) Vroman, I.; Tighzert, L. Biodegradable Polymers. *Materials (Basel).* **2009**, *2*, 307–344.

(87) Berlemont, R. Distribution and Diversity of Enzymes for Polysaccharide Degradation in Fungi. *Sci. Rep.* **2017**, *7* (222), 1–11.

(88) Li, Y.; Thouas, G. a; Chen, Q.-Z. Biodegradable Soft Elastomers: Synthesis/properties of Materials and Fabrication of Scaffolds. *RSC Adv.* **2012**, *2* (22), 8229.

(89) Pomerantseva, I.; Krebs, N.; Hart, A.; Neville, C. M.; Huang, A. Y.; Sundback, C. a. Degradation Behavior of Poly(glycerol Sebacate). *J. Biomed. Mater. Res. A* **2009**, *91* (4), 1038–1047.

(90) Bruggeman, J. P.; de Bruin, B. J.; Bettinger, C. J.; Langer, R. Biodegradable Poly (Polyol Sebacate) Polymers. *Biomaterials* **2008**, *29* (36), 4726–4735.

(91) Rai, R.; Tallawi, M.; Grigore, A.; Boccaccini, A. R. Synthesis, Properties and Biomedical Applications of Poly(glycerol Sebacate) (PGS): A Review. *Prog. Polym. Sci.* **2012**, *37* (8), 1051–1078.

(92) Barrett, D. G.; Yousaf, M. N. Thermosets Synthesized by Thermal Polyesterification for Tissue Engineering Applications. *Soft Matter* **2010**, *6* (20), 5026.

(93) Wang, Y.; Kim, Y. M.; Langer, R. Technical Note In Vivo Degradation Characteristics of Poly (Glycerol Sebacate). **2002**, No. 85.

(94) Chen, Q.; Liang, S.; Thouas, G. A. Synthesis and Characterisation of Poly (Glycerol Sebacate)-Co-Lactic Acid as Surgical Sealants. *Soft Matter* **2011**, *7*, 6484–6492.

(95) Hagandora, C. K.; Gao, J.; Wang, Y.; Almarza, A. J. Poly (Glycerol Sebacate): A Novel Scaffold Material for Temporomandibular Joint Disc Engineering. *Tissue Eng. Part A* **2013**, *19* (5–6), 729–737.

(96) Yi, F.; Lavan, D. A. Poly(glycerol Sebacate) Nanofiber Scaffolds by Core/shell Electrospinning. *Macromol. Biosci.* **2008**, *8*, 803–806.

(97) Yeh, Y.; Highley, C. B.; Ouyang, L.; Burdick, J. A. 3D Printing of Photocurable Poly (Glycerol Sebacate) Elastomers. *Biofabrication* **2016**, *8* (4), 1–10.

(98) Gao, J. I. N.; Crapo, P. M.; Wang, Y. Macroporous Elastomeric Scaffolds with Extensive Micropores for Soft Tissue Engineering. *Tissue Eng.* **2006**, *12* (4), 917–925.

(99) Li, Y.; Cook, W. D.; Moorhoff, C.; Huang, W.-C.; Chen, Q.-Z. Synthesis, Characterization and Properties of Biocompatible Poly(glycerol Sebacate) Pre-Polymer and Gel. *Polym. Int.* **2013**, *62* (4), 534–547.

(100) Li, X.; Hong, A. T.-L.; Naskar, N.; Chung, H.-J. Criteria for Quick and Consistent Synthesis of Poly(glycerol Sebacate) for Tailored Mechanical Properties. *Biomacromolecules* **2015**, *16* (5), 1525–1533.

(101) Liang, S.-L.; Cook, W. D.; Thouas, G. a.; Chen, Q.-Z. The Mechanical Characteristics and in Vitro Biocompatibility of Poly(glycerol Sebacate)-Bioglass® Elastomeric Composites. *Biomaterials* **2010**, *31* (33), 8516–8529.

(102) Bueno, E. M.; Glowacki, J. Cell-Free and Cell-Based Approaches for Bone Regeneration. *Nat. Rev. Rheumatol.* **2009**, *5* (12), 685–697.

(103) Zhao, X.; Wu, Y.; Du, Y.; Chen, X.; Lei, B.; Xue, Y.; Ma, P. X. A Highly Bioactive and Biodegradable Poly(glycerol Sebacate)– Silica Glass Hybrid Elastomer with Tailored Mechanical Properties for Bone Tissue Regeneration. *J. Mater. Chem. B* **2015**, *3*, 3222–3233.

(104) Kerativitayanan, P.; Gaharwar, A. K. Elastomeric and Mechanically Stiff Nanocomposites from Poly(glycerol Sebacate) and Bioactive Nanosilicates. *Acta Biomater.* **2015**, *26*, 34–44.

(105) Zhou, L.; He, H.; Jiang, C.; He, S. Preparation and Characterization of Poly (Glycerol Sebacate)/ Cellulose Nanocrystals Elastomeric Composites. *J. Appl. Polym. Sci.* **2015**, *42196* (132), 42196.

(106) Gaharwar, A. K.; Khademhosseini, A. Elastomeric Nanocomposite Scaffolds Made from Poly(glycerol Sebacate) Chemically Crosslinked with Carbon Nanotubes. *Biomater. Sci.* **2014**, *3* (1), 46–58.

(107) Rosenbalm, T. N.; Teruel, M.; Day, C. S.; Donati, G. L.; Morykwas, M.; Argenta, L.; Kuthirummal, N.; Levi-polyachenko, N. Structural and Mechanical Characterization of Bioresorbable , Elastomeric Nanocomposites from Poly (Glycerol Sebacate)/ Nanohydroxyapatite for Tissue Transport Applications. *J. Biomed. Mater. Res. B. Appl. Biomater.* **2015**, *104* (7), 1366–1373.

(108) Collins, J. M.; Leadbeater, N. E. Microwave Energy: A Versatile Tool for the Biosciences. *Org. Biomol. Chem.* **2007**, *5* (8), 1141–1150.

(109) Gabriel, C.; Gabriel, S.; H. Grant, E.; S. J. Halstead, B.; Michael P. Mingos, D. Dielectric Parameters Relevant to Microwave Dielectric Heating. *Chem. Soc. Rev.* **1998**, *27* (3), 213.

(110) Oliver Kappe, C. Microwave Dielectric Heating in Synthetic Organic Chemistry. *Chem. Soc. Rev.* **2008**, *37* (6), 1127–1139.

(111) Hayes, B. L. *Microwave Synthesis: Chemistry at the Speed of Light*; CEM Publishing: U.S.A., 2002.

(112) Kappe, C. O. Controlled Microwave Heating in Modern Organic Synthesis. *Angew. Chem. Int. Ed. Engl.* **2004**, *43* (46), 6250–6284.

(113) Barlow, B. S.; Marder, S. R. Single-Mode Microwave Synthesis in

Organic Materials Chemistry **. *Adv. Funct. Mater.* **2003**, No. 7, 517–518.

(114) Hoogenboom, R.; Wilms, T. F. A.; Erdmenger, T.; Schubert, U. S. Microwave-Assisted Chemistry : A Closer Look at Heating Efficiency. *Aust. J. Chem.* **2009**, *62*, 236–243.

(115) Razzaq, T.; Kappe, C. O. On the Energy Efficiency of Microwave-Assisted Organic Reactions. *ChemSusChem* **2008**, *1*, 123–132.

(116) Kuhnert, N. Microwave-Assisted Reactions in Organic Synthesis – Are There Any Nonthermal Microwave Effects ? *Angew. Chem. Int. Ed. Engl.* **2002**, *41* (11), 1863–1866.

(117) Strauss, C. R.; Trainor, R. W. Invited Review - Developments in Microwave-Assisted Organic-Chemistry. *Aust. J. Chem.* **1995**, *48*, 1665–1692.

(118) Lovingood, D. D.; Owens, J. R.; Seeber, M.; Kornev, K. G.; Luzinov, I. Controlled Microwave-Assisted Growth of Silica Nanoparticles under Acid Catalysis. *ACS Appl. Mater. Interfaces* **2012**, *4* (12), 6875–6883.

(119) Chen, P.; Rosana, M. Parameters Affecting the Microwave-Specific Acceleration of a Chemical Reaction. *J. Org. Chem.* **2014**, *79*, 7425–7436.

(120) Rosana, M. R.; Hunt, J.; Ferrari, A.; Southworth, T. A.; Tao, Y.; Stiegman, A. E.; Dudley, G. B. Microwave-Specifi c Acceleration of a Friedel − Crafts Reaction: Evidence for Selective Heating in Homogeneous Solution. *J. Org. Chem.* **2014**, *79*, 7437–7450.

(121) Dallinger, D.; Irfan, M.; Suljanovic, A.; Kappe, C. O. An Investigation of Wall Effects in Microwave-Assisted Ring-Closing Metathesis and Cyclotrimerization Reactions. *J. Org. Chem.* **2010**, *75* (15), 5278–5288.

(122) Thommes, M.; Kaneko, K.; Neimark, A. V; Olivier, J. P.; Rodriguez-reinoso, F.; Rouquerol, J.; Sing, K. S. W. Physisorption of Gases , with Special Reference to the Evaluation of Surface Area and Pore Size Distribution (IUPAC Technical Report). *Pure Appl. Chem.* **2015**, *87* (9–10), 1051–1069.

(123) Sing, K. S. W.; Everett, D. .; Haul, R. A. W.; Moscou, L.; Pierotti, R. A.; Rouquerol, J.; Siemieniewska, T. Reporting Physisorption Data for Gas/Solid Systems with Special Reference to the Determination of Surface Area and Porosity. *Pure Appl. Chem.* **1985**, *57* (4), 603–619.

(124) Epple, M.; Ganesan, K.; Heumann, R.; Klesing, J.; Kovtun, A.; Neumann, S.; Sokolova, V. Application of Calcium Phosphate Nanoparticles in Biomedicine. *J. Mater. Chem.* **2010**, *20* (1), 18–23.

(125) Bohner, M.; Tadier, S.; Garderen, N. Van. Synthesis of Spherical Calcium Phosphate Particles for Dental and Orthopedic Applications. *Biomatter* **2013**, *3* (2), 1–15.

(126) Pattanayak, D. K.; Rao, B. T.; Mohan, T. R. R. Calcium Phosphate Bioceramics and Bioceramic Composites. *J. Sol-Gel Sci. Technol.* **2010**, *59* (3), 432–447.

(127) Kumta, P. N.; Sfeir, C.; Lee, D.-H.; Olton, D.; Choi, D. Nanostructured Calcium Phosphates for Biomedical Applications: Novel Synthesis and Characterization. *Acta Biomater.* **2005**, *1* (1), 65–83.

(128) Zhu, X. D.; Zhang, H. J.; Fan, H. S.; Li, W.; Zhang, X. D. Effect of Phase Composition and Microstructure of Calcium Phosphate Ceramic Particles on Protein Adsorption. *Acta Biomater.* **2010**, *6* (4), 1536–1541.

(129) Ginebra, M. P.; Traykova, T.; Planell, J. A. Calcium Phosphate Cements as Bone Drug Delivery Systems: A Review. *J. Control. Release* **2006**, *113* (2), 102–110.

(130) Dasgupta, S.; Bandyopadhyay, A.; Bose, S. Reverse Micelle-Mediated Synthesis of Calcium Phosphate Nanocarriers for Controlled Release of Bovine Serum Albumin. *Acta Biomater.* **2009**, *5* (8), 3112–3121.

(131) Tabata, Y. The Importance of Drug Delivery. *Pharm. Sci. Technolo. Today* **2000**, *3* (3), 80–89.

(132) Bow, J.-S.; Liou, S.-C.; Chen, S.-Y. Structural Characterization of Room-Temperature Synthesized Nano-Sized Beta-Tricalcium Phosphate. *Biomaterials* **2004**, *25* (16), 3155–3161.

(133) Bilecka, I.; Niederberger, M. Microwave Chemistry for Inorganic Nanomaterials Synthesis. *Nanoscale* **2010**, *2* (8), 1358–1374.

(134) Rao, K. J.; Vaidhyanathan, B.; Ganguli, M.; Ramakrishnan, P. A. Synthesis of Inorganic Solids Using Microwaves. *Chem. Mater.* **1999**, *11* (4), 882–895.

(135) Lau, C. C.; Reardon, P. J. T.; Knowles, J.; Tang, J. Phase-Tunable Calcium Phosphate Biomaterials Synthesis and Application in Protein Delivery. *ACS Biomater. Sci. Eng.* **2015**, *1* (10), 947–954.

(136) Xu, J.; Butler, I.; Gilson, D. FT-Raman and High-Pressure Infrared Spectroscopic Studies of Dicalcium Phosphate Dihydrate (CaHPO 4· 2H 2 O) and Anhydrous Dicalcium Phosphate (CaHPO. *Spectrochim. Acta. A. Mol. Biomol. Spectrosc.* **1999**, *55*, 2801–2809.

(137) Jillavenkatesa, A.; Sr., R. A. C. The Infrared and Raman Spectra of β-and α-Tricalcium Phosphate (Ca 3 (Po 4) 2). *Spectrosc. Lett. An Int. J. Rapid Commun.* **1998**, *31* (8), 1619–1634.

(138) Aza, P. N. De; Santos, C.; Pazo, A.; Artu, L. Vibrational Properties of Calcium Phosphate Compounds . 1 . Raman Spectrum of -Tricalcium Phosphate. **1997**, *4756* (10), 912–915.

(139) Kazanci, M.; Fratzl, P.; Klaushofer, K.; Paschalis, E. P. Complementary Information on in Vitro Conversion of Amorphous (Precursor) Calcium Phosphate to Hydroxyapatite from Raman Microspectroscopy and Wide-Angle X-Ray Scattering. *Calcif. Tissue Int.* **2006**, *79* (5), 354–359.

(140) Yin, J.; Gao, F.; Wei, C.; Lu, Q. Water Amount Dependence on Morphologies and Properties of ZnO Nanostructures in Double-Solvent System. *Sci. Rep.* **2014**, *4*, 3736.

(141) Keraliya, R. A.; Soni, T. G.; Thakkar, V. T.; Gandhi, T. R. Effect of

Solvent on Crystal Habit and Dissolution Behavior of Tolbutamide by Initial Solvent Screening. *Dissolution Technol* **2010**, *1*, 16–21.

(142) Veggi, P. C.; Martinez, J.; Meireles, M. A. A. Fundamentals of Microwave Extraction. In *Microwave-assisted Extraction for Bioactive Compounds: Theory and Practice*; Chemat, F., Cravotto, G., Eds.; Springer US: Boston, MA, 2012; pp 15–52.

(143) James, P.; Reardon, T.; Huang, J.; Tang, J. Mesoporous Calcium Phosphate Bionanomaterials with Controlled Morphology by an Energy-Efficient Microwave Method. *J. Biomed. Mater. Res. Part A* **2015**, *103*, 3781–3789.

(144) Dahlsten, P.; Kosmulski, M.; Rosenholm, J. B. Surface-Induced Electrolytic Dissociation of Oxalic and Phosphoric Acid in Mixed Alcohol-Water Solvents. *Colloids Surfaces A Physicochem. Eng. Asp.* **2011**, *376* (1–3), 42–46.

(145) Torres, L. G. Ca-Alginate Spheres Behavior in Presence of Some Solvents and Water-Solvent Mixtures. *Adv. Biosci. Biotechnol.* **2011**, *2* (1), 8–12.

(146) Dorozhkin, S. V. Calcium Orthophosphate Coatings, Films and Layers. *Prog. Biomater.* **2012**, *1* (1), 1.

(147) Perry, D. L. Inorganic Compound Data. In *Handbook of Inorganic Compounds*; CRC Press, Taylor & Francis Group: Boca Raton, 2011; pp 84–85.

(148) Kosmulski, M. Simple Model of Surface-Induced Electrolytic Dissociation of Weak Acids in Organic Solvents. *Adsorption* **2010**, *16* (4–5), 343–349.

(149) Rodrigues, A.; Lebugle, A. Influence of Ethanol in the Precipitation Medium on the Composition, Structure and Reactivity of Tricalcium Phosphate. *Colloids Surfaces A Physicochem. Eng. Asp.* **1998**, *145*, 191–204.

(150) Puvvada, N.; Panigrahi, P. K.; Pathak, A. Room Temperature Synthesis of Highly Hemocompatible Hydroxyapatite, Study of Their Physical Properties and Spectroscopic Correlation of Particle Size. *Nanoscale* **2010**, *2* (12), 2631–2638.

(151) Zeng, H.; Chittur, K. K.; Lacefield, W. R. Analysis of Bovine Serum Albumin Adsorption on Calcium Phosphate and Titanium Surfaces. *Biomaterials* **1999**, *20*, 377–384.

(152) Lee, W.; Loo, C.; Van, K. L.; Zavgorodniy, A. V; Rohanizadeh, R. Modulating Protein Adsorption onto Hydroxyapatite Particles Using Different Amino Acid Treatments. *J. R. Soc. Interface* **2012**, No. 9, 918–927.

(153) Sun, Z.; Deng, Y.; Wei, J.; Gu, D.; Tu, B.; Zhao, D. Hierarchically Ordered Macro-/Mesoporous Silica Monolith: Tuning Macropore Entrance Size for Size-Selective Adsorption of Proteins. *Chem. Mater.* **2011**, *23* (8), 2176–2184.

(154) Shirahama, H.; Suzawa, T. Adsorption of Bovine Serum Albumin onto

Styrene/acrylic Acid Copolymer Latex. *Colloid Polym. Sci.* **1985**, *263* (2), 141–146.

(155) Gao, Y.; Chen, Y.; Ji, X.; He, X.; Yin, Q.; Zhang, Z.; Shi, J.; Li, Y. Controlled Intracellular Release of Doxorubicin in Multidrug-Resistant Cancer Cells by Tuning the Shell-Pore Sizes of Mesoporous Silica Nanoparticles. *ACS Nano* **2011**, *5* (12), 9788–9798.

(156) Liu, T.-Y.; Chen, S.-Y.; Liu, D.-M.; Liou, S.-C. On the Study of BSA-Loaded Calcium-Deficient Hydroxyapatite Nano-Carriers for Controlled Drug Delivery. *J. Control. Release* **2005**, *107* (1), 112–121.

(157) Chen, Q.; Liang, S.; Thouas, G. a. Elastomeric Biomaterials for Tissue Engineering. *Prog. Polym. Sci.* **2013**, *38* (3–4), 584–671.

(158) Sun, Z.-J.; Chen, C.; Sun, M.-Z.; Ai, C.-H.; Lu, X.-L.; Zheng, Y.-F.; Yang, B.-F.; Dong, D.-L. The Application of Poly (Glycerol-Sebacate) as Biodegradable Drug Carrier. *Biomaterials* **2009**, *30* (28), 5209–5214.

(159) Sundback, C. A.; Shyu, J. Y.; Wang, Y.; Faquin, W. C.; Langer, R. S.; Vacanti, J. P.; Hadlock, T. A. Biocompatibility Analysis of Poly(glycerol Sebacate) as a Nerve Guide Material. *Biomaterials* **2005**, *26* (27), 5454–5464.

(160) Sestoft, L. An Evaluation of Biochemical Aspects of Intravenous Fructose , Sorbitol and Xylitol Administration in Man. **1985**, No. mM, 19–29.

(161) Chen, Q.; Jin, L.; Cook, W. D.; Mohn, D.; Lagerqvist, E. L.; Elliott, D. a.; Haynes, J. M.; Boyd, N.; Stark, W. J.; Pouton, C. W.; et al. Elastomeric Nanocomposites as Cell Delivery Vehicles and Cardiac Support Devices. *Soft Matter* **2010**, *6* (19), 4715.

(162) Chen, Q.-Z.; Ishii, H.; Thouas, G. a; Lyon, A. R.; Wright, J. S.; Blaker, J. J.; Chrzanowski, W.; Boccaccini, A. R.; Ali, N. N.; Knowles, J. C.; et al. An Elastomeric Patch Derived from Poly(glycerol Sebacate) for Delivery of Embryonic Stem Cells to the Heart. *Biomaterials* **2010**, *31* (14), 3885–3893.

(163) Shi, R.; Chen, D.; Liu, Q.; Wu, Y.; Xu, X.; Zhang, L. Recent Advances in Synthetic Bioelastomers. *Int. J. Mol. Sci.* **2009**, *10*, 4223–4256.

(164) Wiesbrock, F.; Hoogenboom, R.; Schubert, U. S. Microwave-Assisted Polymer Synthesis: State-of-the-Art and Future Perspectives. *Macromol. Rapid Commun.* **2004**, *25* (20), 1739–1764.

(165) Bayazit, M. K.; Yue, J.; Cao, E.; Gavriilidis, A.; Tang, J. Controllable Synthesis of Gold Nanoparticles in Aqueous Solution by Microwave Assisted Flow Chemistry. *ACS Sustain. Chem. Eng.* **2016**, *4*, 6435.

(166) Li, X.; Hong, A. T.-L.; Naskar, N.; Chung, H.-J. Criteria for Quick and Consistent Synthesis of Poly(glycerol Sebacate) for Tailored Mechanical Properties. *Biomacromolecules* **2015**, *16* (5), 1525–1533.

(167) Loh, X. J.; Karim, A. A.; Owh, C. Poly(glycerol Sebacate) Biomaterial: Synthesis and Biomedical Applications. *J. Mater. Chem. B* **2015**, *3* (39), 7641–7652.

(168) Barlow, S.; Marder, S. R. Single-Mode Microwave Synthesis in Organic Materials Chemistry. *Adv. Funct. Mater.* **2003**, *13* (7), 517–518.

(169) Lau, C. C.; Bayazit, M. K.; Knowles, J. C.; Tang, J. Tailoring Degree of Esterification and Branching of Poly(glycerol Sebacate) by Energy Efficient Microwave Irradiation. *Polmer Chem.* **2017**, *8*, 3937–3947.

(170) Dallinger, D.; Kappe, C. O. Microwave-Assisted Synthesis in Water as Solvent. *Chem. Rev.* **2007**, *107* (6), 2563–2591.

(171) Adam, D. Out of the Kitchen. *Nature* **2003**, *421*, 571.

(172) Hoogenboom, R.; Schubert, U. S. Microwave-Assisted Polymer Synthesis: Recent Developments in a Rapidly Expanding Field of Research. *Macromol. Rapid Commun.* **2007**, *28* (4), 368–386.

(173) Ergan, B. T.; Bayramoğlu, M.; Özcan, S. Emulsion Polymerization of Styrene under Continuous Microwave Irradiation. *Eur. Polym. J.* **2015**, *69*, 374–384.

(174) Velmathi, S.; Nagahata, R.; Sugiyama, J.; Takeuchi, K. A Rapid Eco-Friendly Synthesis of Poly(butylene Succinate) by a Direct Polyesterification under Microwave Irradiation. *Macromol. Rapid Commun.* **2005**, *26* (14), 1163–1167.

(175) Coates, J. Interpretation of Infrared Spectra , A Practical Approach. *Encyclopedia of Analytical Chemistry*; 2006.

(176) Nijst, C. L. E.; Bruggeman, J. P.; Karp, J. M.; Ferreira, L.; Zumbuehl, A.; Bettinger, C. J.; Langer, R. Synthesis and Characterization of Photocurable Elastomers from Poly(glycerol-Co-Sebacate). *Biomacromolecules* **2007**, *8* (10), 3067–3073.

(177) Bodakhe, S.; Verma, S.; Garkhal, K.; Samal, S. K.; Sharma, S. S.; Kumar, N. Injectable Photocrosslinkable Nanocomposite Based on Poly(glycerol Sebacate) Fumarate and Hydroxyapatite: Development, Biocompatibility and Bone Regeneration in a Rat Calvarial Bone Defect Model. *Nanomedicine (Lond).* **2013**, *8* (11), 1777–1795.

(178) Jia, Y.; Wang, W.; Zhou, X.; Nie, W.; Chen, L.; He, C. Synthesis and Characterization of Poly(glycerol Sebacate)-Based Elastomeric Copolyesters for Tissue Engineering Applications. *Polym. Chem.* **2016**, *7* (14), 2553–2564.

(179) Shi, H.; Gan, Q.; Liu, X.; Ma, Y.; Hu, J.; Yuan, Y.; Liu, C. Poly(glycerol Sebacate)-Modified Polylactic Acid Scaffolds with Improved Hydrophilicity, Mechanical Strength and Bioactivity for Bone Tissue Regeneration. *RSC Adv.* **2015**, *5* (97), 79703–79714.

(180) Liu, Q.; Tian, M.; Ding, T.; Shi, R.; Feng, Y.; Zhang, L.; Chen, D.; Tian, W. Preparation and Characterization of a Thermoplastic Poly (Glycerol Sebacate) Elastomer by Two-Step Method. *J. Appl. Polym. Sci.* **2007**, *103*, 1412–1419.

(181) Kafouris, D.; Kossivas, F.; Constantinides, C.; Nguyen, N. Q.; Wesdemiotis, C.; Patrickios, C. S. Biosourced Amphiphilic Degradable

Elastomers of Poly(glycerol Sebacate): Synthesis and Network and Oligomer Characterization. *Macromolecules* **2013**, *46* (3), 622–630.

(182) Nagahata, R.; Sano, D.; Suzuki, H.; Takeuchi, K. Microwave-Assisted Single-Step Synthesis of Poly(lactic Acid) by Direct Polycondensation of Lactic Acid. *Macromol. Rapid Commun.* **2007**, *28* (4), 437–442.

(183) Guo, X.-L.; Lu, X.-L.; Dong, D.-L.; Sun, Z.-J. Characterization and Optimization of Glycerol/sebacate Ratio in Poly(glycerol-Sebacate) Elastomer for Cell Culture Application. *J. Biomed. Mater. Res. A* **2014**, *102* (11), 3903–3907.

(184) Chen, Q.-Z.; Bismarck, A.; Hansen, U.; Junaid, S.; Tran, M. Q.; Harding, S. E.; Ali, N. N.; Boccaccini, A. R. Characterisation of a Soft Elastomer Poly(glycerol Sebacate) Designed to Match the Mechanical Properties of Myocardial Tissue. *Biomaterials* **2008**, *29* (1), 47–57.

(185) Soh, M. S.; Yap, A. U. J. Influence of Curing Modes on Crosslink Density in Polymer Structures. *J. Dent.* **2004**, *32* (4), 321–326.

(186) Gillham, J. K. Formation and Properties of Network Polymeric Materials. *Polym. Eng. Sci.* **1979**, *19* (10), 676–682.

(187) Safranski, D. L.; Gall, K. Effect of Chemical Structure and Crosslinking Density on the Thermo-Mechanical Properties and Toughness of (Meth)acrylate Shape Memory Polymer Networks. *Polymer (Guildf).* **2008**, *49* (20), 4446–4455.

(188) Yang, B.; Lv, W.; Deng, Y. Drug Loaded Poly(glycerol Sebacate) as a Local Drug Delivery System for the Treatment of Periodontal Disease. *RSC Adv.* **2017**, *7* (59), 37426–37435.

(189) Kamaly, N.; Yameen, B.; Wu, J.; Farokhzad, O. C. Degradable Controlled-Release Polymers and Polymeric Nanoparticles: Mechanisms of Controlling Drug Release. *Chem. Rev.* **2016**, *116* (4), 2602–2663.

(190) Lyu, S.; Untereker, D. Degradability of Polymers for Implantable Biomedical Devices. *Int. J. Mol. Sci.* **2009**, *10* (9), 4033–4065.

(191) Wu, L.; Ding, J. Effects of Porosity and Pore Size on in Vitro Degradation of Three-Dimensional Porous poly(D,L-Lactide-Co-Glycolide) Scaffolds for Tissue Engineering. *J. Biomed. Mater. Res. A* **2005**, *75* (4), 767–777.

(192) Zhu, X.; Zhou, Y.; Yan, D. Influence of Branching Architecture on Polymer Properties. *J. Polym. Sci. Part B Polym. Phys.* **2011**, *49* (18), 1277–1286.

(193) Bosco, R.; Beucken, J. Van Den; Leeuwenburgh, S.; Jansen, J. Surface Engineering for Bone Implants: A Trend from Passive to Active Surfaces. *Coatings* **2012**, *2*, 95–119.

(194) Conejero-garcía, Á.; Gimeno, H. R.; Sáez, Y. M.; Vilariño-feltrer, G.; Ortuño-lizarán, I.; Vallés-lluch, A. Correlating Synthesis Parameters with Physicochemical Properties of Poly (Glycerol Sebacate). *Eur. Polym. J.* **2017**, *87*, 406–419.

(195) Kim, M. J.; Hwang, M. Y.; Kim, J.; Chung, D. J. Biodegradable and

Elastomeric Poly (Glycerol Sebacate) as a Coating Material for Nitinol Bare Stent. *BioMed Reserach Int.* **2014**, 1–7.

(196) Paital, S. R.; Dahotre, N. B. Calcium Phosphate Coatings for Bio-Implant Applications : Materials , Performance Factors , and Methodologies. *Mater. Sci. Eng. R* **2009**, *66*, 1–70.

(197) Bayazit, M. K.; Cao, E.; Gavriilidis, A.; Tang, J. A Microwave Promoted Continuous Flow Approach to Self-Assembled Hierarchical Hematite Superstructures. *Green Chem.* **2016**, *18*, 3057–3065.

(198) Zhou, C.; Ye, X.; Fan, Y.; Ma, L.; Tan, Y.; Qing, F.; Zhang, X. Biomimetic Fabrication of a Three-Level Hierarchical Calcium Phosphate/collagen/hydroxyapatite Scaffold for Bone Tissue Engineering. *Biofabrication* **2014**, *6* (3), 35013.

(199) Gibson, I. R.; Rehman, I.; Best, S. M.; Bonfield, W. Characterization of the Transformation from Calcium-Deficient Apatite to B -Tricalcium Phosphate. *J. Mater. Sci. Med.* **2000**, *11*, 533–539.

(200) Carrodeguas, R. G.; De Aza, S. α-Tricalcium Phosphate: Synthesis, Properties and Biomedical Applications. *Acta Biomater.* **2011**, *7* (10), 3536–3546.

(201) Huang, J.; Ten, E.; Liu, G.; Finzen, M.; Yu, W.; Lee, J. S.; Saiz, E.; Tomsia, A. P. Biocomposites of pHEME with HA/b-TCP (60/40) for Tissue Engineering : Swelling , Hydrolytic Degradation , and in Vitro Behavior. *Polymer (Guildf).* **2013**, *54* (3), 1197–1207.

(202) Petta, D.; Fussell, G.; Hughes, L.; Buechter, D. D.; Sprecher, C. M.; Alini, M.; Eglin, D.; Este, M. D. Calcium Phosphate / Thermoresponsive Hyaluronan Hydrogel Composite Delivering Hydrophilic and Hydrophobic Drugs. *J. Orthop. Transl.* **2016**, *5*, 57–68.

(203) Kester, M.; Heakal, Y.; Sharma, A.; Robertson, G. P.; Morgan, T. T.; Altinogly, E. I.; Tabakovic, A.; Parette, M. R.; Rouse, S.; Ruiz-Velasco, V.; et al. Calcium Phosphate Nanocomposite Particles for in Vitro Imaging and Encapsulated Chemotherapeutic Drug Delivary to Cancer Cells. *Nano Lett.* **2008**, *8* (12), 4116–4121.

(204) Park, C.; Kyo, E.; Tijing, L. D.; Amarjargal, A.; Raj, H.; Sang, C.; Kyong, H. Preparation and Characterization of LA / PCL Composite Fi Bers Containing Beta Tricalcium Phosphate (β -TCP) Particles. *Ceram. Int.* **2014**, *40* (3), 5049–5054.

(205) Kobayashi, T.; Shimizu, K.; Konishi, S. Novel Combination of Hydrophilic / Hydrophobic Surface for Large Wettability Difference and Its Application to Liquid Manipulation. *Lab Chip* **2011**, *11*, 639–644.

(206) Wenzel, R. N. Resistance of Solid Surfaces to Wetting by Water. *Ind. Eng. Chem.* **1936**, *28*, 988–994.

(207) Yang, F.; Cui, W.; Xiong, Z.; Liu, L.; Bei, J.; Wang, S. Poly (L , L - Lactide- Co -Glycolide)/ Tricalcium Phosphate Composite Scaffold and Its Various Changes during Degradation in Vitro. *Polym. Degrad. Stab.* **2006**, *91*, 3065–3073.

(208) Sung, H.; Meredith, C.; Johnson, C.; Galis, Z. S. The Effect of Scaffold Degradation Rate on Three-Dimensional Cell Growth and Angiogenesis. *Biomaterials* **2004**, *25*, 5735–5742.

(209) Yi, J.; Xiong, F.; Li, B.; Chen, H.; Yin, Y.; Dai, H.; Li, S. Degradation Characteristics , Cell Viability and Host Tissue Responses of PDLLA-Based Scaffold with PRGD and B -TCP Nanoparticles Incorporation. *Regen. Biomater.* **2016**, 159–166.

(210) Kim, C. H.; Khil, M. S.; Kim, H. Y.; Lee, H. U.; Jahng, K. Y. An Improved Hydrophilicity via Electrospinning for Enhanced Cell Attachment and Proliferation. *J. Biomed. Mater. Res. Part B Appl. Biomater.* **2005**, 283–290.

(211) Gratiela, T.; Daniela, M.; Gabriela, R.; Iordachescu, D. Effect of Hydrophilic – Hydrophobic Balance on Biocompatibility of Poly (Methyl Methacrylate) (PMMA)– Hydroxyapatite (HA) Composites. *Mater. Chem. Phys.* **2009**, *118*, 265–269.

(212) Ghasemi-mobarakeh, L.; Prabhakaran, M. P.; Morshed, M. Bio-Functionalized PCL Nano Fi Brous Scaffolds for Nerve Tissue Engineering. *Mater. Sci. Eng. C* **2010**, *30* (8), 1129–1136.

(213) Park, H.; Guo, X.; Temenoff, J. S.; Tabata, Y.; Caplan, A. I.; Kasper, F. K.; Mikos, A. G. Effect of Swelling Ratio of Injectable Hydrogel Composites on Chondrogenic Differentiation of Encapsulated Rabbit Marrow Mesenchymal Stem Cells in Vitro. *Biomacromolecules* **2009**, *10* (3), 541–546.

(214) Roy, T. D.; Simon, J. L.; Ricci, J. L.; Rekow, E. D.; Thompson, V. P.; Parsons, J. R. Performance of Degradable Composite Bone Repair Products Made via Three-Dimensional Fabrication Techniques. *J. Biomed. Mater. Res. Part A* **2003**, *66* (2), 283–291.

(215) Maliger, R. B.; Halley, P. J.; Cooper-White, J. J. Poly (Glycerol-Sebacate) Bioelastomers: 2. Synthesis Using Brabender Plasticoder ® as a Batch Reactor. *J. Appl. Polym. Sci.* **2016**, *133* (1), 42852.

(216) Lee, S. H.; Lee, K.; Gade, P. S.; Robertson, A. M.; Yadong, W. Microwave-Assisted Facile Fabrication of Porous Poly (Glycerol Sebacate) Scaffolds. *J. Biomater. Sci.* **2017**, 1–10.

(217) Liu, Q.; Tian, M.; Shi, R.; Zhang, L.; Chen, D.; Tian, W. Structure and Properties of Thermoplastic Poly (Glycerol Sebacate) Elastomers Originating from Prepolymers with Different Molecular Weights. *J. Appl. Polym. Sci.* **2007**, *104*, 1131–1137.

(218) Jaafar, I. H.; Ammar, M. M.; Jedlicka, S. S.; Pearson, R. A.; Coulter, J. P. Spectroscopic Evaluation , Thermal , and Thermomechanical Characterization of Poly (Glycerol-Sebacate) with Variations in Curing Temperatures and Durations. *J. Mater. Sci.* **2010**, *45*, 2525–2529.